Synchronisation, Resonance and Reliability in Auditory Receptor Neurons

DISSERTATION

zur Erlangung des akademischen Grades
doctor rerum naturalium
(Dr. rer. nat.)
im Fach Biologie

eingereicht an der
Mathematisch-Naturwissenschaftlichen Fakultät I
Humboldt-Universität zu Berlin

von
Herrn dipl. zool. Samuel Glauser
geboren am 23.12.1975 in Zug, Schweiz

Präsident der Humboldt-Universität zu Berlin:
Prof. Dr. Christoph Markschies

Dekan der Mathematisch-Naturwissenschaftlichen Fakultät I:
Prof. Dr. Christian Limberg

Gutachter:

1. Prof. Dr. Andreas V. M. Herz
2. Prof. Dr. Bernd Ronacher
3. Prof. Dr. Oliver Behrend

eingereicht am:	3. Dezember 2007
Tag der mündlichen Prüfung:	26. Mai 2008

Abstract

This thesis deals with the effect of resonance and synchronisation on the precision and reliability of receptor neurons. Precision of individual neurons at the periphery of a nervous system, for example sensory neurons, is very important for later stages of processing. Different forms of resonance lead to an increase of precision in a neuron. Here, we examine neuronal timing resonance: a neuron produces action potentials (spikes) with greater precision around its resonance frequency – its firing rate – than at other frequencies. By using electrophysiological experiments on auditory receptor neurons of the locust *Locusta migratoria*, spike responses are generated whose precision is investigated using different reliability measures. Different types of auditory stimuli and stimulus parameters are used to examine locking of the spike response to the frequency of the stimulus, and the influence this locking has on spike time reliability, phase coupling and spike jitter. By varying the stimulus amplitude, so-called Arnold tongues become visible. The most prominent effect is seen for stimulus frequencies around the average firing rate, where the width of the Arnold tongue and the values of the reliability measures increases for increasing stimulus amplitudes.

Keywords:
Receptor Neurons, Resonance, Reliability, Locust

Zusammenfassung

Diese Dissertation befasst sich mit dem Einfluss von Resonanz und Synchronisation auf die Präzision und die Zuverlässigkeit von Rezeptorneuronen. Präzision von individuellen Neuronen an der Peripherie eines Nervensystems, beispielsweise in sensorischen Neuronen, ist äusserst wichtig für höhere Stufen der Verarbeitung. Verschiedene Formen von Resonanz können dazu führen, dass sich die Präzision eines Neurons erhöht. Hier wird neuronale Timing-Resonanz untersucht: diese kommt vor, wenn ein Neuron für Signale mit Frequenzen um seine Resonanzfrequenz – seiner Feuerrate – Aktionspotentiale (Spikes) mit höherer Präzision produziert, als für andere Frequenzen. Mit Hilfe von elektrophysiologischen Experimenten an auditorischen Rezeptorneuronen der Heuschrecke *Locusta migratoria* werden Spike-Antworten gewonnen, welche mit verschiedenen Zuverlässigkeitsmassen auf ihre Präzision untersucht werden. Verschiedene auditorische Stimulus-Typen und Stimulus-Parameter werden verwendet, um Kopplungsverhältnisse zwischen der Stimulusfrequenz und der Spike-Antwort und deren Einfluss auf Spike-Zeiten-Zuverlässigkeit, Phasen-Kopplung, und Spike-Jitter zu untersuchen. Dabei werden durch Variation der Stimulusamplitude sogenannte Arnold-Zungen sichtbar. Der deutlichste Effekt ist für Stimulusfrequenzen in der Nähe der mittleren Feuerrate zu sehen, wo die Breite der Arnold-Zunge ansteigt, wenn die Stimulusamplitude erhöht wird und erhöhte Werte für die Zuverlässigkeitsmasse vorhanden sind.

Schlagwörter:
Rezeptorneurone, Resonanz, Zuverlässigkeit, Heuschrecke

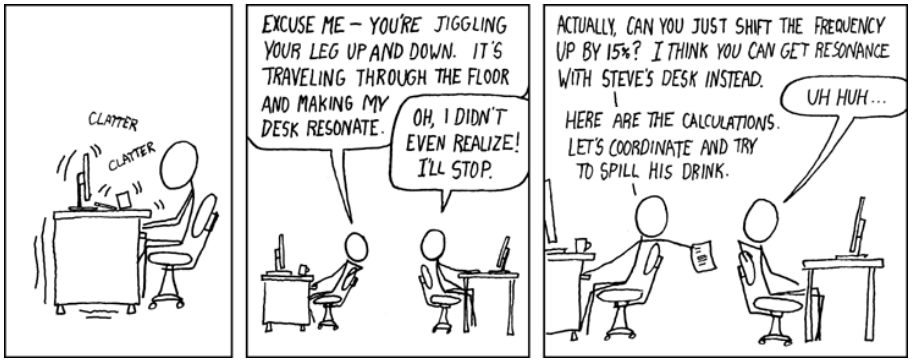

Resonance in daily use. (Cartoon by Randall Munroe)

Für meine Eltern

Contents

List of Figures

About this Thesis

Just as the stylus of a turntable's cartridge transforms the vibrations it receives in the groove of a vinyl record into electrical signals, the ears transform sound waves in the environment into electrical signals called spikes, generated by auditory receptor neurons. And, much like the turntable and its cartridge have an influence on the fidelity of the reproduction to the original musical performance, the design of a sensory system like the auditory system has a great influence on the fidelity with which the resulting ensembles of spikes represent the stimulus.

Thus, like the source component in a Hi-Fi system, the receptor neurons in a sensory organ such as the ear provide all the information that is available to the following stages of processing, be it amplifier and loudspeakers in the former, or higher stages of neuronal processing in the latter case. From this, we already see the importance of this first stage of processing: Information that is lost at the beginning is not available to subsequent stages.

Receptor neurons are the interface between an animal's brain and its environment, and they provide the information on which the animal bases its decisions and actions. Thus, to ensure survival and reproductive success, receptor neurons must encode information with sufficient fidelity. In this thesis, we study the fidelity of the response of a model system, locust auditory receptor neurons, to different types of stimuli. Specifically, we investigate whether synchronisation and resonance effects occur, which influence the neuronal response, possibly leading to greater reliability.

In Chapter 1, we start by introducing synchronisation and resonance. Synchronisation describes the process of two or more oscillators, matching the respective frequencies of their oscillations to a common one, due to a weak interaction between them. Examining synchronisation will bring us to the phenomenon of Arnold tongues: Areas where the frequency of an oscillator becomes closely coupled to the frequency of an external driving force, due to interactions between specific frequencies and amplitudes of the driving force and the oscillator. Resonance is the property of a system to oscillate with a maximal amplitude when excited at a certain frequency, the system's resonance frequency.

After the introduction, Chapter 2, *Reliability Through Resonance*, brings us to different types of resonance found in neural systems, and we will examine how a property such as resonance can improve the temporal precision and the reliability of spike generation of a neuron. We learn why improving precision and reliability of individual neurons at the periphery of a nervous system is of fundamental importance to higher stages of processing. Furthermore, three reliability measures are presented, which will be used to assess the spike timing of the neurons investigated in this thesis.

Chapter 3 presents the model system we studied: *The Locust Ear*. This chapter deals with the behavioral relevance of the locust ear, its anatomy and, specifically, the auditory

receptor neurons it contains, which are at the center of interest in this thesis. In Chapter 4, *Experiments*, the hardware and software involved in the experiments are presented, as well as the different stimulation protocols.

In the next chapter, *Neuronal Resonance with Sine Wave Stimuli*, we will analyse whether resonance effects with respect to spike timing can be observed in the responses of locust auditory receptor neurons under acoustic stimulation. Using sine wave stimuli, we will investigate if there are resonance effects present for different ratios between the neuron's firing rate and the stimulus frequency. By varying the stimulus amplitude we will examine the phenomenon of Arnold tongues, and investigate the influence of the firing rate on the reliability of the spike response of the neuron. To further analyse how timing resonance may depend on the presence of certain frequencies in the stimulus, we employ white noise stimuli with different cut-off frequencies and frequency gaps.

In Chapter, 6, *Neuronal Resonance with Square Wave Stimuli*, we will examine the spike time reliability of neurons using square wave stimuli, which due to the sharper transitions between the amplitude extremes resemble communication signals used by grasshoppers and locusts more closely than sine wave stimuli. Moreover, square waves give us the opportunity to control the fraction of the stimulus cycle which is above-threshold by varying the duty cycle.

Finally, Chapter 7, *Discussion and Outlook* will revisit the experimental findings from Chapters 5 and 6. We will discuss the results, compare them and put them into a context with respect to other studies in the field. This is followed by an outlook, which will deal with possible future directions of investigations.

Chapter 1

Synchronisation and Resonance

In 1665, when Christiaan Huygens was lying in his bed and recovering from an illness, he noticed something peculiar: The pendula of the two clocks in his room were moving synchronously in antiphase. Even when this synchrony was disturbed, the synchronous motion between the two pendula would reappear after a certain time:

> *"While I was forced to stay in bed for a few days, and made observations on my two clocks of the new workshop, I noticed a wonderful effect that nobody could have thought of before. The two clocks, while hanging [on the wall] side by side with a distance of one or two feet between, kept in pace relative to each other with a precision so high that the two pendula always swung together, and never varied [...] when I made the pendula swing at differing paces, I found that half an hour later, they always returned to synchronism and kept it constantly afterwards, as long as I let them go."*
>
> Huygens, as quoted in Pikovsky *et al.* (2001a)

Eight years before, in 1657, Huygens had patented the pendulum clock, so such an unexpected behaviour from his own invention baffled him: Why did the frequencies of those two pendula always converge to the same frequency?

Huygens went on to move the two clocks to different positions in the room, sometimes disrupting the synchrony, sometimes not. He also concealed one clock from the other with a wooden board, as to determine whether any air-turbulences from the pendula were the reason for the synchrony. They were not, as the synchrony was still there. After a few days of experimenting, he correctly determined the reason for the phenomenon: The tiny vibrations, transmitted from one clock to the other via the support on which both of them sat, were responsible for the synchronisation of the pendula.

Huygens discovered that two oscillators – the two pendulum clocks – can influence each other in a way that leads to a synchronised motion. He could not have imagined however, that the very same effect he discovered – synchronisation – was already exploited by the neurons in his brain to tackle the challenges of the environment.

Synchronisation in the brain was discovered almost three hundred years later, when, in 1929, Hans Berger published his electroencephalograph (EEG) work on humans (Berger,

1929), where he describes *brain waves*, caused by the synchronized electrical activity of neurons in the brain. Since then, our knowledge on synchronisation in nervous systems has grown considerably. As a first step towards understanding how synchronisation is used in a nervous system to process information coming from the environment, let us examine some basic principles of synchronisation.

1.1 Synchronisation

Synchronisation describes the process of two or more oscillators, such as the pendulum clocks in the example above, synchronising the frequencies of their oscillations to a common one, due to a weak interaction between them. Oscillators in such systems are usually considered to be *self-sustained*, meaning that they will continue to oscillate as long as there is enough energy present to drive the oscillation.

The oscillatory motion depends on the internal parameters of the oscillator, not on the way the oscillation was started. For example, the oscillation of the pendulum of an (isolated) clock is determined by the mechanism of the clock, and not by the amount of energy put into setting its pendulum in motion. Also, the oscillation is stable against small perturbations, as it will return to its original shape after it has been perturbed.

The rhythm or frequency of an oscillation, f, is given by the inverse of its period T,

$$f = \frac{1}{T}, \tag{1.1}$$

also known as the cyclic frequency. For example, the simple harmonic oscillator is described by a sine function

$$\sin(2\pi \cdot f \cdot t) = \sin(\omega \cdot t), \tag{1.2}$$

where the *angular frequency* ω,

$$\omega = 2\pi \cdot f = 2\pi/T, \tag{1.3}$$

is another natural measure and is often just called *frequency*. Later on we will see that the frequency can be changed by an external influence on the oscillator, or due to its interaction with another system. To avoid ambiguity, we call the frequency of the autonomous isolated system the *natural frequency* and denote it with ω_0.

In the above mentioned example of Huygens, there was not one oscillator but two: The two clocks in his room. Compared to today's standards, clock manufacturing inconsistencies were high, so it is not surprising that they did not oscillate identically, but rather that each had its own frequency. However through the weak interaction, or *coupling*, via the support on which both of the clocks sat, both clocks could influence each other's oscillation.

This effect is called *phase locking*, and whether it takes place or not depends on the *coupling strength*, which determines the strength of the interaction between the two oscillators, and on the *frequency detuning* (also called *mismatch*), which quantifies the difference between the natural frequencies of the two oscillators. If this mismatch is not too big, the two frequencies become equal, or *entrained*, and are thus synchronised. In the following four subsections, we will have a closer look at some phenomena of synchronisation (For more details, see also Pikovsky *et al.*, 2001b).

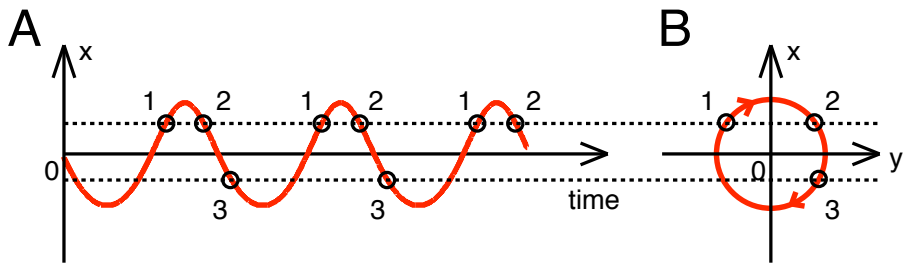

Figure 1.1: A periodic oscillation and its phase portrait. **(A)** A periodic oscillation, with x being the angle of the pendulum with respect to the vertical, changing over time. **(B)** Phase portrait of the oscillation. The angle x of the pendulum with respect to the vertical and its angular velocity y, define the phase space. A point with the coordinates x and y is called a phase point. A periodic oscillation that repeats itself after the period T corresponds to a closed curve (limit cycle) in the phase space.

1.1.1 Self-Sustained Oscillators

Let us look at self-sustained oscillators in more detail. In general, self-sustained oscillators (also called auto-oscillatory systems) derive their oscillation from an internal energy source, and therefore still oscillate when isolated from their environment. Such a system is called *dissipative*. The opposite, a *conservative* system, does not have an internal energy source – the movement of a planet around a sun is an example for a conservative system undergoing self-sustained oscillation. The stability of the oscillation with respect to perturbations is another quality that sets self-sustained, dissipative oscillators apart from conservative oscillators. A conservative oscillator neither dissipates nor replenishes energy, it remains disturbed after perturbation. To describe a self-sustained oscillator, a *phase portrait* of the oscillation can be helpful. Two variables, e.g., the angle x of the pendulum with respect to the vertical and its angular velocity y, define the *phase space*. A point with the coordinates x and y is called a *phase point*. Since the oscillation is periodic, repeating itself after the period T, $x(t)$ and $y(t)$ correspond to a closed curve in the phase space, a curve which is called the *limit cycle* (Figure 1.1).

If an oscillation takes on the form of a sine wave, the limit cycle in the phase portrait is a circle. Oscillators whose phase portraits are close to circular are often termed quasi-linear. For example, adding a weak cubic nonlinearity to the equations of motion for a simple harmonic oscillator yields the quasilinear oscillation of the van der Pol oscillator. The van der Pol oscillator, named after the Dutch physicist Balthasar van der Pol, is a type of dissipative, stable oscillator with nonlinear damping. Van der Pol found limit cycles in electrical circuits employing vacuum tubes. When these circuits are driven near the limit cycle they become entrained, i.e., the driving signal pulls the current along with it. The van der Pol equation has a long history of being used in both the physical and biological sciences. For example, in biology, the equation was extended to a model for action potentials of neurons (FitzHugh, 1955), and in seismology, the equation has been found to be equivalent to models used to understand earthquake faults with viscous friction (Cartwright *et al.*, 1999).

Pushing the phase point off the stable limit cycle corresponds to a perturbation of the oscillation. After a while, the point will return to the limit cycle due to the dissipative nature of the oscillator, and the original rhythm is restored. This is an essential feature of dissipative self-sustained oscillators. Since the limit cycle attracts phase point trajec-

tories, it is also called an attractor of the dynamical system. The maintenance of stable limit cycle oscillations requires nonlinearity.

1.1.2 Weakly Driven Quasilinear Oscillators

What happens if a self-sustained oscillator is perturbed by an external force from another oscillator? If, for example, the pendulum of a pendulum clock is made out of magnetic material and an AC electromagnet is put next to it, perturbing the self-sustained oscillation of the pendulum by a periodic magnetic field?

For the phase point on the limit cycle of an oscillation, a perturbation changes phase and amplitude. But the perturbation of the amplitude decays as the phase point moves back to the limit cycle, whereas the perturbation of the phase neither grows or decays, but remains at the new value until the system is disturbed again.

Consider a self-sustained linear harmonic oscillator,

$$x(t) = A \cdot \sin(\omega_0 t + \phi_0), \tag{1.4}$$

where A is the amplitude, ω_0 is the frequency and ϕ_0 is the phase of the oscillator. Suppose the external force F_{ext} that perturbs the oscillator is defined as

$$F_{ext} = \epsilon \cdot \cos(\omega t + \phi_{ext}), \tag{1.5}$$

where ϵ is the amplitude, ω is the frequency and ϕ_{ext} is the phase of the external force F_{ext} which drives the oscillator. In general, the natural frequency ω_0 of the oscillator is different from the frequency ω of the external driving force F_{ext}. The difference between these two frequencies $\omega_0 - \omega$ is called *detuning*. Under certain circumstances, the driven oscillator's frequency Ω (the *observed frequency*) may become equal to the frequency ω of the external driving force F_{ext}, and a stable relation between the phases is established: The motion of the oscillator is synchronised with the external driving force F_{ext}.

1.1.3 Arnold Tongues

For any fixed amplitude ϵ of the external driving force F_{ext}, the frequency Ω of the driven oscillator depends on the detuning $\omega_0 - \omega$. If the detuning is within a certain range, i.e., not too high and not too low, then the external driving force F_{ext} entrains the oscillator, so that the frequency Ω of the driven oscillator becomes equal to ω. However, if the detuning is outside of this range, then Ω is no longer equal to ω (Figure 1.2A).

When multiple curves of $\Omega - \omega$ vs. ω are plotted for different values of the amplitude ϵ of the external driving force F_{ext}, these curves determine a region in the ϵ vs. ω plane, where the frequency Ω of the oscillator is equal to the frequency ω of the external driving force F_{ext}. Such a region is called *synchronisation region* or *Arnold tongue* (Figure 1.2B), after the Russian mathematician Vladimir Arnold.

1.1.4 Synchronisations of Higher Order

Up to now we have looked at phase-coupled oscillators. But the synchronisation of an oscillator with an external driving force F_{ext} can also occur through a sequence of pulses.

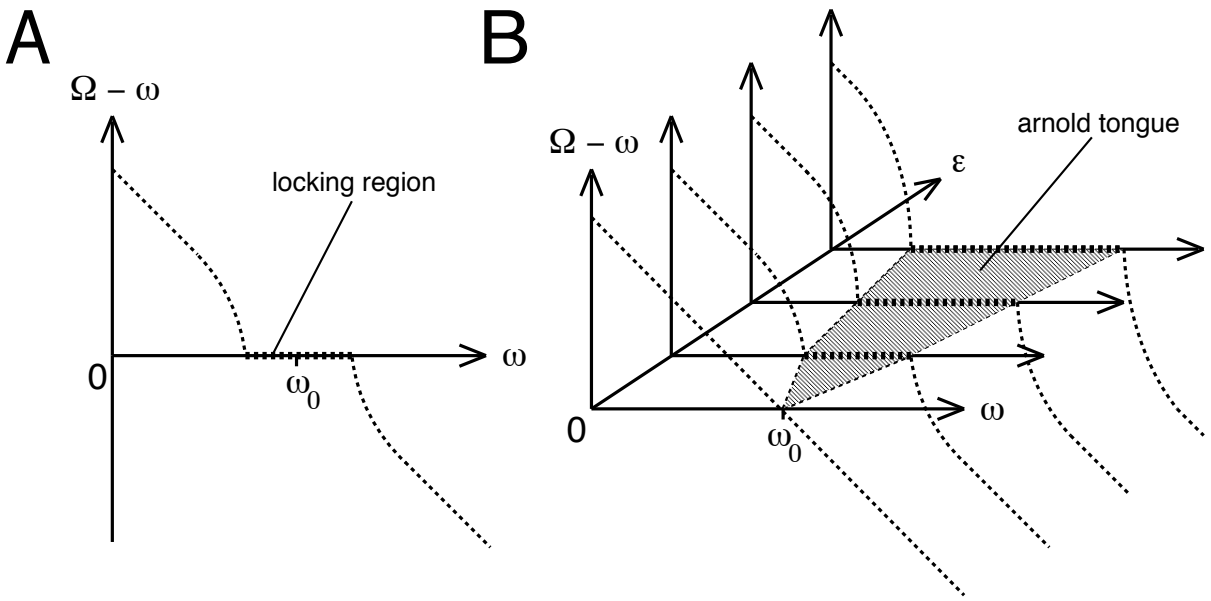

Figure 1.2: **(A)** Difference between the frequency Ω of the driven oscillator and the frequency ω of the external driving force F_{ext} as a function of ω for a fixed value of the external driving amplitude ϵ. In the vicinity of the natural frequency ω_0 of the oscillator, $\Omega - \omega$ is exactly 0, this is denoted frequency locking. **(B)** The family of $\Omega - \omega$ vs. ω plots for different values of the external driving amplitude ϵ determines the domain where the frequency Ω of the driven oscillator is equal to that of the driving frequency ω. This domain is known as the synchronisation region or Arnold tongue, which grows larger for higher values of ϵ.

An example is a radio controlled clock, which periodically receives a signal from a very precise, central, atomic clock, in order to maintain a very high precision. The atomic clock is not constantly coupled to the radio controlled clock, but sends its signal only at certain intervals.

Treating the entrainment as a series of pulses can give insight into more complicated forms of synchronisation. For example, if every second pulse is skipped, but the pulses have an amplitude that is strong enough to compensate for the lack of every other pulse, then an oscillator with a natural frequency ω_0 can be entrained by an external driving force having a frequency equal or close to $\omega/2$. Such a regime is called synchronisation of the order $2:1$. In general, synchronous regimes of arbitrary order $n{:}m$ (n oscillatory cycles for m pulses, with n and m being integers) can be observed, resulting in Arnold tongues at the respective locations (Figure 1.3).

1.2 Examples of Synchronisation

Two pendulum clocks synchronizing the motion of their pendula are an example of mechanical synchronisation. Synchronisation has also been observed in biological systems, from the macroscopic level, such as in social systems, down to a microscopic level, such as in neural systems.

Let us consider a clapping concert audience as a social system. It consists of individuals that express their appreciation of a performance by clapping their hands, in the beginning with different frequencies. Over time however, the individuals in the audience

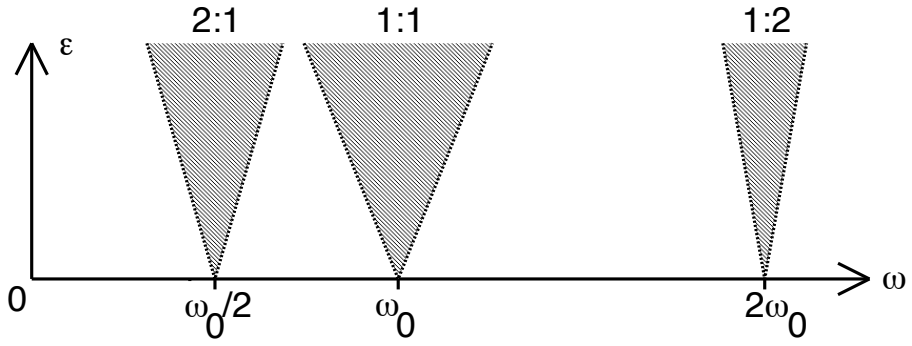

Figure 1.3: Schematic representation of three Arnold tongues for the 2 : 1, the 1 : 1 and the 1 : 2 synchronisation. For example, 2 : 1 means that the relation $0.5\omega = \Omega$ is fulfilled, i.e., that the frequency ω of the external driving force F_{ext} is twice as high as the frequency Ω of the driven oscillator.

will synchronize their frequencies to one global frequency (Neda *et al.*, 2000). In invertebrates, male fireflies of the genus *Pteroptyx malaccae* emit rhythmic light pulses to attract females and they are able to synchronize their flashes with their neighbours (Buck and Buck, 1968).

On a microscopic level, populations of neurons in the mammalian brain transmit signals using different rhythms, in response to a variety of internal and external stimuli. As the individual neurons synchronise their signals, the rhythms develop: Slow rhythms, such as the *delta* rhythm between 1 – 4 Hz, have been associated with some sleep states in humans, while faster rhythms between 20 – 60 Hz, such as *beta* and *gamma* rhythms, often characterise brain-active states of waking or REM (rapid eye movement) sleep (Steriade, 2006). The existence of these rhythms demonstrates that neuronal synchronisation is a part of normal brain functioning. But neuronal synchrony can also be pathological: In so-called *grand-mal* epileptic seizures, abnormal synchronisation tends to spread over the whole neocortex, involving also subcortical structures, and leads to comatose states (Uhlhaas and Singer, 2006).

Nervous systems might even exploit the transition from synchronisation to desynchronisation and vice versa as a code for a signal. In the weakly electric fish *Apteronotus leptorhynchus*, electric organ discharge (EOD) is used for echolocation as well as communication. In communication, *chirps*, transient increases of the frequency of the EOD, play an important role. These chirps either synchronize or desynchronize the activity of the electroreceptor cells of the receiving fish. The change from synchrony to asynchrony or vice versa might be a relevant signal for the next level of neural processing in contrast to synchrony alone (Benda *et al.*, 2006).

1.3 Resonance

The following phenomenon is well known to owners of old cars: When the car's engine operates at a certain number of revolutions per minute, the mechanical vibration of the engine can cause the car's door to vibrate with the same frequency, whereas at other frequencies, the door is unaffected by the vibration of the motor. The property of a system to oscillate with a maximal amplitude when excited at a certain frequency is called *resonance*. The frequency at which the amplitude is maximal is known as the

system's *resonance frequency*.

When subjected to a complex excitation such as wideband noise, the system is filtering out all frequencies except a more or less broad frequency band around the system's resonance frequency, depending on how narrow the system is tuned. Depending on the complexity of the dynamical system, there may be more than one resonance frequency. Typically, the *harmonics* (an integer multiple of a given frequency) of the strongest resonance frequency will also drive the system to oscillate strongly.

For a linearly oscillating system with a resonance frequency Ω, which is driven with a driving frequency ω, the intensity I of the oscillation is given by

$$I(\omega) \propto \frac{\frac{\Gamma}{2}}{(\omega - \Omega)^2 + (\frac{\Gamma}{2})^2}. \tag{1.6}$$

The intensity of an oscillation is defined as the square of its amplitude. Γ is a parameter dependent on the damping of the oscillator, and is known as the linewidth of the resonance. Heavily damped oscillators tend to have broad linewidths, and respond to a wider range of driving frequencies around the resonance frequency.

1.4 Examples of Resonance

Similar to synchronisation, resonance is often put to use in human artifacts, for example, in technical devices, but it can also have catastrophic consequences, for example when the frequency of the oscillation of the earth's crust during an earthquake corresponds to the resonance frequency of a building.

In AM (amplitude modulated) radio, a station is sending its signal on a specific frequency and encodes it with amplitude modulation. The user determines the target frequency (the frequency of the radio station) on the radio receiver and resonance enables the receiver to filter out unwanted frequencies and amplify the frequency of the desired radio station from a mixture of several radio stations transmitting at different frequencies. Since there is only a limited frequency band available for radio transmission, the technical challenge is to construct radio receivers with a very low Γ, which are able to tune in to precisely defined frequencies.

An example for catastrophic resonance is the collapse of the Nimitz Freeway, near San Francisco, USA, due to a magnitude 7.1 earthquake on October 17 1989. It turned out that only a specific 1.4 km section of the freeway collapsed, while the other sections survived the earthquake with only minor damage. Upon inspection, it turned out that the collapsed section was built on loosely structured mudfill, which transmitted the vibrations of the earthquake at the resonance frequency of the bridge. This resulted in the section oscillating at high amplitudes which eventually led to its collapse. The other sections, built on rock deposits which transmitted vibrations at a different frequency, survived the earthquake with only minor damage (Hough *et al.*, 1990).

Resonance can also be found in biological systems. In the mammalian ear, the basilar membrane in the cochlea is deflected in response to sound waves that reach it via the bones of the middle ear. The deflection of the basilar membrane is a traveling wave, diminishing rapidly in both amplitude and velocity as it moves from the basal end toward the apical end of the basilar membrane. Each location on the basilar membrane resonates

for a specific, narrowly tuned range of frequencies, based on the local physical properties. High frequencies lead to resonance at the basal end of the basilar membrane, where it is narrow and stiff, and low frequencies lead to resonance at the apical end, where it is wide and more compliant.

The male Australian field cricket *Teleogrillus oceanicus* uses resonance to regulate the frequency of its mating song. The mating song is produced by the two fore wings, when a plectrum on the posterior side of the left wing engages with file teeth on the underside of a vein of the right wing. Capture, then release, of successive file teeth by the plectrum provides the frequency which excites resonance in a small section on the fore wings, producing a nearly pure tone sound at around 4.5 kHz (Bennet-Clark, 2003).

In the next Chapter, *Neural Resonance*, we will look more closely and more specifically at resonance phenomena that occur in neurons.

1.5 Synchronisation versus Resonance

In the previous four sections, we have learned about synchronisation and resonance. But how are they different? Let us re-examine synchronisation: Synchronisation is a process that takes place between two or more oscillators. In the example of the pendulum clocks, all the clocks involved already have a rhythm of their own, which they synchronise. In the example of one-way synchronisation, such as, for example, the circadian rhythm, the influence is unidirectional, however both systems still oscillate on their own.

In resonance, on the other hand, an external oscillator imposes its frequency on an object that would not oscillate on its own. Consider the above mentioned example of the car door: The car door does not oscillate with a rhythm of its own, only the car's engine does. Thus, only when the car's engine reaches the door's resonance frequency, the door will vibrate. However, identifying resonance is not always straightforward. The famous collapse of the Tacoma Narrows bridge on November 7 1940 in Washington, USA is often cited as *the* example for resonance in many physics textbooks. But according to Billah and Scanlan (1991), the collapse was not due to resonance, because the wind forces which acted on the bridge did not have a periodicity[1], but instead the collapse was related to an aerodynamically induced condition of self-excitation in a torsional degree of freedom.

1.6 Chapter Summary

In this chapter we examined synchronisation and resonance. Synchronisation describes the process of two or more oscillators synchronising their individual frequencies to a common one, due to a weak interaction between them. Oscillators in such systems are usually considered to be self-sustained, their limit cycle corresponding to a closed curve in the phase space (Figure 1.1). This means that they will continue to oscillate as long as there is enough energy present to drive the oscillation. The oscillation is stable against small perturbations and will return to its original shape after it has been perturbed.

[1]The frequency of vortex shedding was long considered to be identical with the resonance frequency of the Tacoma Narrows bridge, thus leading to its collapse. However, this frequency was determined to be close to 1 Hz, and thus not in synch with the observed frequency of the final destructive oscillation, which was 0.2 Hz.

This synchronisation effect is called phase locking, and whether it takes place or not depends on the strength of the interaction (the coupling strength) between the oscillators, and on the difference between the individual frequencies of the oscillators (the frequency detuning). If these two parameters are within a certain range, the frequencies of the oscillators become equal, or entrained, and are thus synchronised or phase-locked. Examining synchronisation has brought us to the phenomenon of Arnold tongues: The range of frequencies for which an external driving force (exerted by another oscillator) entrains the driven oscillator increases for higher values of the amplitude of the external driving force, and a region called Arnold tongue results (Figure 1.2).

When the synchronisation of an oscillator with an external driving force occurs through a sequence of pulses, more complicated forms of synchronisation may emerge. For example, if every second pulse is skipped, but the amplitude of the pulses is strong enough to compensate for the lack of the missing pulse, then an external driving force having a frequency equal or close to *half* the oscillator's natural frequency may be able to entrain it, leading to a locking regime called synchronisation of the order $2:1$. Synchronous regimes of arbitrary order $n{:}m$ (n oscillatory cycles for m pulses, with n and m being integers) can be observed, resulting in Arnold tongues at the respective locations (Figure 1.3).

Learning about synchronisation helped us to differentiate this phenomenon from resonance, the property of a system to oscillate with a maximal amplitude when excited at a certain frequency – the system's resonance frequency. Unlike synchronisation, resonance does not require that the system oscillates on its own. But similar to synchronisation, there may be more than one resonance frequency, and typically, the harmonics of the strongest resonance frequency will also drive the system to oscillate strongly. When applying complex input signals such as wideband noise, the system may filter out all frequencies except a frequency band around it's resonance frequency.

Chapter 2

Reliability Through Resonance

Resonance is the property of a system to oscillate maximally when excited at a certain frequency. This frequency is known as the system's *resonance frequency*. As we will see in this chapter, neurons are also able to resonate, responding best to inputs that are modulated at the resonance frequency. Neurons communicate through electrical signals, also called *spikes*. Spikes are rapid ($\sim 1\,\text{ms}$), transient and stereotypical changes of the electrical potential across the neuron's membrane. Due to its stereotypical nature, the voltage time course of the spikes of a neuron can be considered uniform across all spikes, and thus a reduced representation of the neuron's output consists of the times at which the neuron produced a spike. Such a representation is also called a *spike train*.

In a controlled experiment, a stimulus that elicits spikes can be repeated many times, the stimulus being identical each time. Even so, the resulting spike trains can show a certain degree of variability. The timing of individual spikes in these spike trains can be examined relative to a point of reference, for example the stimulus that elicited the spikes. But since neurons are 'noisy', the spikes may not always be precisely timed relative to the stimulus, a spike may not always be generated, even though the stimulus is sufficient for the neuron to react, or a spike may appear spontaneously. Thus, the precision of spike timing and the reliability of spike generation are two aspects that make up the fidelity of a neuron's response to a stimulus.

In this chapter, we examine how a property such as resonance can improve the precision of spike timing and the reliability of spike generation of a neuron, and we investigate three reliability measures that are used to analyse the spike timing of the neurons investigated in this thesis.

2.1 Resonance in Neural Systems

In Section 1.3, resonance was defined as the property of a system to oscillate maximally if excited at a certain frequency. However, since spikes are considered to be stereotypical events, then what is it exactly that resonates in a neural system? Let us therefore define resonance more generally: As a maximum of a dynamical parameter as a function of frequency. In the example of the car's door reacting to the engine's frequency of revolutions, the dynamical parameter is the *amplitude* of the oscillation of the door, as a reaction of a system that is being driven at different frequencies by the motor's vibrations. For the resonance frequency, the amplitude of the oscillation is maximal, and the further

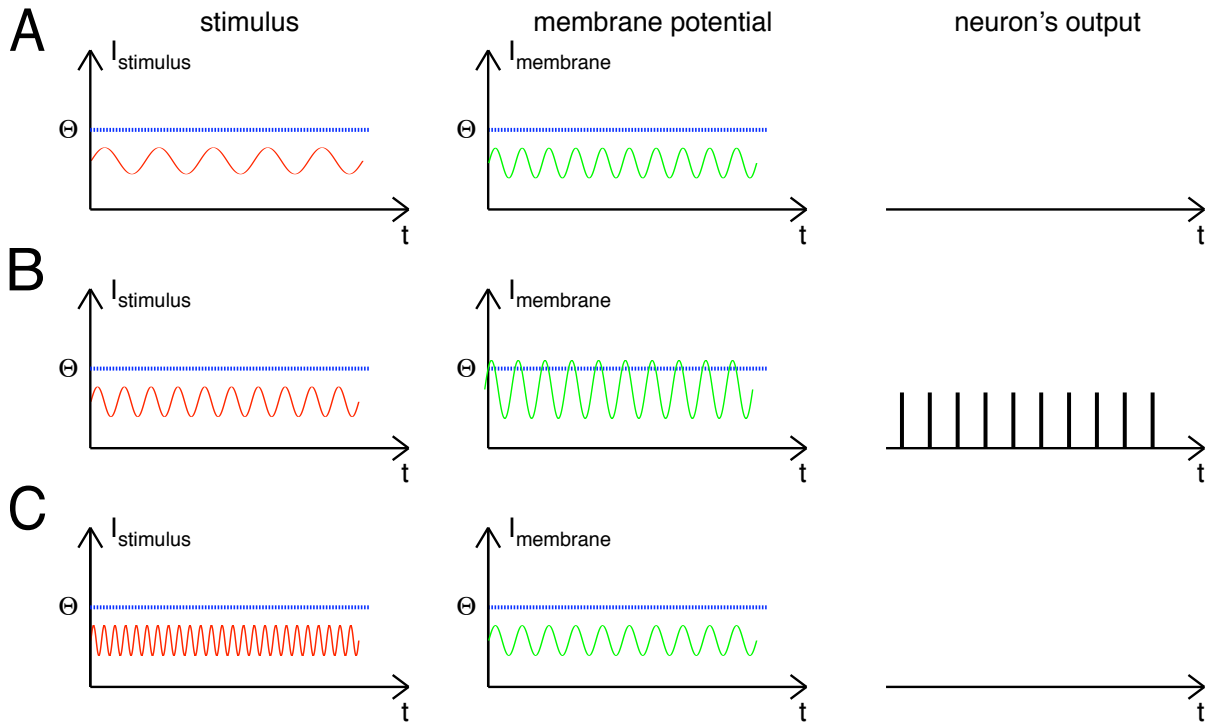

Figure 2.1: Subthreshold resonance occurs in neurons, when a small input signal (red) below the neuron's firing threshold Θ (blue) influences the neurons subthreshold membrane potential (green). **(A)** and **(C)** The input signal's frequency does not influence the membrane potential. **(B)** If the input signal contains a certain frequency, the amplitude of the neuron's membrane potential increases. The increase may lead to the membrane potential crossing the threshold Θ, eliciting spikes.

the motor's vibration frequency moves away from the resonance frequency of the door, the smaller the amplitude of the oscillations will be. In neural systems however, different types of resonance can be found, as we will see in the following three sections.

2.1.1 Subthreshold Resonance

Subthreshold resonance can occur, when a small subthreshold input signal is applied to a neuron, influencing its subthreshold membrane potential. When the input signal contains a certain frequency, the neuron's membrane potential starts to resonate by increasing its amplitude (Figure 2.1). Thus, subthreshold resonance can be seen as the maximum of the dynamical parameter *amplitude* of a neuron's membrane potential as a function of frequency. When the amplitude of the membrane potential crosses threshold at the resonance frequency, thus eliciting a spike, subthreshold resonance can act as a frequency-dependent amplifier for small amplitude signals. Such a mechanism is likely to play an important role in the frequency dependent gating of signals in nervous systems (Schreiber *et al.*, 2004b). Subthreshold resonance has been found in different types of neurons, from cortical neurons (Haas and White, 2002) to neurons at the periphery (Hudspeth, 1985), and has also been suggested to be involved in brain rhythm generation by cortical neurons (Hutcheon and Yarom, 2000).

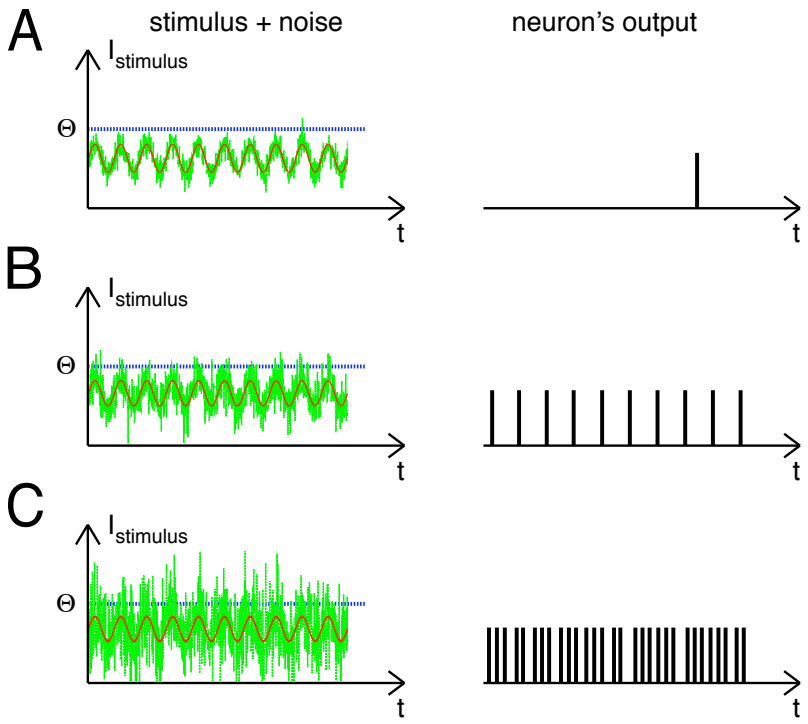

Figure 2.2: Stochastic resonance in neurons enhances the detection of a subthreshold input signal (red) through the introduction of a large wide band stochastic input, the noise (green). The resulting spike train of the neuron is influenced by the combination of the input signal and the noise. **(A)** For low noise intensities, the threshold Θ (blue) is reached in very few cases, mainly at random, and the periodicity of the input signal is not significantly represented in the neuron's spike train. **(B)** An optimal noise intensity allows the periodic input signal to reach threshold, but the noise intensity is not so high as to mask the periodic input signal, leading to a maximal signal-to-noise ratio. **(C)** When the noise intensity is very high, the threshold is reached many times and the resulting spike train of the neuron is dominated by the noise and does not represent the periodicity of the input signal, leading to a low signal-to-noise ratio.

2.1.2 Stochastic Resonance

Stochastic resonance describes a phenomenon whereby the detection of a low-level signal in a non-linear system is enhanced by the introduction of noise. In its simplest form – threshold stochastic resonance – it occurs, when a subthreshold input signal is applied together with a large wide band stochastic input, the noise (Moss *et al.*, 2004). For low noise intensities, very few threshold crossings occur, mainly at random, and the input signal is not significantly represented in the system's output, leading to a low signal-to-noise ratio. When the noise intensity is very high, a large number of threshold crossings occur and the system's output is dominated by the noise and does not represent the input signal either, again leading to a low signal-to-noise ratio. However, between those two extremes, an optimal noise intensity exists that allows the input signal to reach threshold, but the noise intensity is not so large as to mask the signal, thus leading to a maximal signal-to-noise ratio. Stochastic resonance can thus be understood as the maximum of the dynamical parameter *signal-to-noise ratio* as a function of the noise intensity (Figure 2.2).

Stochastic resonance occurs in almost all mechanical and biological threshold systems.

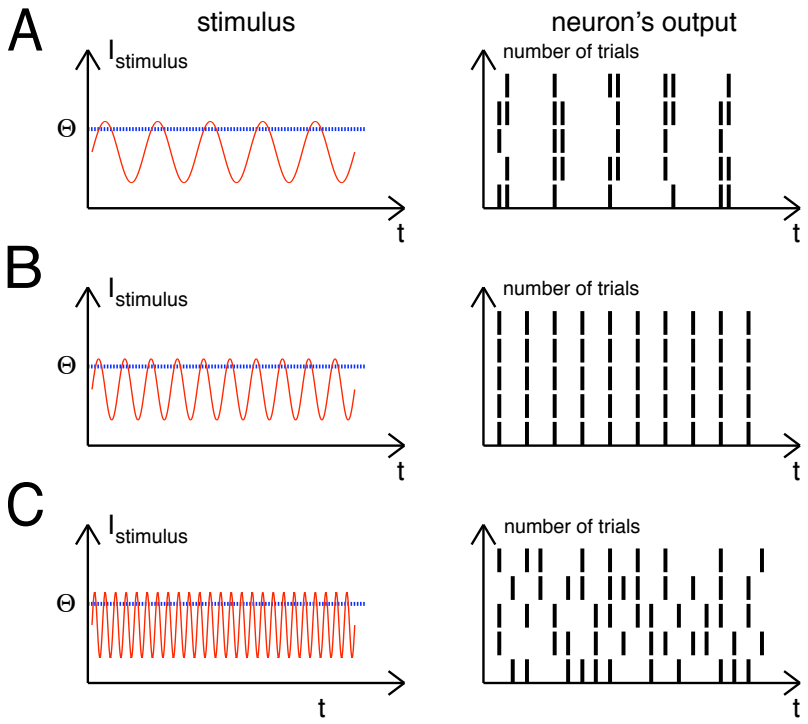

Figure 2.3: Timing resonance occurs when an above-threshold input signal (red) is presented multiple times to a neuron. For the resulting spike trains, the neuron generates more precisely timed spikes at one input signal frequency than at other frequencies. **(A)** The input signal frequency allows the neuron to sometimes fire one or two spikes per input signal cycle in every trial. **(B)** In every trial, the neuron fires only one spike per input signal cycle, thus the neuron's spike train closely resembles the input signal. **(C)** The neuron is unable to fire spikes for every stimulus cycle, because the input signal frequency is too high, thus, in every trial there are many spikes missing.

In sensory systems, the effect of stochastic resonance is an enhancement of input signal detection in noisy systems (Kosko and Mitaim, 2004); in terms of detection of any particular input signal, any other input that is uncorrelated with the input signal can be considered as 'noise'. However, in the central nervous system of mammals, determining what is 'input' and what is 'noise' is a complex task. For example, hippocampal CA1 neurons receive tens of thousands of inputs from other neurons via large dendritic trees which attenuate the input signal significantly. In such a noisy environment, stochastic resonance can enhance the detection of signals from the distal ends of the dendritic tree and may help to explain why these signals are detected as well as signals from proximal synapses (Stacey and Durand, 2000). Neural systems may even be able to adapt the noise level to changing conditions to influence stochastic resonance, thereby using noise as information (Stemmler, 1996).

2.1.3 Timing Resonance

The third type of resonance, which is at the center of attention in this thesis, is neural timing resonance. Neural timing resonance occurs, when, given an above-threshold input signal, a neuron produces more precisely timed spikes at its resonance frequency than at other frequencies (Figure 2.3). Thus, the dynamical parameter is the *spike time reliability*,

which reaches a maximum for a specific frequency.

In nervous systems, such timing resonance effects have been observed in many different neuron types, such as interneurons in the sea snail *Aplysia* (Hunter *et al.*, 1998), spinal cord interneurons of rats (Beierholm *et al.*, 2001) and eccentric cells (an ommatidial bipolar cell type) in the horse shoe crab *Limulus polyphemus* (Knight, 1972). Spike timing responses of these neurons turned out to be most precise when the frequency of the stimulus matched the mean firing rate of the neuron's response. As we have learned in Section 1.3, depending on the complexity of a dynamical system, there may be more than one resonance frequency and typically, the harmonics of the strongest resonance frequency will also drive the system to oscillate strongly. Neurons may thus have more than one timing resonance frequency: When Hunter *et al.* (1998) stimulated *Aplysia* interneurons with a modulated periodic current stimulus, not only were the spikes more precisely timed at the firing rate of the interneuron, but also at the harmonics of the firing rate, compared to input stimuli at other frequencies.

2.1.4 Relevance of Resonance in Neural Systems

We have now seen examples where neural resonance has improved the precision and the reliability of neurons. But why are these two properties relevant? Let us look at how neurons encode information. On one hand, neurons may integrate information over a large number of spikes, without taking into account their exact timing. In such cases, stimulus attributes are encoded in the mean neuronal firing rate. Such a code is called a *rate code* (Shadlen and Newsome, 1994; Rieke *et al.*, 1997). Obviously, a rate code is not dependent on the precise timing of spikes, but its overall precision benefits from pooling the output from more than one neuron.

On the other hand, neurons may act as *coincidence detectors*, firing only if small numbers of spikes from other neurons arrive simultaneously on a millisecond time scale. Under these circumstances, detailed timing information can in principle be used to transmit information efficiently (Rieke *et al.*, 1997; Hudspeth and Logothetis, 2000). Coincidence detection plays an important role for the localisation of sound sources through interaural time differences (Jeffress, 1948; Carr, 1993). In the nucleus laminaris of the auditory system of the barn owl, this computation is performed through a system of axonal delay lines and coincidence detection neurons (Carr and Konishi, 1990). If such a *time code* is used in higher brain structures, spikes from receptor neurons in the periphery must be generated with high precision.

Thus, precision and reliability of individual neurons at the periphery of a nervous system, such as receptor neurons, can be of fundamental importance to higher stages of processing because it allows them to correlate inputs from different neurons more efficiently. Resonance plays a role in tuning neurons to inputs with a specific frequency (Izhikevich, 2001), but the question of *how* neurons tune themselves – or get tuned – to a resonance frequency is still under consideration. Hudspeth (1985) suggested different tuning possibilities for the hair cells of the bull frog *Lithobates catesbeianus*, such as by regulating the number of ion channels involved in spike generation, by adjusting the kinetics of channel gating, by changing the membrane capacitance, or by regulating the intracellular buffering capacity for certain ions or the rate at which they are removed.

Billimoria *et al.* (2006) investigated the effect of two neuromodulatory substances,

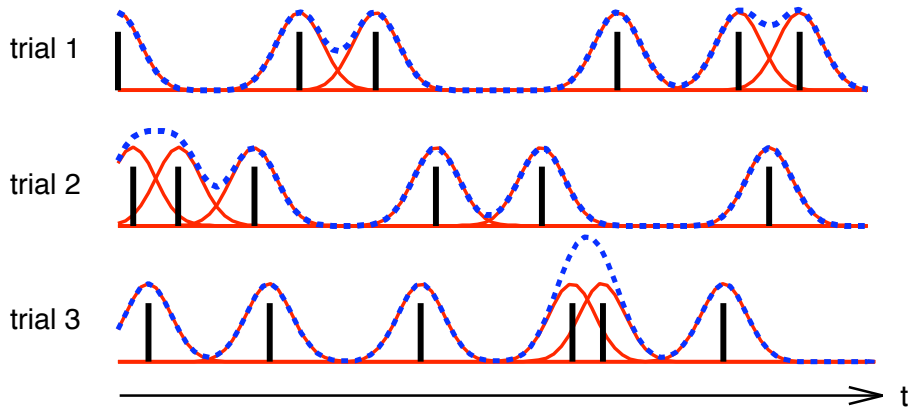

Figure 2.4: Correlation-based reliability measure. Convolution (blue) of three spike trains with a Gaussian kernel (red) with an appropriate value of the standard deviation σ. The value for σ is chosen based on the phenomenological time scale of interest. The convolved spike trains are then pairwise cross-correlated, and the average of the cross-correlations yields the reliability value R, ranging between 0 (low reliability) and 1 (high reliability).

allatostatin (AST) and serotonin, on the precision of the spike response of mechanoreceptors in two species of crabs, *Cancer borealis* and *Cancer maenas*, and found that AST decreased parameters such as jitter, membrane resistance, receptor potential and integration time. AST helps to keep jitter low by increasing sensitivity to faster transients in stimuli, leading to better defined threshold crossings. On the other hand, serotonin increased jitter, membrane resistance, receptor potential and membrane potential noise. Thus, neuromodulation has a functional significance by influencing jitter and other parameters important for circuit dynamics, which in turn are responsible for precision and reliability of a neuron.

2.2 Reliability Measures

In this thesis, we use three different reliability measures to analyse the precision of spike timing. The first measure, *correlation-based reliability*, measures the correlation between spike trains, the second, *vector strength* measures the precision of the phase locking of a neuron to a stimulus, and the third measure, the *spike time jitter* is based on the standard deviation of each spike's timing across all trials. In the following three sections, these reliability measures and their implications are examined more closely.

2.2.1 Correlation-Based Reliability

This reliability measure was proposed by Schreiber *et al.* (2003). It assesses the spike time reliability based on the correlation between the N spike trains s obtained by presenting the same stimulus N times to the same neuron. The reliability is computed by first convolving the spike trains with a *Gaussian* kernel with a standard deviation σ (Figure 2.4). The convolved spike trains $\vec{s}_N$, represented as vectors, are then pairwise cross-

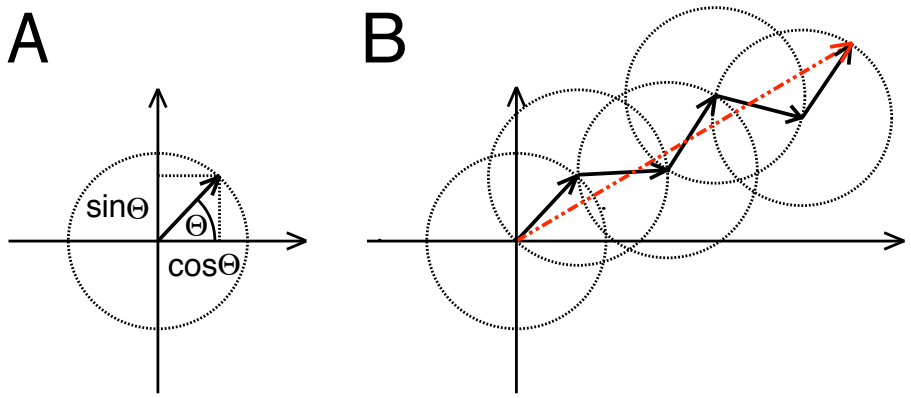

Figure 2.5: Vector strength. This measure assesses the degree of phase locking of a neuron to a periodic stimulus. The periodic stimulus provides the period T, so each spike can be considered as defining a vector of unit length with a phase angle of $\Theta = 2\pi t_i/T$. **(A)** The x and y coordinates of the vector on the unit circle are computed using $x_i = \cos\Theta_i, y_i = \sin\Theta_i$. **(B)** The n vectors that characterize a spike train are distributed on a unit circle. The vector strength is the length of the vector $r = \sqrt{(\sum_{i=1}^{n} x_i)^2 + (\sum_{i=1}^{n} y_i)^2}$ (red) divided by n, the number of spikes in the spike train. If the stimulus has been presented multiple times to the neuron, the average vector strength over all presentations is computed.

correlated, and the average of the cross-correlations is termed the reliability value R,

$$R = \frac{2}{N(N-1)} \sum_{i=1}^{N} \sum_{j=i+1}^{N} \frac{\vec{s}_i \vec{s}_j}{|\vec{s}_i||\vec{s}_j|}. \tag{2.1}$$

R takes on a value between 0 (low reliability) to 1 (high reliability). Note that the only free parameter is the value of the standard deviation σ. An appropriate choice for σ is determined by the phenomenological time scale of interest, in the present work, we used values of 0.6, 1.1 and 1.6 ms.

2.2.2 Vector Strength

The vector strength (Goldberg and Brown, 1969) provides a measure of phase locking or synchronisation to a periodic input stimulus. Such a stimulus provides the period T, so each spike can be considered as defining a vector of unit length with a phase angle,

$$\Theta = 2\pi t_i/T, \tag{2.2}$$

where t_i is the time in which the spike occurs. We then compute the x and y coordinates of the vector on the unit circle,

$$x_i = \cos\Theta_i, \quad y_i = \sin\Theta_i. \tag{2.3}$$

If the spike train contains n spikes, we take the sum of these vectors. The n vectors characterize the spike train, distributed on a unit circle. The vector strength is the length of the normalized mean vector,

$$R = \frac{1}{n}\sqrt{(\sum_{i=1}^{n} x_i)^2 + (\sum_{i=1}^{n} y_i)^2}, \tag{2.4}$$

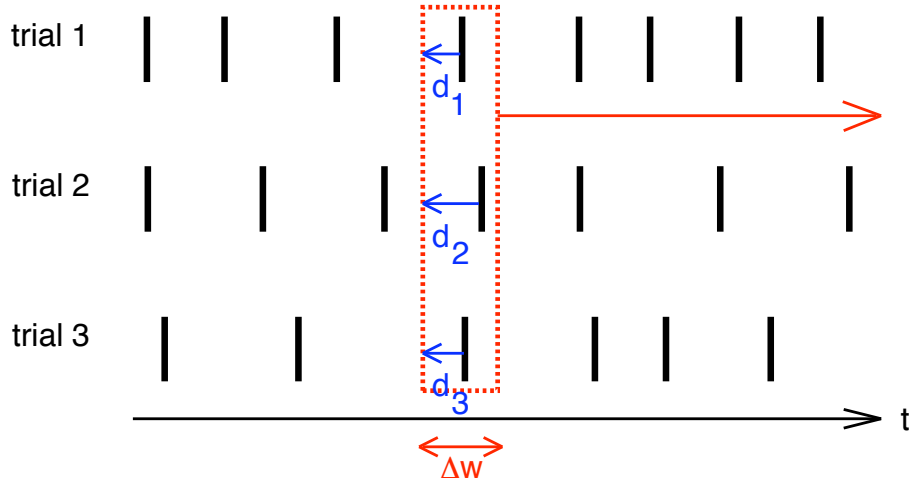

Figure 2.6: The spike time jitter assesses the jitter of the spikes in ms. A sliding window spanning from some time t_0 to $t_0 + \Delta w$ is used. The width Δw is chosen small enough so that there is a high probability of finding at most a single spike per trial inside the window, yet large enough to encompass the typical amounts of jitter found in the system. The amount of jitter associated with the spikes inside the sliding window t_0, $t_0 + \Delta w$ is defined as the standard deviation j of spike occurrence times d_1, d_2 and d_3 in all $n = 3$ trials. To avoid ambiguities, only trials containing one single spike in the window are used, and for a given t_0, at least 50 % of the trials are required to have a single spike in the window in order to participate in the calculation of the mean jitter value $J = 1/n(\sum_{i=1}^{n} j_i)$. This measure has the advantage of having units of time and thus provides an intuitive notion of the temporal dispersion in a raster plot.

and takes on values between 0 (no phase locking) and 1 (perfect phase locking) (Figure 2.5). If a stimulus is presented to the neuron multiple times, the average vector strength is computed over all presentations. The advantage of the vector strength measure lies in the fact that it is not dependent on any additional parameters. However, additional spikes that may appear spontaneously, influence this measure strongly, resulting in a lower value even though there might still be a high degree of phase locking present.

2.2.3 Spike Time Jitter

The third measure, proposed by Rokem *et al.* (2006), measures spike time jitter in ms. First, the standard deviation of each spike's timing is calculated across all trials. To identify aligned spikes automatically, a sliding window spanning some time from t_0 to $t_0 + \Delta w$ is used. The width Δw is chosen small enough so that there is a high probability of finding at most a single spike per trial inside the window, yet large enough to encompass the typical amounts of jitter found in the system (Figure 2.6). The amount of jitter associated with the spikes inside the sliding window t_0, $t_0 + \Delta w$ is defined as the standard deviation j of spike occurrence times in all n trials. To avoid ambiguities, only trials containing one single spike in the window are used, and for a given t_0, at least 50% of the trials are required to have a single spike in the window in order to participate in the calculation of the mean jitter value J,

$$J = \frac{1}{n} \sum_{i=1}^{n} j_i. \tag{2.5}$$

In this study, we used a window size of 5 ms, as the mean interspike interval observed during most of the experiments was 10 ms. Measuring spike time jitter has the advantage of dealing with units of time and thus provides an intuitive notion of the temporal dispersion of spikes.

2.3 Chapter Summary

In this chapter, we examined different types of resonance that can be found neural systems, and we investigated three reliability measures that were used to assess the spike timing of the neurons investigated in this thesis.

Spikes are electrical signals, produced by neurons to transmit information whithin a nervous system. When presenting a stimulus to a neuron multiple times, the resulting spike trains may not be identical – neurons are 'noisy': Spikes may not always be generated, even though the stimulus is sufficient for the neuron to react, or spikes may be generated, but not precisely timed relative to the stimulus.

In neurons, different types of resonance can improve the precision of spike timing and the reliability of spike generation. Subthreshold resonance occurs when a subthreshold input signal containing a certain frequency leads to increased amplitudes of the subthreshold membrane potential of the neuron (Figure 2.1). Stochastic resonance enhances the detection of a sub-threshold input in a system by introducing noise. There is an optimal noise intensity that allows the input signal to reach threshold, but it does not dominate the signal, leading to an output that reflects the signal more than the noise (Figure 2.2). The third type of resonance is neural timing resonance. Neural timing resonance occurs when a neuron produces more precisely timed spikes at its resonance frequency – the mean firing rate, or harmonics of it – than at other frequencies (Figure 2.3).

Neurons may integrate information over a large number of incoming spikes, without taking into account their exact timing. In this case, stimulus attributes are encoded in the mean neuronal firing rate, a coding principle called a rate code. Neurons may also act as coincidence detectors, firing only if small numbers of spikes arrive at the neuron simultaneously on a millisecond time scale. Under these circumstances, detailed timing information can be used to transmit information efficiently using a time code. Therefore, the precision and reliability of a neuron is of fundamental importance to subsequent stages, and receptor neurons at the periphery of a nervous system must be very precise.

Three different reliability measures are presented to assess the precision of spike timing. The correlation-based reliability measure assesses the spike time reliability based on the pairwise cross-correlation between filtered individual spike trains. It takes on values between 0 (low reliability) and 1 (high reliability) (Figure 2.4). The vector strength measures phase locking to a periodic input stimulus with values ranging from 0 (no phase locking) to 1 (perfect phase locking) (Figure 2.5). The third measure quantifies spike time jitter in ms (Figure 2.6).

Chapter 3

The Locust Ear

In insects, hearing is widespread in many orders, and it has evolved independently many times (Hoy and Robert, 1996). Notable examples are crickets and grasshoppers, both belonging to the order *Orthoptera*, for which acoustic communication plays an important role in courtship and mating. These orthopteran species produce mating songs; hearing is needed to identify the position of potential mates and to assess their condition. Since the selection pressure on such an organ is high due to its direct involvement in mate choice, we can assume that the ear and the auditory receptor neurons are constructed to perform with the highest possible efficiency given the physical constraints. In this chapter, we will have a closer look at these aspects.

3.1 Behavioral Relevance of Hearing

In many species of the order *Orthoptera*, acoustic communication plays an important role in courtship behaviour: Potential mates attract each other using acoustic signals, in the case of the grasshopper *Chorthippus biguttulus*, typical communication distances are between 1 – 2.2 m (Lang, 2000). But why choose acoustic communication in the first place? The habitat in which most species of the order *Orthoptera* live, features dense, thick vegetation in meadows and fields, making e.g. visual communication difficult. Visual communication can also be too risky for the sender of such a signal: The sender must display a conspicuous behaviour to be noticed by the receiver, a behaviour which will inevitably also attract predators. For insects, which have a low position on the food chain, this is a high risk.

Generation of acoustic communication signals in orthopteran species can be achieved by a process called *stridulation*. For example, *Chorthippus biguttulus* does this by rubbing a toothed file on the inside of the hind leg against a protruding vein on the ipsilateral wing. The short impact or sound impulse produced by each 'tooth' strike results in the production of a broadband sound with frequency maxima around 6 – 7 kHz and 35 kHz (Klappert and Reinhold, 2003, see also Figure 3.1).

The auditory neural system in animals of the order *Orthoptera* shows a mixture of convergence and homology: The ordering of receptor fibres responding to airborne sound and vibration within the central neuropile has evolved independently in at least two different families, *Tettigoniidae* and *Acrididae*, of the order *Orthoptera* (Römer, 1985). However, many species that are not directly related to each other use the same neurons

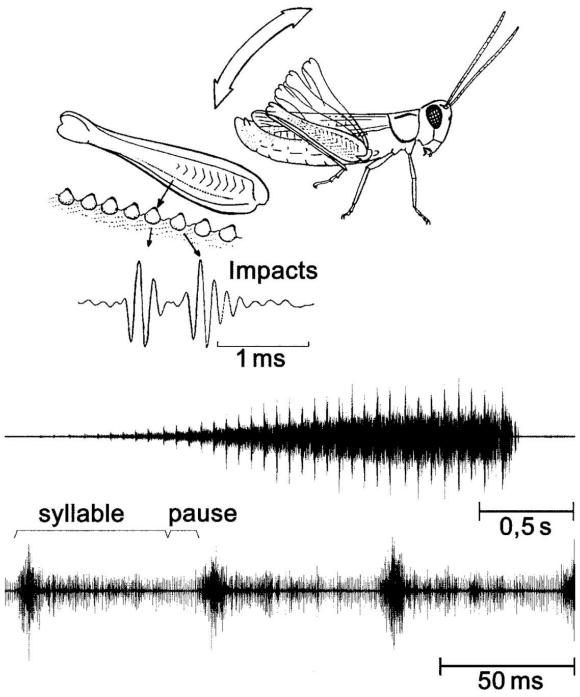

Figure 3.1: The production of the acoustic signals of *Chorthippus biguttulus* via stridulation and the acoustic signal's structure. The acoustic communication signals are produced by rubbing a toothed file on the inside of the hind leg against a protruding vein on the ipsilateral wing. Each 'tooth' strike results in the production of a short sound impulse or impact. This produces a broadband sound with frequency maxima around 6 – 8 kHz and 20 – 30 kHz. The trace below shows an oscillogram of a verse of a male song. The second trace shows a magnified view of a section of the verse, illustrating the syllable-pause structure of the signal. Figure adapted from Balakrishnan *et al.* (2001), used with permission.

for the different processing stages of the auditory pathway (Ronacher and Stumpner, 1988).

The production and recognition of these conspecific signals are important for two reasons. First, they are an important barrier against hybridisation: In the case of the genus *Chorthippus*, the species *Chorthippus biguttulus* and *Chorthippus mollis* can be found in the same habitat, and their physical appearances are almost indistinguishable. However, their respective signals differ and are filtered out by members of the other species (von Helversen and von Helversen, 1975). Second, the structure of these signals also contains information about the condition of the producer of the signal: Males use these signals to attract females, and a given female responds to inform the male of its position, provided that the male produces an 'attractive' song. Such an attractive song signals a good condition, which in turn is correlated with higher fitness. For example, male grasshoppers that have lost one of their hind legs produce different songs than males with both legs. Female grasshoppers are able to distinguish these songs from those produced by males who still have both hind legs, and respond less to the songs from one-legged males (von Helversen, 1972). Thus, the auditory neurons must encode the acoustic signals with sufficient fidelity. Indeed, it has been shown that the spike trains of single auditory receptor neurons of grasshoppers contain sufficient information to discriminate conspecific calling songs (Machens *et al.*, 2003).

For *Locusta migratoria*, whose auditory receptor neurons are examined in this study, acoustic communication plays a minor role. The species is predominantly known for its swarming behaviour which can cause great damage to crops. In a swarm, potential mates are not difficult to locate. However, acoustic communication plays a role in aggressive behaviour (Jacobs, 1953). Given the lower level of sophistication of *Locusta migratoria's* acoustic communication, it is therefore surprising that comparative studies have revealed hardly any difference in number and electrophysiological properties of the thoracic audi-

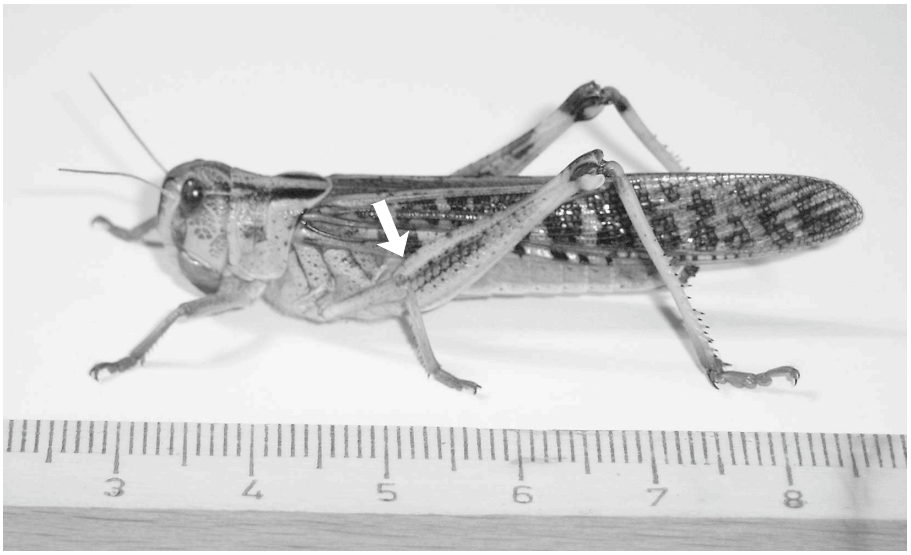

Figure 3.2: The locust *Locusta migratoria*. The arrow indicates the position of the ear. The ears of locusts are situated at the anterior end of the first abdominal tergite of the adult. Each ear has a thin cuticular bean-shaped tympanum with a size of approximately 2.5 mm x 1.5 mm. Figure from Gollisch (2004), used with permission.

tory interneurons between the subfamily *Locustinae* and the subfamily *Gomphocerinae*, to which the above mentioned genus *Chorthippus* belongs (Ronacher and Stumpner, 1988). The consistency between *Locusta migratoria* and *Chorthippus biguttulus* with respect to the auditory system, from the anatomy of the ear to the physiology of the neurons of the auditory pathway, thus allows the use of *Locusta migratoria* to examine problems which are at first glance exclusive to *Chorthippus biguttulus* and its intricate courtship behaviour. However, specimens of *Locusta migratoria* are commercially available and comparatively large, which facilitates preparation, as discussed in the next chapter.

3.2 Anatomy of the Ear

Like almost all ears of insects (with one exception being lacewings, see Miller, 1970), the locust ear is a tympanal organ backed by air filled tracheal cavities (Stumpner and von Helversen, 2001; Yack and Fullard, 1993). The ears of locusts are situated at the anterior end of the first abdominal tergite of the adult (Figure 3.2). Each ear has a thin cuticular bean-shaped tympanum with a size of approximately 2.5 mm x 1.5 mm. On the inside of the tympanum, a structure called *Müller's organ* is attached to it via four attachment parts: The *elevated process*, the *styliform body*, the *folded body* and the *pyriform vesicle* (Figure 3.3).

When the tympanum vibrates due to sound, Müller's organ vibrates with it, showing complex rotary motion and squeezing strains of its four attachment parts containing the auditory receptor neurons. The strains differ in different parts of Müller's organ and change with frequency, and they appear to be the basis of adequate stimulation of the auditory receptor neurons. The axons of the auditory receptor neurons are connected to the metathoracic ganglion via the auditory nerve, but Müller's organ is otherwise mechanically disconnected from the rest of the body (Stephen and Bennet-Clark, 1982;

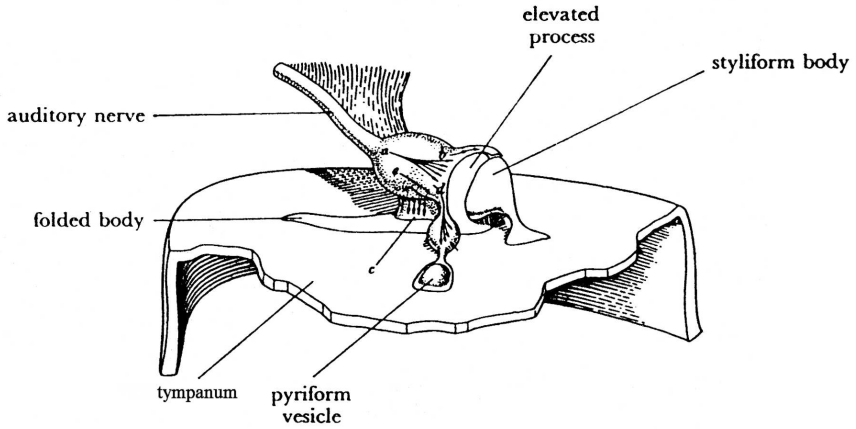

Figure 3.3: Müller's organ, situated on the inside of the tympanum. This organ is attached to the tympanum via four attachment parts: The *elevated process*, the *styliform body*, the *pyriform vesicle* and the *folded body*. These attachment parts contain auditory receptor neurons, whose axons are connected to the metathoracic ganglion via the auditory nerve. Otherwise, Müller's organ is mechanically disconnected from the rest of the body. When the tympanum vibrates, Müller's organ vibrates with it. Its four attachment parts then undergo complex rotary motions which appear to be the basis of adequate stimulation of the auditory receptor neurons. Figure adapted from Gray (1960), used with permission.

Breckow and Sippel, 1985).

The inner face of the tympanum and Müller's organ are covered by the cuticle of one of a series of air sacs situated between the ears. These air sacs, *trachea*, provide the tympanum with the necessary space to perform the movements elicited by sound waves. However, the air pressure in the trachea varies during ventilation, thus introducing a further parameter that influences the movement of the tympanum and the response of the auditory receptor neurons (Meyer and Hedwig, 1995).

3.3 Receptor Neurons

Receptor neurons can be seen as an interface between a nervous system and the environment an animal lives in. They are used to collect information necessary for maximising reproductive success, locating food, and to avoid predators. Both issues are of key importance for an individual to compete against other individuals of the same species and against other species in the same habitat. The receptor neurons, be they visual, auditory or touch-sensitive, are providing information on which an individual is basing its actions. Thus, to understand what kind of information the receptor neurons pass on, and in what manner, helps to understand how further stages, closer to the 'decision-making' instance of an animal, function.

Auditory receptor neurons are essentially mechanoreceptors, meaning that they transduce movement into electrical signals. In mammals, for example, these mechanoreceptors are hair cells, which are located within the organ of Corti on the basilar membrane in the cochlea. Hair cells derive their name from the tufts of stereocilia, a structure known as the hair bundle, which protrudes from the apical surface of the hair cell into the scala media (a fluid-filled tube within the cochlea). Inside the scala media, the hair bundle contacts the tectorial membrane. Sound waves in the environment result in a motion of

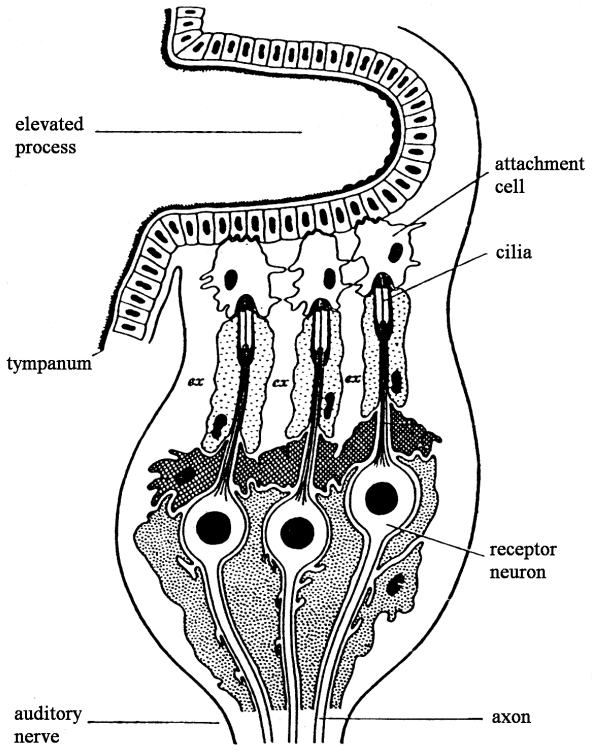

Figure 3.4: Schematic drawing of three auditory receptor neurons of *Locusta migratoria* as part of a chordotonal sensillum. Auditory receptor neurons are essentially mechanoreceptors, meaning that they transduce movement into electrical signals. The cilia of these mechanoreceptors are connected via attachment cells to the tympanum and react to its movements. In the locust, Müller's organ contains around 60 – 80 auditory receptor neurons per ear. Figure adapted from Gray (1960), used with permission.

the tectorial membrane relative to the basilar membrane, and the hair cells react to this movement (Møller, 2000). In insects, ears derived from stretch receptors, *chordotonal organs*, which were modified such that these mechanoreceptors became attached to thin cuticular membranes (serving as tympani), which are backed by air filled tracheal cavities. The cilia of the mechanoreceptors are connected to the tympanum via attachment cells and react to its movements (Stumpner and von Helversen, 2001; Gray, 1960, see also Figure 3.4).

In both mammals and insects, it is not yet clear how physical motion of the structures of a mechanoreceptor is transduced into electrical signals, or, more precisely, how the detailed molecular composition of a mechanically activated ion channel protein in a neuron is constituted. Results from *C. elegans* suggest that microtubule subunits, membrane associated structural proteins and collagen could plausibly convey mechanical force to an ion channel protein, since mutations that result in touch insensitivity involve genes encoding for these proteins (Gu *et al.*, 1996).

In the locust, Müller's organ contains around 60 – 80 auditory receptor neurons per ear (Popov and Svetlogorskaya, 1971; Michelsen, 1971a). These auditory receptor neurons can be subdivided into four groups (*a*, *b*, *c* and *d*), based on their morphology: The elevated process contains ca. 35 *a* neurons, the styliform body contains ca. 12 *b* neurons, the folded body contains ca. 10 *c* neurons and the pyriform vesicle contains ca. 8 *d* neurons. The axons of the auditory receptor neurons project to the metathoracic ganglion via the auditory nerve (Gray, 1960).

The *a*, *b* and *c* auditory receptor neurons are in contact with different structures on the tympanum, so-called *sclerites*, and thus receive mechanical input from different regions of the tympanum. As shown for the closely related species *Schistocerca gregaria*, the *a*, *b* and *c* auditory receptor neurons mainly receive input from the thick membrane (or the

interaction between the thick and the thin membrane) and respond best to frequencies below approximately 10 kHz, with the *b* receptor neurons being the most sensitive. The *d* auditory receptor neurons are less sensitive than the low frequency *a*, *b* and *c* auditory receptor neurons, they receive input from the thin membrane and are tuned to frequencies above 10 kHz (Michelsen, 1971a,b).

3.4 Chapter Summary

Hearing is widespread in many insect orders, and notable examples are crickets and grasshoppers, for which acoustic communication plays an important role in courtship and mating. In some orthopteran species, acoustic communication signals are generated by rubbing a toothed file on the inside of the hind leg against a protruding vein on the ipsilateral wing, a process called stridulation (Figure 3.1). The production and recognition of these conspecific signals are an important barrier against hybridisation and their structure contains information about the fitness of the producer of the signal. For *Locusta migratoria*, whose auditory receptor neurons are examined in this study, acoustic communication plays a minor role. However, comparative studies have revealed hardly any difference in number and electrophysiological properties of its auditory system compared to other species for which acoustic communication is more important. Locusts can thus also be used to study aspects of hearing, which are more difficult to assess experimentally in grasshoppers.

Like almost all ears of insects, the locust ear is a tympanal organ situated at the anterior end of the first abdominal tergite (Figure 3.2). On the inside of the tympanum, Müller's organ is attached via four attachment parts which contain the auditory receptor neurons, around 60 – 80 per ear (Figure 3.3). When the tympanum vibrates, Müller's organ vibrates with it, and the resulting rotary motion and squeezing strains of its four attachment parts stimulate the auditory receptor neurons. The axons of the auditory receptor neurons project to the metathoracic ganglion via the auditory nerve.

For a nervous system, a receptor neuron is an interface to the environment. Any type of receptor neuron is providing the information on which an individual is basing its actions, in order to optimise its reproductive success. Auditory receptor neurons are essentially mechanoreceptors, meaning that they transduce movement, e.g., elicited by soundwaves, into electrical signals. In insects, ears derived from stretch receptors, which were modified such that these mechanoreceptors became attached to thin cuticular membranes, serving as tympani (Figure 3.4).

Chapter 4

Experiments

In-vivo experiments on neural systems require several considerations: How challenging is the preparation of the animal? How difficult is the data acquisition? How reproducible are the experiments? The nervous system of the locust *Locusta migratoria* is, like all nervous systems of invertebrates, decentralised. It is organised in several *ganglia*, accumulations of neurons, rather than in one brain, as it is the case with vertebrates. Thus, the structure of the locust's nervous system allows for an invasive preparation with the goal to expose the auditory nerve, which contains the axons of the auditory receptor neurons and ends in the metathoracic ganglion. Even though the preparation necessitates the removal of all extremities, some internal organs and tissue, and the head, the decentralised nature of the nervous system still allows it to function for several hours.

Data is acquired by physically penetrating the axons of auditory receptor neurons using intracellular 'sharp' electrodes and recording the membrane potential during acoustic stimulation. Acoustic stimulation is well suited for experiments: The main stimulus parameters, frequency and amplitude, can be controlled easily via a computer. The hardware necessary to emit the stimuli as well as to contain them in a controllable environment to avoid reflections is also manageable, both from a technical point of view as well as regarding the spatial requirements. In this chapter, we examine the hardware and the software involved in the experiments, the experimental protocols that were used to obtain the data, as well as the stimuli used for the experiments.

4.1 Hardware and Software

The hardware used for the experimental setup consisted of an experimental chamber which had its insides, as well as its door, covered with sound-absorbing foam. Inside this chamber, an air-suspended platform (Newport Corporation, Irvine CA, USA) carried an animal holder, as well as two micromanipulators and the headstage of the intracellular amplifier. The air-suspended platform isolates the animal holder and the two micromanipulators from mechanical vibrations in the environment.

One micromanipulator, a standard model from Leica (Leica Microsystems, Bensheim, Germany) held the electrode by means of an electrode holder (PPH-1P-BNC90, 90° angle with Ag wire, npi electronic, Tamm, Germany). The other micromanipulator (MM33, Märzhäuser, Wetzlar, Germany), held a modified pair of tweezers that were used to stabilize the auditory nerve. The tweezers were modified such that they ended in rings,

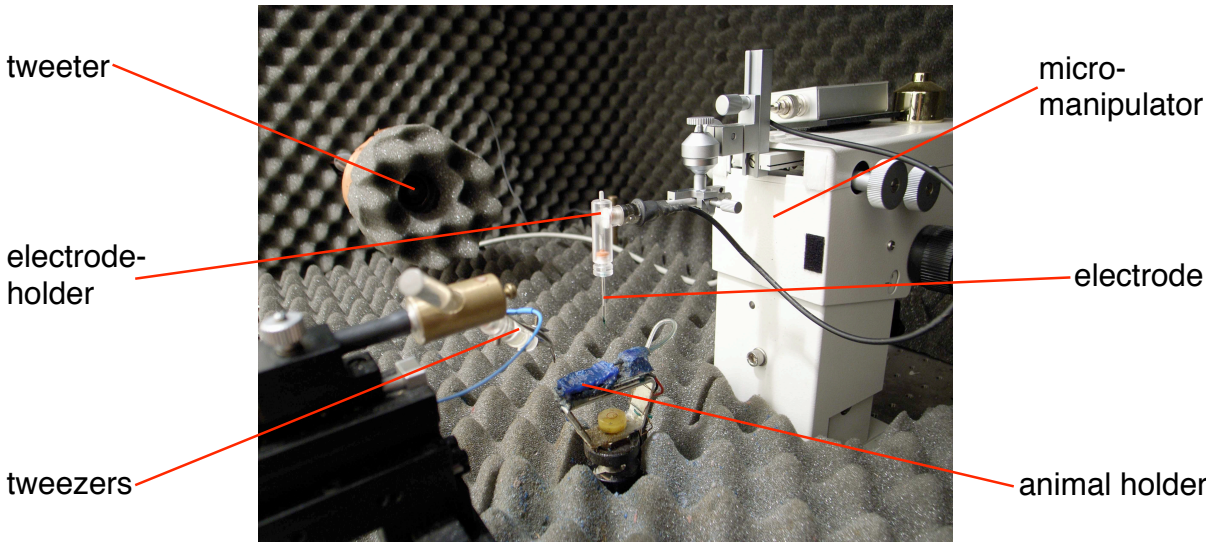

Figure 4.1: The experimental setup used to perform the intracellular recordings on *Locusta migratoria*. The picture shows the micromanipulator holding the electrode holder with the electrode, on top of the animal holder in front of one of the two tweeters. To the right are the tweezers used to to stabilise the auditory nerve. For the purpose of the picture, the sound absorbing foam which is used extensively in the chamber is removed on the front of the micromanipulator.

rather than tips, in order to gently clamp the auditory nerve and thus exert counter pressure to the electrode (Figure 4.1). The headstage of the intracellular amplifier was also placed on the air suspended platform in order to keep the length of cable from the electrode to the headstage as short as possible, as the changes in membrane potential recorded from the receptor neurons are very weak and thus susceptible to interference from the environment.

Electrodes used for the experiments were 1.5 mm outer diameter/0.84 mm inner diameter borosilicate glass (World Precision Instruments, Sarasota FL, USA). The electrodes were pulled with a P-87 electrode puller (Sutter Instrument Company, Novato CA, USA). The electrodes were filled with either 3 M or 1 M KCL solution. To prevent the preparation from drying out, *Ringer* solution was used. The solution was applied with a pipette directly into the thorax. See Appendix for further details on the electrodes and the Ringer solution.

The experiments took place at room temperature (approximately 22° Celsius). Usually, these types of preparations are directly heated via the animal holder with a *Peltier* element to keep the temperature constant. However, this causes increased evaporation of the Ringer solution. Normally, this is not a problem, as this can be compensated by adding fresh Ringer solution after a recording – adding Ringer solution during a recording usually causes the electrode to lose contact with the neuron. In our experiments however, the stimuli presented to the locust varied a high number of parameter values (more on this in Section 4.3), meaning that long intracellular recordings of 50 minutes and longer were necessary.

For stimulus generation, a data acquisition board (PCI-MIO-16E-1, National Instruments, Austin TX, USA) with a sampling rate of 100 kHz was used. The stimulus was sent via an interface (model 2090, National Instruments, Austin TX, USA) to an attenuator (produced in-house) which attenuated the stimulus in the digital domain in order

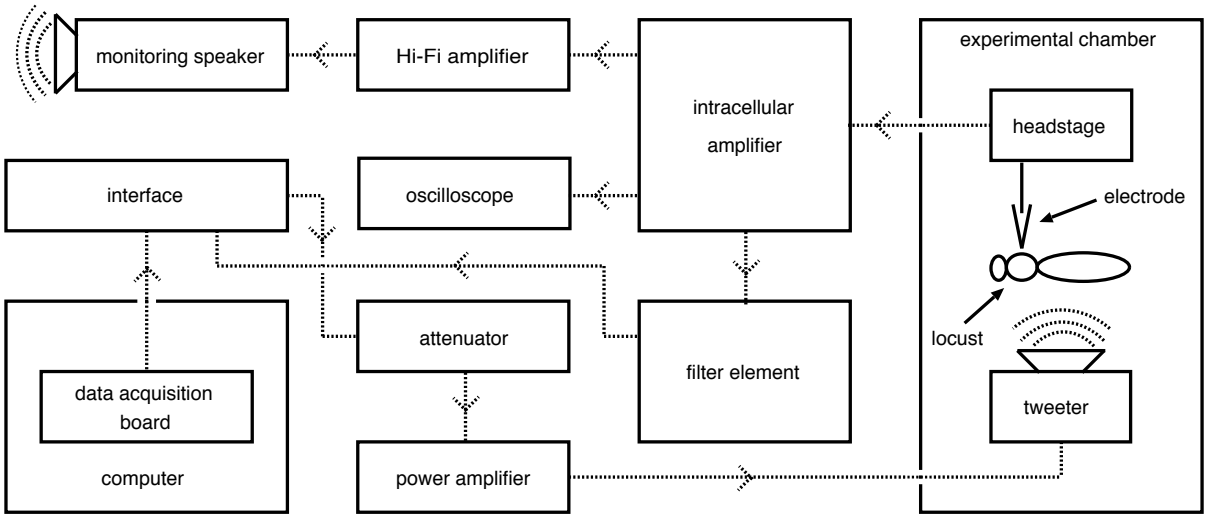

Figure 4.2: Schematic diagram of the experimental setup. *Stimulus generation*: Using the *OEL* programming environment on the computer, the stimulus was produced by the data acquisition board and sent via the interface to an attenuator, which attenuated the stimulus in the digital domain in order to avoid loss of fidelity. The attenuator sent the stimulus to a power amplifier, which was used to drive the speakers (two tweeters) in the experimental chamber. *Data acquisition*: In the experimental chamber, the membrane voltage was recorded from an auditory receptor neuron of a locust by an electrode connected via a headstage to an intracellular amplifier. The amplified membrane potential was monitored visually on an oscilloscope and acoustically on a monitoring loudspeaker driven by a Hi-Fi amplifier. A filter element, receiving the membrane potential signal from the intracellular amplifier, band-pass filtered it and sent it via an interface, which digitized the membrane potential signal, to the data acquisition board in the computer.

to avoid loss of fidelity. The attenuator sent the stimulus to a power amplifier (DCA450, Denon Electronic, Tokyo, Japan) which was used to drive the speakers in the experimental chamber. The speakers were two tweeters (Esotec D-260, Dynaudio, Skanderborg, Denmark), facing each other, with the prepared animal in between, positioned at a distance of 60 cm from each tweeter. The stimulus was emitted by the tweeter ipsilateral to the ear from which an intracellular recording took place.

In order to record membrane potential changes, electrodes were connected via a headstage to an intracellular amplifier (BRAMP 01, npi electronic, Tamm, Germany) which amplified the signal from the electrode. The intracellular amplifier was connected to a filter element (DPA 2F, npi electronic, Tamm, Germany), both components were housed in an EPMS 07 housing (also made by npi electronic) which provided power and earthing. The filter element was used to filter out electrical noise present in the setup. The settings were 30 Hz for the high-pass filter and 10 kHz for the low-pass filter. The filter element was connected via the 2090 interface to the PCI-MIO-16E-1 data acquisition board in the computer. We used a sampling rate of 20 kHz for data acquisition. A schematic of the setup is shown in Figure 4.2.

The software used for stimulus generation and data acquisition was *OEL*, the *Online Electrophysiology Lab* programming environment, written in C++ by Jan Benda and Christian Machens (Figure 4.3). OEL runs on the Linux operating system and provides the user with various possibilities regarding the management of stimulus presentation,

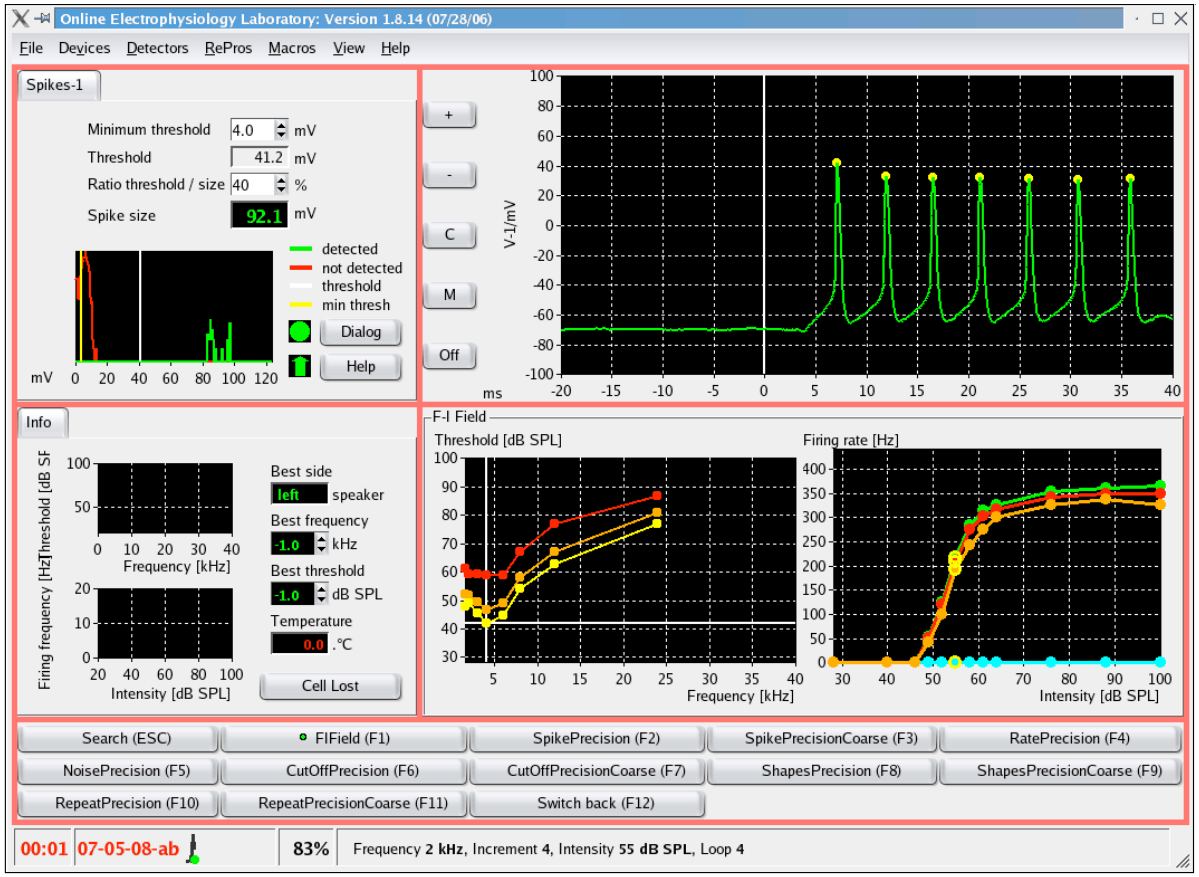

Figure 4.3: Screenshot of the *Online Electrophysiology Lab* software used for stimulus generation and data acquisition. The top right section shows the membrane potential. Individual spikes are identified by OEL; and the respective spike times are written to a file. The bottom right section shows the sensitivity of the receptor neuron in an intensity vs. frequency plot (left) and its response curve in a firing rate vs. intensity plot (right).

including online data analysis. OEL analyzes the incoming membrane potential signal and identifies individual spikes by employing an algorithm presented by Todd and Andrews (1999), and writes the spike times to a file. Further data analysis and processing was done using MATLAB (The MathWorks, Natick MA, USA).

An oscilloscope (TDS 224, Tektronix Inc., Beaverton OR, USA) was used to monitor the spike size. A Hi-Fi amplifier (A-109, Pioneer Electronics Inc., Long Beach CA, USA) connected to the intracellular amplifier, and driving a small monitoring speaker (Maxi300, Quadral, Hannover, Germany) was used to receive acoustic feedback while searching for an axon inside the auditory nerve.

4.2 Experimental Protocol

Adult locusts of both sexes were used in the experiments. Care was taken to avoid old animals, since their auditory nerve membrane is tougher to penetrate. Also, animals that just molted were avoided, since their chitin is too soft, making the preparation difficult. The preparation began by removing the head, the legs, and the wings. Then, about

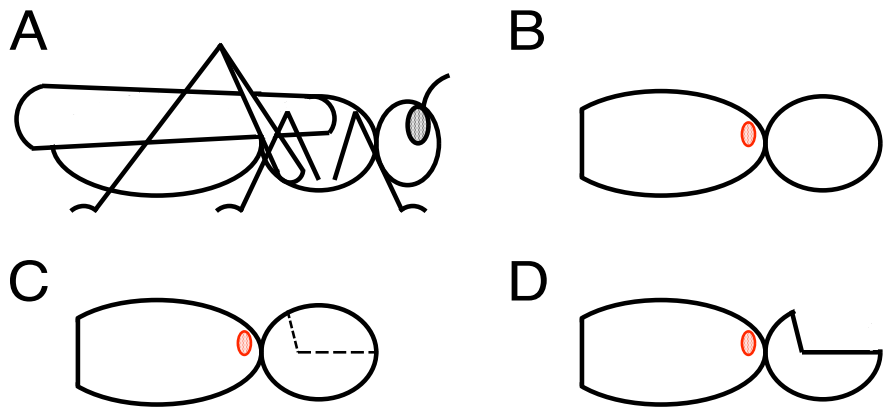

Figure 4.4: Schematic diagram of the locust preparation. The position of the tympanum is indicated in red. **(A)** The intact locust. **(B)** First, the head, the legs, and the wings are abscised. Then, about 3 mm of the abdomen are removed to gain access to the gut, in order to completely extract it. **(C)** After that, a large part of the upper half of the thorax is excised by first making two cuts on both sides of the thorax, in caudal direction to about 3/4 of the length of the thoracal segment (dashed line). Subsequently, the locust is fixated on the animal holder using wax. Then, two cuts, originating dorsally from the end of the thoracal segment downwards to the end of the two cuts left and right of the thoracal segment, are made (dotted line). **(D)** By pulling on the upper half of the thorax with a pair of tweezers, while at the same time cutting the locust's flight muscles, it is then removed completely. Further tissue needs to be removed inside the animal in order to gain access to the auditory nerve.

3 mm of the abdomen were removed, in order to remove the gut. After that, the upper half of the thorax was removed by first making two cuts on both sides of the thorax, in *caudal* direction to about 3/4 of the length of the thoracal segment. Subsequently, the locust was fixated on the animal holder using wax. Next, two cuts were made, originating dorsally from the end of the thoracal segment downwards to the end of the two cuts left and right of the thoracal segment. By pulling on the upper half of the thorax with a pair of tweezers, while at the same time cutting the locusts flight muscles, the upper half of the thorax was removed completely. Finally, further removal of flight muscles, as well as fat and tissue, was necessary in order to get access to the auditory nerve (Figure 4.4). The auditory nerve was stabilised with a modified pair of tweezers, discussed in Section 4.1, in order to exert counter pressure to the electrode. By gently clamping the auditory nerve between the two rings and moving the tweezers slightly upwards, a slight tension was applied.

The electrode was put into position over the auditory nerve in an orientation orthogonal to the suspended platform. Using the micromanipulator, the electrode was moved downwards, while at the same time the micromanipulator was gently tapped. The tapping elicited vibrations, which were transmitted from the micromanipulator to the tip of the electrode, where they facilitated the physical penetration of, firstly, the membrane of the auditory nerve and, secondly, the membrane of an axon of a receptor neuron in the nerve. When the penetration of the latter was successful, an intracellular recording could take place. During the search for an axon, the oscilloscope was used to monitor the changes in membrane potential. The Hi-Fi amplifier, connected to the intracellular amplifier, and driving the monitoring speaker, was used to give acoustic feedback on the progress that the electrode made inside the auditory nerve. During the actual data acquisition phase of an experiment, output from the monitoring speaker was switched off.

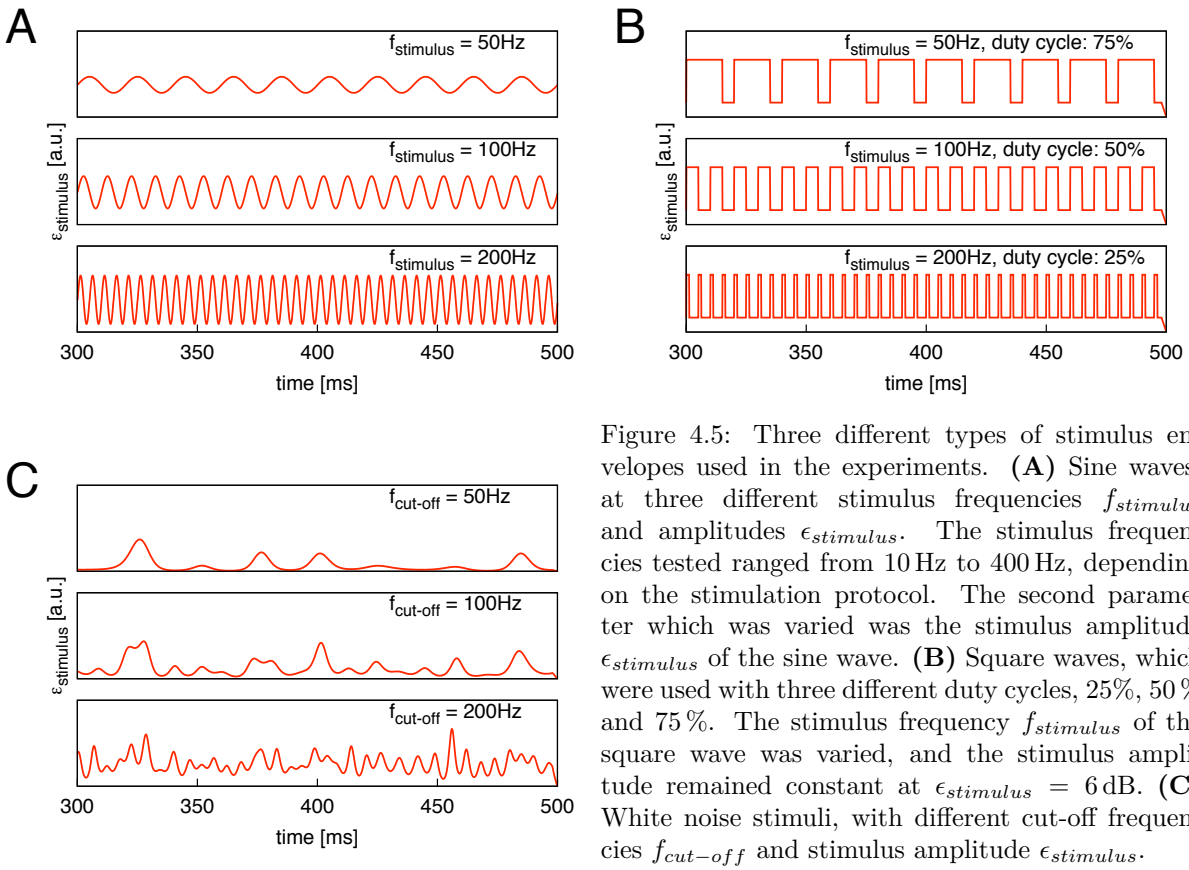

Figure 4.5: Three different types of stimulus envelopes used in the experiments. **(A)** Sine waves, at three different stimulus frequencies $f_{stimulus}$ and amplitudes $\epsilon_{stimulus}$. The stimulus frequencies tested ranged from 10 Hz to 400 Hz, depending on the stimulation protocol. The second parameter which was varied was the stimulus amplitude $\epsilon_{stimulus}$ of the sine wave. **(B)** Square waves, which were used with three different duty cycles, 25%, 50 % and 75 %. The stimulus frequency $f_{stimulus}$ of the square wave was varied, and the stimulus amplitude remained constant at $\epsilon_{stimulus} = 6$ dB. **(C)** White noise stimuli, with different cut-off frequencies $f_{cut-off}$ and stimulus amplitude $\epsilon_{stimulus}$.

4.3 Stimuli Used for the Experiments

When the electrode had entered an axon of a receptor neuron, the neuron's *best frequency* – the sound frequency where the neuron is most sensitive – was determined. This frequency was then used as the carrier frequency for all subsequent stimuli. After determination of the carrier frequency, the intensity needed to elicit a certain firing rate, specified by the experimental protocol, was adjusted. This firing rate is called the *target firing rate*. Ideally, the resulting average firing rate should be as close as possible to the target firing rate however in most cases it was only met approximately by the receptor neuron. The carrier frequency was then modulated with different envelopes, and these envelopes served as the stimuli for the receptor neuron.

Three different types of amplitude modulated stimuli were used: Sine wave stimuli, square wave stimuli and white noise stimuli. For the sine wave stimuli, the stimulus frequency $f_{stimulus}$ and the stimulus amplitude $\epsilon_{stimulus}$ were varied (Figure 4.5A). For the square wave stimuli, $\epsilon_{stimulus}$ remained at a constant value, while the duty cycle of the square wave and the $f_{stimulus}$ were varied. Three duty cycles were tested: 25 %, 50 % and 75 % (Figure 4.5B). For the white noise stimuli, $\epsilon_{stimulus}$ denotes the standard deviation of the white noise, not the stimulus amplitude. The standard deviation was varied, and the cut-off frequency $f_{cut-off}$ of the stimulus was decreased, thus deceasing the frequency content of the stimulus (Figure 4.5C). A variation of the white noise stimulus which was also used had different relative frequency gaps around different band-stop frequencies f_{gap}

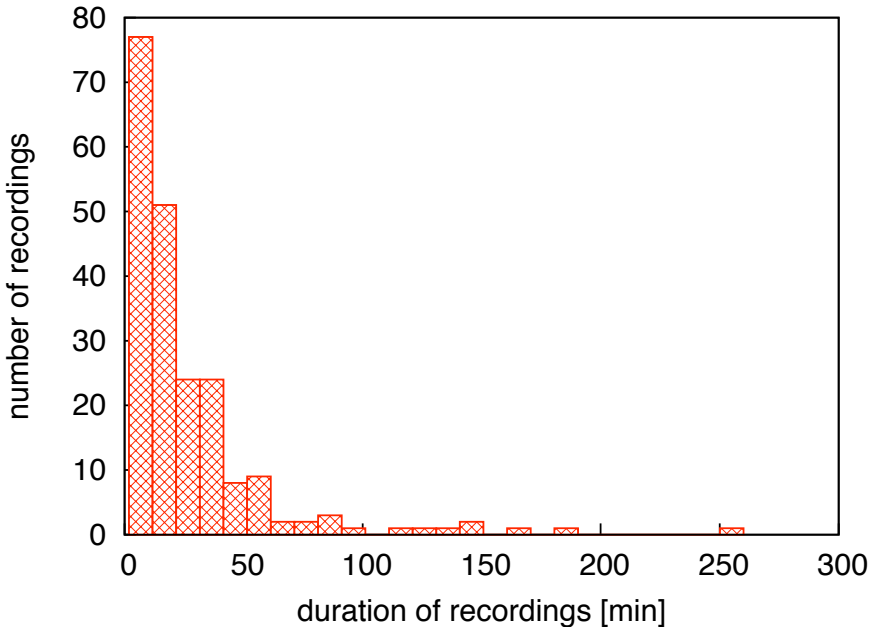

Figure 4.6: A histogram of the durations of all 209 intracellular recordings performed on receptor neurons, using a bin size of 10 minutes. Due to the high number of parameter values varied in every stimulus type, long intracellular recordings were particularly interesting, since they allowed testing of all combinations of parameter values in the same neuron. Depending on the exact stimulus protocol and the stimuli used, intracellular recordings of up to 50 minutes were necessary in order to test, e.g., all combinations of stimulus frequency $f_{stimulus}$ and stimulus amplitude $\epsilon_{stimulus}$ on a neuron.

at a constant standard deviation of the white noise (not shown). The white noise stimuli were based on the same noise sample in all experiments ('frozen noise'). The length of all stimuli was 500 ms. The first 300 ms were discarded in the analysis, in order to avoid adaptation effects in the receptor neurons. Every stimulus was repeated 10 times, and there was a pause of 1000 ms between every stimulus presentation. The spike responses that these three different stimuli types elicited in the receptor neurons will be discussed in more detail in the following two chapters.

The focus on the high number of parameter values that were varied in every stimulus type meant that long intracellular recordings were particularly interesting, since they allowed testing of all combinations of parameter values in the same receptor neuron. Depending on the exact stimulus protocol and the stimuli used, intracellular recordings of up to 50 minutes were necessary in order to test, e.g., all combinations of $f_{stimulus}$ and $\epsilon_{stimulus}$ on a receptor neuron. However, recordings of such length are difficult to achieve, and the majority of recordings performed were less than 10 minutes (Figure 4.6). During the course of this thesis, a total of 209 recordings were made, and in the following three chapters, 27 will be analysed more closely, as they have a minimal duration in order to test a suitable amount of stimulus parameter values.

4.4 Chapter Summary

In this chapter, the hardware and software involved in the experiments, the experimental protocols that were used to obtain the data, as well as the stimuli used for the experiments

were presented. The experiments took place in an experimental chamber, containing an air-suspended platform which carried an animal holder, two micromanipulators and the headstage of the intracellular amplifier. One micromanipulator held the electrode, while the other held a modified pair of tweezers that were used to stabilize the auditory nerve (Figure 4.1). For the stimulus generation, two computer-controlled tweeters were used (Figure 4.2). The software used for stimulus generation and data acquisition was *OEL*, the *Online Electrophysiology Lab* programming environment (Figure 4.3).

Adult locusts of both sexes were used to perform the experiments. First, a preparation was performed in order to expose the auditory nerve (Figure 4.4). Then, an electrode was used to penetrate the membrane of an axon of a receptor neuron in the nerve to record changes in the membrane potential. When the electrode had entered an axon of a receptor neuron, a carrier frequency for all subsequent stimuli was established. This carrier frequency was then modulated with different envelopes, the stimuli for the receptor neuron.

Three different types of stimuli were used: Sine wave stimuli, square wave stimuli and white noise stimuli (Figure 4.5). For the sine wave stimuli, the stimulus frequency and the stimulus amplitude were varied. For the square wave stimuli, the stimulus amplitude was constant, while the frequency and the duty cycle were varied (25 %, 50 % and 75 %). For the white noise stimuli, the standard deviation was varied, and the cut-off frequency of the stimulus was decreased, thus deceasing the frequency content of the stimulus. A variation of the white noise stimulus involved different band-stop frequencies and relative frequency gaps around these band-stop frequencies at a constant standard deviation. In every stimulus type, a high number of parameter values was varied. Thus, long intracellular recordings were particularly interesting, because they allowed testing of many combinations of parameter values in the same receptor neuron – however, recordings of such length are difficult to achieve (Figure 4.6).

Chapter 5

Neuronal Resonance with Sine Wave Stimuli

In this chapter, we examine neural timing resonance of locust auditory receptor neurons using *sine wave stimuli* as described in Section 4.3. Sine wave stimuli were chosen as a starting point in our investigations, because a sine wave is a simple wave form, having by definition only one frequency. Additionally, using sine waves will allows us to compare our model system – the locust auditory receptor neuron – with other systems that have been tested with sine wave stimuli, such as neurons of the prefrontal cortex of rats (Schreiber *et al.*, 2004a), motor neurons of *Aplysia* (Hunter *et al.*, 1998) and interneurons of the spinal cord of rats (Beierholm *et al.*, 2001).

The last section of this chapter will deal with findings gained with *white noise stimuli*, also described in Section 4.3. White noise is a random signal consisting of a superposition of sine waves with a flat power spectrum, meaning that all the frequencies have the same power. Much like white light, which is the combination of all the colors of the visible light spectrum in equal proportions, white noise contains sine waves of all frequencies up to a specific cut-off frequency. White noise stimuli have also been used in the aforementioned study by Hunter *et al.* (1998) in order to investigate resonance phenomena.

5.1 Specific Stimulus Frequencies Elicit Timing Resonance

The goal of the experiments presented in this section is to examine timing resonances present in locust auditory receptor neurons; namely finding stimulus frequencies that elicit more precisely timed spikes than other stimulus frequencies. Furthermore, if such a timing resonance is present, can an increased spike response reliability also be observed at higher or lower harmonics of the resonance frequency? We stimulated receptor neurons with sine wave stimuli, using 26 stimulus frequencies, ranging from 10 Hz to 260 Hz in 10 Hz increments. These stimulus frequencies were presented at different stimulus amplitudes, ranging from 4 dB to 8 dB in 1 dB increments. The overall stimulus intensity was adjusted such that the average firing rate elicited by the neuron was approximately 100 Hz; each stimulus was presented 10 times.

Let us examine the neuron's spike response to six different stimulus frequencies $f_{stimulus}$,

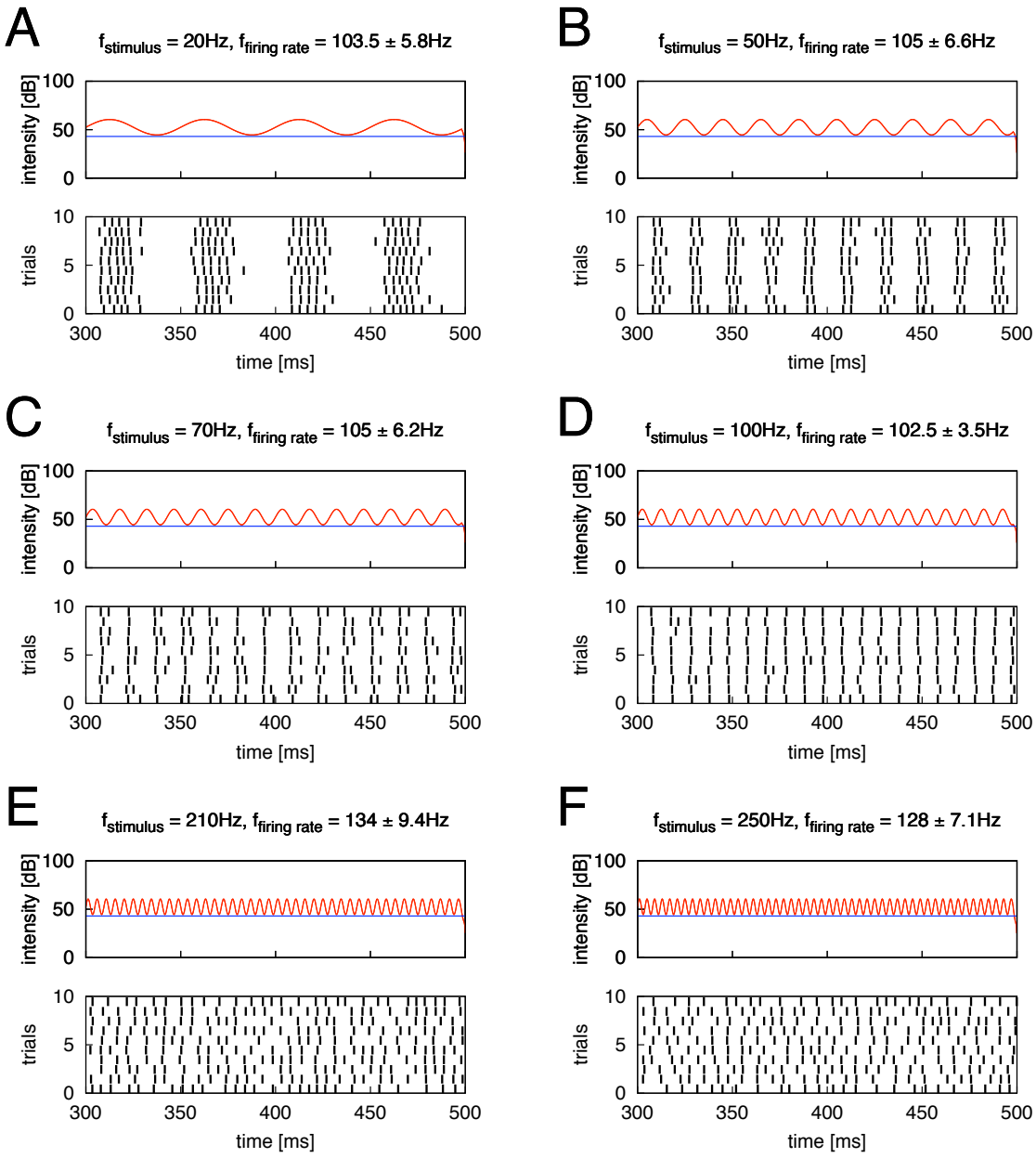

Figure 5.1: Spike responses of a receptor neuron stimulated with a sine wave stimulus (red), using six stimulus frequencies $f_{stimulus}$, at a stimulus amplitude of $\epsilon_{stimulus} = 8\,\mathrm{dB}$. The firing threshold of the neuron (blue) was 43 dB SPL. The neuron's spike responses are depicted as raster plots (upper plots), the stimuli were presented 10 times (lower plots). The overall stimulus intensity was adjusted in order to elicit a target firing rate of 100 Hz. **(A)** At $f_{stimulus} = 20\,\mathrm{Hz}$, the neuron spiked approximately five times per stimulus cycle. The firing rate $f_{firing\ rate}$ was $103.5 \pm 5.8\,\mathrm{Hz}$. **(B)** At $f_{stimulus} = 50\,\mathrm{Hz}$, there is a ratio of approximately 2 : 1 between $f_{firing\ rate} = 105 \pm 6.6\,\mathrm{Hz}$ and $f_{stimulus}$. The stimulus elicited approximately two spikes per stimulus cycle. **(C)** At $f_{stimulus} = 70\,\mathrm{Hz}$, the number of spikes per stimulus cycle became less consistent, there were almost as many cases where the neuron fired two spikes per stimulus cycle, as there were cases where it fired only one spike. $f_{firing\ rate} = 105 \pm 6.2\,\mathrm{Hz}$. **(D)** At $f_{stimulus} = 100\,\mathrm{Hz}$, an almost perfect 1 : 1 locking was established, at $f_{firing\ rate} = 102.5 \pm 3.5\,\mathrm{Hz}$: One spike was generated per stimulus cycle. **(E)** At $f_{stimulus} = 210\,\mathrm{Hz}$, the neuron was no longer able to produce a spike for every stimulus cycle. $f_{firing\ rate} = 134 \pm 9.4\,\mathrm{Hz}$. **(F)** At $f_{stimulus} = 250\,\mathrm{Hz}$, the raster plot shows that spikes were still locked to the stimulus, even though many spikes were missing. The ratio between $f_{stimulus} = 250\,\mathrm{Hz}$ and $f_{firing\ rate} = 128 \pm 7.1\,\mathrm{Hz}$ is approximately 1 : 2. (Data from neuron 05-07-21-ac)

Figure 5.2: Reliability of a receptor neuron's spike response to sine wave stimuli and its firing rate for different stimulus frequencies $f_{stimulus}$ at a stimulus amplitude of $\epsilon_{stimulus} = 8\,\mathrm{dB}$. The average firing rate, calculated over all $f_{stimulus}$, is $119 \pm 14.6\,\mathrm{Hz}$. **(A)** $f_{stimulus}$ vs. firing rate $f_{firing\ rate}$. The dashed lines indicate 2 : 1 (first line), 1 : 1 (second line) and 1 : 2 (third line) ratios between $f_{stimulus}$ and the firing rate of the neuron. The neuron changed its firing rate most prominently from $f_{stimulus} = 90\,\mathrm{Hz}$ to $f_{stimulus} = 150\,\mathrm{Hz}$. It exhibited 1 : 1 locking by increasing $f_{firing\ rate}$ in order to match $f_{stimulus}$, until $f_{stimulus}$ was too high, and the locking was no longer upheld. $f_{firing\ rate}$ remained at an elevated level compared to $f_{firing\ rate}$ before 1 : 1 locking. **(B)** Slope of $f_{firing\ rate}$ relative to the 1 : 1 line in the plot above. The data points are smoothed using a median filter with a sliding window containing five data points. For the locking region between 90 and 150 Hz, the slope is > 0, indicating that the stimulus 'pulls' $f_{firing\ rate}$ up to the 1 : 1 locking. **(C)** Difference between firing rate and stimulus frequency $f_{firing\ rate} - f_{stimulus}$. This difference is close to 0 from $f_{stimulus} = 90\,\mathrm{Hz}$ to $f_{stimulus} = 150\,\mathrm{Hz}$. **(D)** Spikes per stimulus cycle. The range of $f_{stimulus}$, for which the number of spikes elicited per stimulus cycle is whole-numbered, is shown as data points that are parallel to the dashed lines at $spikes/cycle = 2$ (2 : 1 locking), $spikes/cycle = 1$ (1 : 1 locking) and $spikes/cycle = 0.5$ (1 : 2 locking). Between 90 and 150 Hz, the number of spikes per cycle is close to 1. **(E)** Correlation-based reliability with different values for σ: 1.6, 1.1 and 0.6 ms, from top to bottom. The most reliably timed spikes were elicited by $f_{stimulus}$ close to the average firing rate of the neuron. This indicates an increased reliability for 1 : 1 locking of the neuron's spike response to the stimulus. Next to this main peak, there is a smaller peak for $f_{stimulus} = 50\,\mathrm{Hz}$, approximately half of the $f_{stimulus}$ for which 1 : 1 locking begins, indicating a comparatively weaker increased reliability for 2 : 1 locking. **(F)** Vector strength. Phase locking of the neuron's response is best for $f_{stimulus}$ between 90 and 150 Hz. **(G)** Spike time jitter. The lowest spike time jitter was elicited by $f_{stimulus} = 90\,\mathrm{Hz}$. Next to this main trough is a smaller trough between $f_{stimulus} = 40\,\mathrm{Hz}$ and $f_{stimulus} = 50\,\mathrm{Hz}$, indicating a comparatively weaker lower spike time jitter. (Data from neuron 05-07-21-ac)

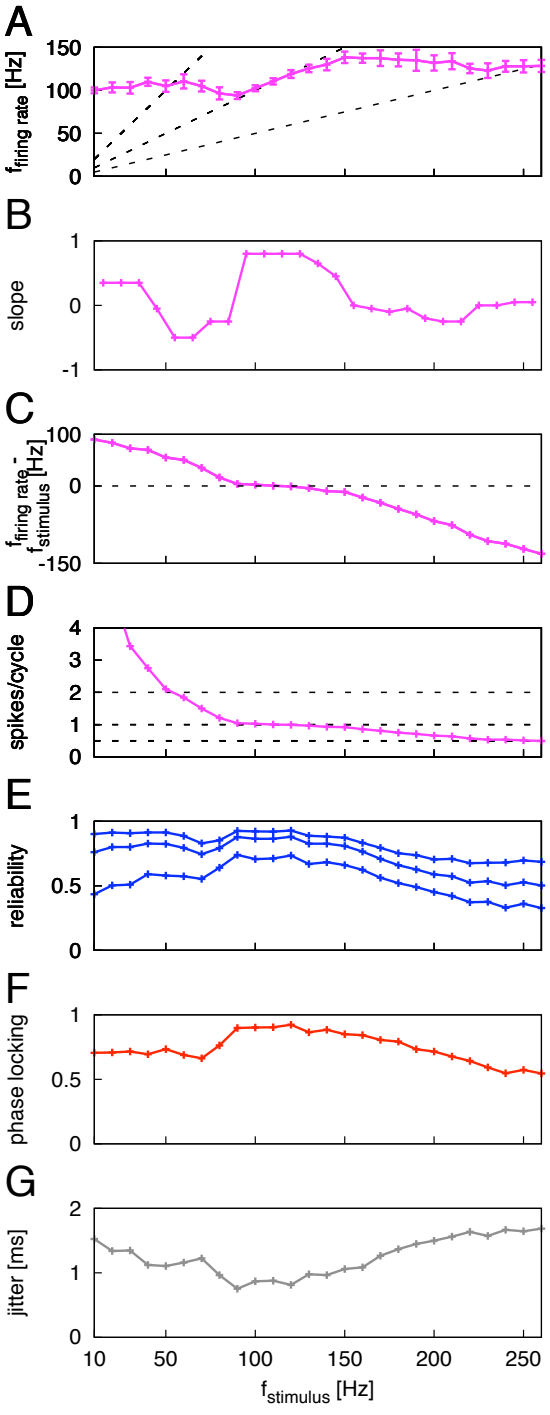

at a stimulus amplitude $\epsilon_{stimulus} = 8\,\text{dB}$: $f_{stimulus} = 20, 50, 70, 100, 210$ and $250\,\text{Hz}$. For $f_{stimulus} = 50\,\text{Hz}$, there was a ratio of approximately $2:1$, as the firing rate $f_{firing\ rate}$ of $105 \pm 6.6\,\text{Hz}$, was approximately twice as high as $f_{stimulus}$. A ratio of approximately $1:1$ was achieved for $f_{stimulus} = 100\,\text{Hz}$ with $f_{firing\ rate} = 102.5 \pm 3.5\,\text{Hz}$; and a ratio of approximately $1:2$ for a firing rate of $128 \pm 7.1\,\text{Hz}$ and $f_{stimulus} = 250\,\text{Hz}$. On the other hand, for $f_{stimulus} = 70$ and $210\,\text{Hz}$, the ratios between $f_{stimulus}$ and $f_{firing\ rate}$ did not follow an $n:m$ ratio, with n and m being integers, as described in Section 1.1.4. As $f_{stimulus}$ was increased, a change in stimulus locking was observed. For $f_{stimulus} = 20\,\text{Hz}$, the neuron spiked five times per stimulus cycle and for $f_{stimulus} = 50\,\text{Hz}$ two times, in both cases with very few exceptions (Figures 5.1A and B). However, as $f_{stimulus}$ was increased further, the number of spikes per stimulus cycle became less consistent, and for $f_{stimulus} = 70\,\text{Hz}$ there were almost as many cases where the neuron fired two spikes per stimulus cycle, as there were cases where it fired only one spike (Figure 5.1C). As $f_{stimulus}$ was increased further, an almost perfect $1:1$ locking for $f_{stimulus} = 100\,\text{Hz}$ was established (Figure 5.1D). For higher values of $f_{stimulus}$, the neuron had difficulties following the stimulus: It was no longer able to produce a spike for every stimulus cycle (Figures 5.1E and F).

However, even though spikes are missing for high stimulus frequencies, the remaining spikes produced by a neuron may retain a high degree of precision. In order to investigate this possibility, we analysed the behaviour of the neuron's spike response for all stimulus frequencies tested with different reliability and locking measures.

The neuron changed its firing rate most prominently from $f_{stimulus} = 90\,\text{Hz}$ to $f_{stimulus} = 150\,\text{Hz}$, matching it with $f_{stimulus}$ and thereby exhibiting $1:1$ locking. At $f_{stimulus} = 150\,\text{Hz}$, the locking was no longer upheld. However, the firing rates remained at an elevated level compared to the firing rates before $1:1$ locking, and did not decrease back to the lower firing rates obtained for $f_{stimulus} < 90\,\text{Hz}$ (Figure 5.2A). Computing the slope of $f_{firing\ rate}$ relative to the $1:1$ line where $f_{stimulus} = f_{firing\ rate}$ reveals that the slope is positive for the locking region between $f_{stimulus} = 90\,\text{Hz}$ to $f_{stimulus} = 150\,\text{Hz}$. This indicates that the stimulus 'pulls' the firing rate up to the $1:1$ locking. The data points are filtered using a median filter with a sliding window containing five data points, in order to counteract the noise generated by taking derivatives. This procedure produces artefacts at the beginning and the end of the data set, as there are not enough data points to fill the window (Figure 5.2B). When we compute the number of spikes per cycle and the difference between firing rate and stimulus frequency, we arrive at the same range of $f_{stimulus} = 90\,\text{Hz}$ to $f_{stimulus} = 150\,\text{Hz}$, with one spike per cycle and the firing rate equal to the stimulus frequency (Figures 5.2C and D).

Finally, the three reliability measures introduced in Section 2.2 are used to examine the reliability for the different stimulus frequencies. We find a good agreement between all three reliability measures: The most reliably timed spikes, the highest phase locking and the lowest spike time jitter were elicited for values of $f_{stimulus}$ for which the neuron locked on well to the stimulus (Figures 5.2E, F and G). This indicates an increased reliability of the spikes elicited during $1:1$ locking of the neuron's spike response to the stimulus. Next to this main peak, the correlation-based reliability reveals a smaller peak at $f_{stimulus} = 50\,\text{Hz}$ – approximately half of the $f_{stimulus}$ for which $1:1$ locking begins – indicating a comparatively weaker increased reliability for $2:1$ locking. For the correlation-based reliability measure, three different values for σ, 0.6, 1.1 and 1.6 ms,

were tested. The value of $\sigma = 1.1\,\text{ms}$ turned out to be a good compromise between a too broadly tuned filter, which would correlate spikes which are not elicited by the same stimulus cycle, and a filter that is too narrow, which would treat spikes of every trial, elicited by a stimulus cycle, as uncorrelated events. For this reason, we will from now on use $\sigma = 1.1\,\text{ms}$ when applying the correlation-based reliability measure. Thus, the stimulus frequency increases the firing rate of the neuron, and the increase is sustained, even when the reliability of the spike response decreases again, as $f_{stimulus}$ increases further.

5.2 Increasing the Stimulus Amplitude Reveals Arnold Tongue Structures

Arnold tongues were introduced in Section 1.1.3 as regions in the ϵ vs. ω plane (amplitude ϵ vs. frequency ω of the external driving force F_{ext}) where the frequency Ω of the driven oscillator is equal to ω of F_{ext}. In the present case, Ω corresponds to the firing rate of the neuron, the amplitude ϵ of the external driving force F_{ext} corresponds to the stimulus amplitude $\epsilon_{stimulus}$, and the frequency ω to the stimulus frequency $f_{stimulus}$.

We start by analysing data from an example neuron. When we evaluate the difference between the neuron's firing rate $f_{firing\ rate}$ and the stimulus frequency $f_{stimulus}$, we see that the range of $f_{stimulus}$ for which the difference between $f_{stimulus}$ and $f_{firing\ rate}$ is 0, or close to 0, is increasing, as $\epsilon_{stimulus}$ increases, revealing an Arnold tongue structure (Figure 5.3A). In the following, we analyse whether this Arnold tongue structure can also be seen with other measures of locking and reliability, and if Arnold tongue structures also occur for sub- and higher harmonics of the neuron's firing rate. As a first measure of stimulus locking we consider the slope of the curve of evoked firing rate $f_{firing\ rate}$ vs. $f_{stimulus}$: If the neuron is not influenced by the stimulus at all, the firing rate would be constant for every $f_{stimulus}$, resulting in a slope of 0. If the stimulus increases the neuron's firing rate, leading to perfect $1:1$ locking, the slope would be 1. We find that the slope is positive for values of $f_{stimulus}$ around the average firing rate (calculated over all $f_{stimulus}$) for each value of $\epsilon_{stimulus}$, indicating that the stimulus indeed 'pulls' the firing rate up to the $1:1$ locking (Figure 5.3B). Note that the data points for all $f_{stimulus}$ at all values of $\epsilon_{stimulus}$ are smoothed by applying the same filter used in Section 5.1.

The correlation-based reliability using $\sigma = 1.1\,\text{ms}$ changes for increasing $\epsilon_{stimulus}$, and we see two areas of increased spike time reliability, one around the average firing rates, and a weaker area around their subharmonics (half of the respective average firing rates). Decreasing $\epsilon_{stimulus}$ also decreases the range of $f_{stimulus}$ eliciting more reliably timed spikes, giving rise to Arnold tongue-like structures (Figure 5.3C). The vector strength on the other hand, shows maximal phase locking of the neuron to the stimulus only around the average firing rates. The area of increased phase locking in Figure 5.3D corresponds well to the Arnold tongue seen for the difference between $f_{firing\ rate}$ and $f_{stimulus}$ in Figure 5.3A. In the analysis of the spike time jitter, we see two areas of decreased jitter, one around the average firing rates, and one at their subharmonics (Figure 5.3E). These areas are similar to the areas of increased reliability found with the correlation-based reliability measure in Figure 5.3C.

But what about higher harmonics, an increase in spike time reliability at stimulus

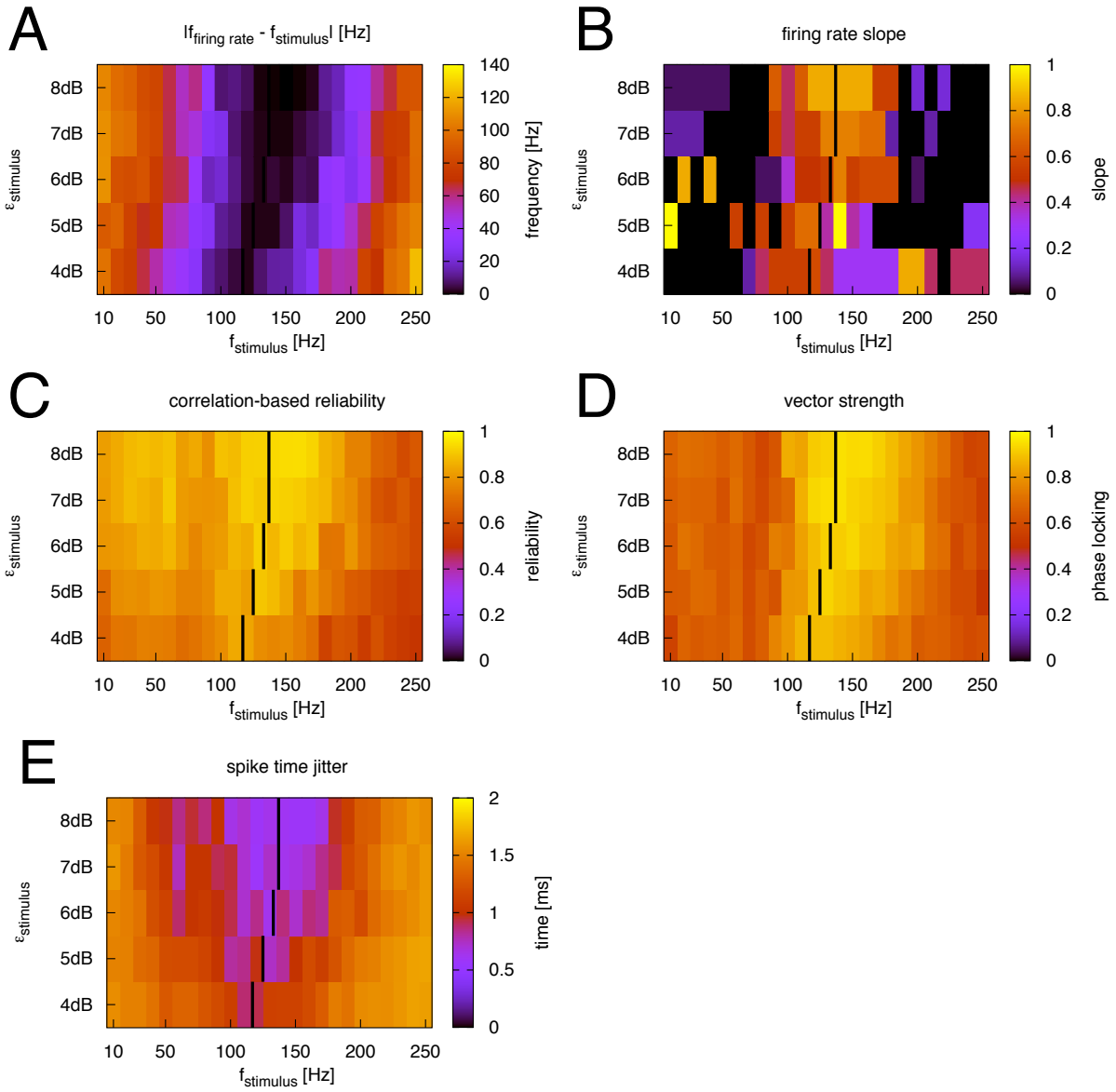

Figure 5.3: Arnold tongue and areas of increased reliability of the spike response for different stimulus frequencies $f_{stimulus}$ and amplitudes $\epsilon_{stimulus}$ of the sine wave stimulus for a receptor neuron. The average firing rates (indicated with a black bar) calculated over all $f_{stimulus}$ for $\epsilon_{stimulus} = 4$, 5, 6, 7 and 8 dB were 122 ± 14.6, 130 ± 16.4, 138 ± 19.6, 142 ± 19.0 and 142 ± 20.6 Hz. **(A)** Arnold tongue, defined as the area where the absolute value of the difference between the firing rate $f_{firing\ rate}$ and $f_{stimulus}$ is 0, or close to 0. This area is increasing, as $\epsilon_{stimulus}$ increases. **(B)** Increasing slopes (> 0) of the $f_{firing\ rate}$ vs. $f_{stimulus}$ plot. The data points are smoothed using a median filter with a sliding window containing five data points. The slope increases most prominently around the average firing rates, indicating a high degree of $1:1$ locking for $f_{stimulus}$ **(C)** Correlation-based reliability, using $\sigma = 1.1$ ms. Two areas of increased spike time reliability can be seen around the average firing rates and their subharmonics, resembling Arnold tongues. **(D)** Vector strength, showing maximal phase locking around the average firing rates. **(E)** Spike time jitter. Two areas with low amounts of jitter are present, around the average firing rates and their subharmonics. (Data from neuron 05-08-01-am)

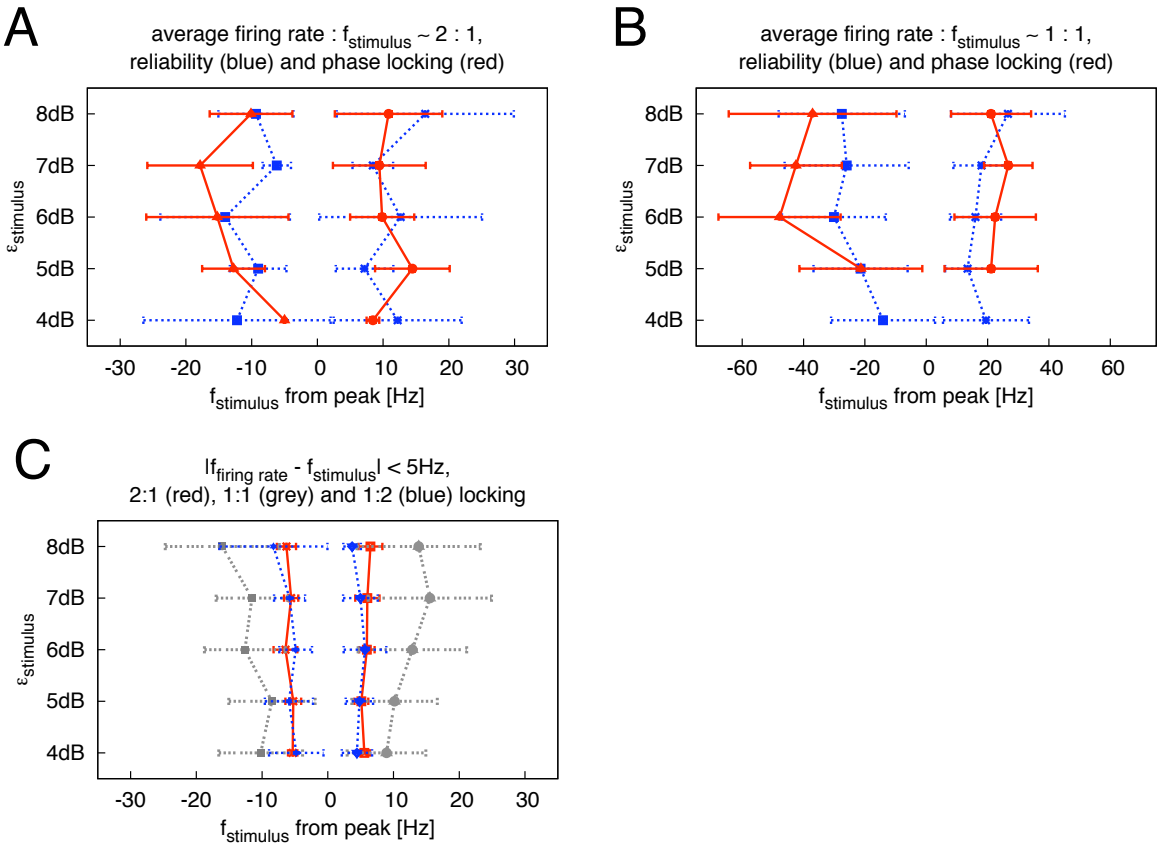

Figure 5.4: Widths of Arnold tongues and areas of increased reliability for different values of $\epsilon_{stimulus}$, averaged over 11 receptor neurons stimulated with sine wave stimuli. The target firing rate was 100 Hz. **(A)** For a ratio of approximately 2 : 1 between the average firing rate and the stimulus frequency, neither the reliability (blue), determined using the correlation-based reliability with $\sigma = 1.1$ ms, nor the phase locking (red), determined by the vector strength, show an increase in Arnold tongue width, as $\epsilon_{stimulus}$ is increased from 4 dB to 8 dB. The sample size ranges from $n = 2$ to $n = 8$, with a median of 5.5. **(B)** For a ratio of approximately 1 : 1 between the average firing rate and the stimulus frequency, the correlation-based reliability (blue) with $\sigma = 1.1$ ms and the phase locking (red) the Arnold tongue width increases, as $\epsilon_{stimulus}$ is increased from 4 dB to 8 dB. The sample size ranges from $n = 5$ to $n = 9$, with a median of 7. **(C)** The width of the Arnold tongues for which $|f_{firing\ rate} - f_{stimulus}| < 5$ Hz increases for a 1 : 1 ratio (grey) between $f_{stimulus}$ and $f_{firing\ rate}$, for higher values of $\epsilon_{stimulus}$, but remains constant for 2 : 1 (red) and 1 : 2 (blue) ratios. The sample size ranges from $n = 6$ to $n = 11$, with a median of 11.

frequencies around twice the average firing rate? Increased reliability at such a higher harmonic would indicate 1 : 2 locking: A regime where a reliably timed spike is generated only at every other stimulus cycle. When we reconsider the rasterplots in Figures 5.1E and F, where high stimulus frequencies were used, we see that indeed the neuron has difficulty locking onto the stimulus, resulting in many missing spikes. It would still be possible, though, for the remaining spikes to be precisely timed. Such a precision, if it existed, would be detected by the correlation-based reliability, as this measure is relatively tolerant to missing spikes (Schreiber *et al.*, 2003). However, for this neuron, the correlation-based reliability measure reveals Arnold tongue-like structures only for areas where $f_{firing\ rate} : f_{stimulus} \approx 1 : 1$, and to a lesser degree for areas where $f_{firing\ rate} : f_{stimulus} \approx 2 : 1$. For the resolution and the range of $f_{stimulus}$ used, an increase in spike timing precision for the second harmonic, indicating 1 : 2 locking, was not observed, regardless of the measure.

Let us now examine the width of the Arnold tongues and the areas of increased reliability for all 11 neurons from which the recordings were long enough to test all the necessary parameters of the stimulus protocol. For the correlation-based reliability and the vector strength, the width has been calculated using a procedure that will be explained in more detail in Section 5.4 below. For the spike time jitter, this procedure has not yielded any meaningful results.

Analysing the results of the averaged areas of increased spike-time reliability and phase locking around the subharmonics of the average firing rates, we see that the increase, though weakly present in approximately nine of the 11 recordings, is not significant when averaged. This is due to the difficulty of estimating the width of peaks in reliability around the subharmonics, since these peaks are very weak (Figure 5.4A). Around the average firing rates, we see an increase of the range of $f_{stimulus}$ for which the spikes are more reliably timed, as $\epsilon_{stimulus}$ increases. The vector strength on the other hand does not show a significant increase (Figure 5.4B). In order to compare the width of the Arnold tongues for the different locking regimes, the values of $f_{stimulus}$ are multiplied with a factor of 2, in order to achieve a $2:1$ ratio between $f_{stimulus}$ and $f_{firing\ rate}$; and with a factor of 0.5, in order to achieve a $1:2$ ratio between $f_{stimulus}$ and $f_{firing\ rate}$. In both cases, the width of the Arnold tongue is determined as the range of $f_{stimulus}$ for which $f_{stimulus} - f_{firing\ rate} < \pm 5\,\text{Hz}$. An increase of the width of the Arnold tongue is only observed for $1:1$ locking between $f_{stimulus}$ and $f_{firing\ rate}$, for higher values of $\epsilon_{stimulus}$, while for ratios of $2:1$ and $1:2$, the data points remain at a distance of approximately 10 Hz, a result of the threshold measure of $\pm 5\,\text{Hz}$ (Figure 5.4C). From these findings we can conclude that the Arnold tongues and the areas of increased reliability are present for $1:1$ ratios. For the $2:1$ ratios, both effects are only seen in some recordings and are not significant when averaged.

5.3 Timing Resonance Increases with Average Firing Rate

We now turn to a set of experiments, where the average firing rates of the neurons and the stimulus frequency $f_{stimulus}$ were varied, and the stimulus amplitude was held constant at $\epsilon_{stimulus} = 6\,\text{dB}$. The goal of these experiments was to investigate if the timing resonance effect described in Section 5.1 is dependent on the *average firing rate* of the neuron. Let us therefore examine the data from an experiment where a receptor neuron was tested at six different firing rates. Overall stimulus intensities were adjusted in order to elicit target firing rates, ranging from 25 Hz to 150 Hz in 25 Hz increments. The resulting average firing rates when calculated over all $f_{stimulus}$, were 22 ± 3.4, 48 ± 5.7, 85 ± 9.3, 116 ± 11.8, 133 ± 14.9 and $172 \pm 17.3\,\text{Hz}$, respectively. For every target firing rate, the range of $f_{stimulus}$ and its increments were chosen accordingly, in order to obtain 25 values of $f_{stimulus}$ with fixed ratios between $f_{stimulus}$ and the target firing rate.

To test if the phenomenon of timing resonance is dependent on the average firing rate, we analyse the $1:1$ locking regime, where one spike is generated per stimulus cycle, and investigate if this type of locking took place at all six different average firing rates. When we stimulated the neuron with the six different stimulus frequencies which are identical to the target firing rates mentioned above – $f_{stimulus} = 25$, 50, 75, 100, 125 and 150 Hz –

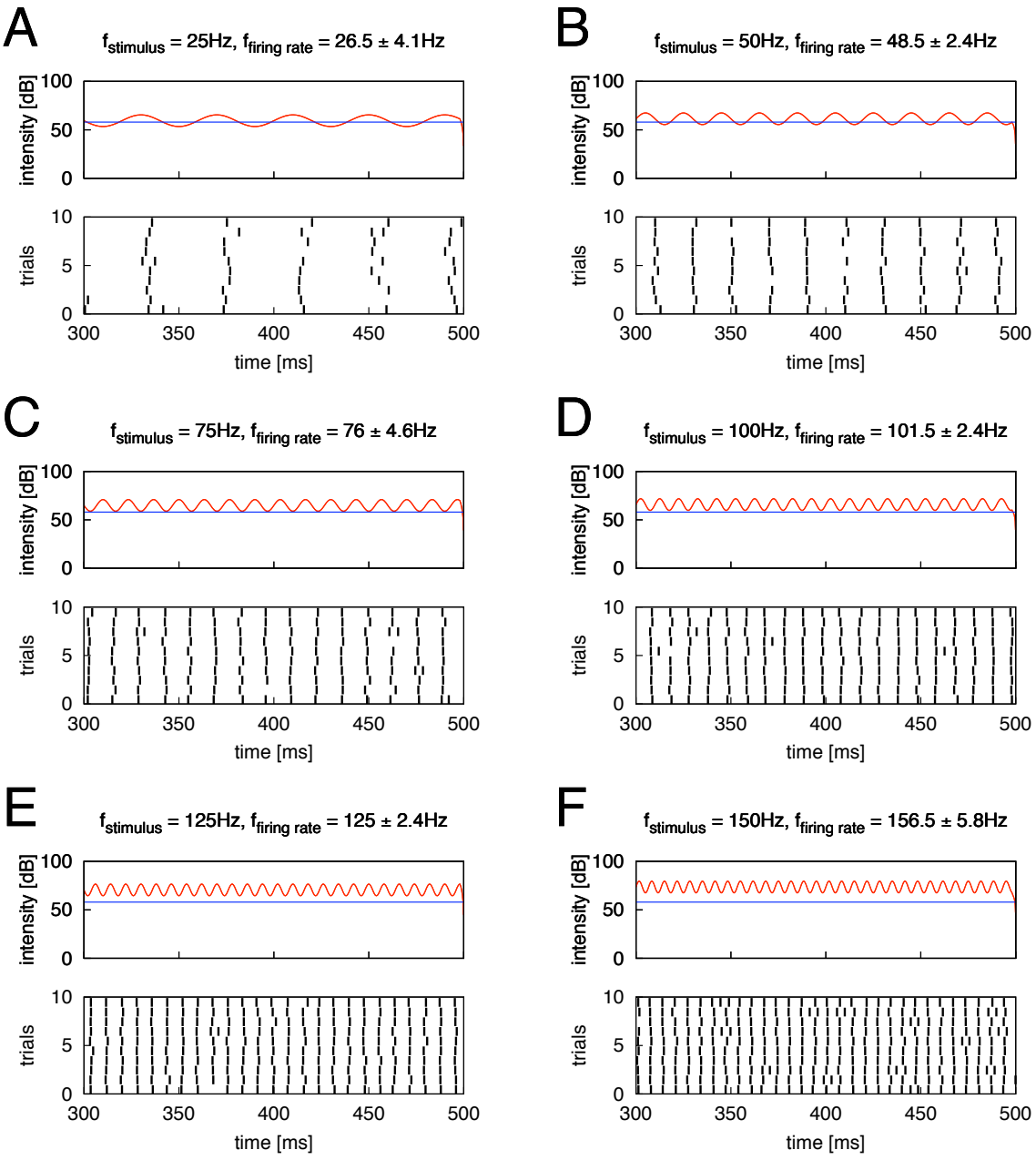

Figure 5.5: A receptor neuron stimulated with a sine wave stimulus, using six stimulus frequencies $f_{stimulus}$ at an amplitude of $\epsilon_{stimulus} = 6\,\text{dB}$. The firing threshold of the neuron (blue) was 58 dB SPL. Overall stimulus intensities were adjusted in order to elicit six different target firing rates, ranging from 25 to 150 Hz in 25 Hz increments. $f_{stimulus}$ was chosen such that there is a $1:1$ ratio with the target firing rate. In each sub-figure, the upper plot shows the stimulus (red) and the neuron's firing threshold (blue), and the lower plot shows the neuron's spike response as a raster plot of 10 trials. $1:1$ locking took place in all six cases: Almost always, one spike is generated per stimulus cycle, regardless of the firing rate. **(A)** $f_{stimulus} = 25\,\text{Hz}$, $f_{firing\ rate} = 26.5 \pm 4.1\,\text{Hz}$. **(B)** $f_{stimulus} = 50\,\text{Hz}$, $f_{firing\ rate} = 48.5 \pm 2.4\,\text{Hz}$. **(C)** $f_{stimulus} = 75\,\text{Hz}$, $f_{firing\ rate} = 76 \pm 4.6\,\text{Hz}$. **(D)** $f_{stimulus} = 100\,\text{Hz}$, $f_{firing\ rate} = 101.5 \pm 2.4\,\text{Hz}$. **(E)** $f_{stimulus} = 125\,\text{Hz}$, $f_{firing\ rate} = 125 \pm 2.4\,\text{Hz}$. **(F)** $f_{stimulus} = 150\,\text{Hz}$, $f_{firing\ rate} = 156.5 \pm 5.8\,\text{Hz}$. (Data from neuron 05-08-29-ad)

we see that 1 : 1 locking takes place in all six cases: The neuron generates one spike per stimulus cycle with very few exceptions, regardless of the average firing rate (Figure 5.5).

How does the reliability of the spike response change for other values of $f_{stimulus}$? To investigate this, we plot the reliability of the neuron's spike response against $f_{stimulus}$ for every target firing rate. For the resulting average firing rates, there is an increase in spike timing precision, as well as a corresponding decrease in spike time jitter, for stimulus frequencies around the average firing rate of the neuron. Similar to our results in Section 5.1, these peaks are not only present for values of $f_{stimulus}$ around the average firing rate, but also – to a lesser degree – around its subharmonic. For the higher harmonic, the peaks are not present. The reliability peaks become more pronounced for higher average firing rates. Phase locking, determined by the vector strength, remains high for low average firing rates, but as the average firing rate is increased, phase locking decreases for all values of $f_{stimulus}$ except for values around the average firing rate. When plotting the firing rate $f_{firing\ rate}$ against $f_{stimulus}$, we see that the neuron's spike response starts to lock onto the stimulus as the average firing rate is increased (Figure 5.6).

Figure 5.7 presents the averaged results for all five neurons from which the recordings were long enough to test all the necessary parameters of this stimulus protocol. Here, the widths of the peaks for the correlation-based reliability and the vector strength are calculated for every target firing rate, using a procedure that will be explained in more detail in the next section. For the spike time jitter, this procedure has not yielded any meaningful results. Analysing these average 'Arnold tongue-like' structures, we see that the peak widths are increasing for both the spike time reliability and the vector strength around the subharmonics of the firing rates (Figure 5.7A) and in a more pronounced way around the firing rates (Figure 5.7B). When we consider the relative width of the locking ranges for every target firing rate, the effect is less pronounced. The width of the Arnold tongues based on the difference between $f_{stimulus}$ and $f_{firing\ rate}$ was computed in a similar way as for Figure 5.4C and shows that the range of $f_{stimulus}$ increases for a 1 : 1 ratio between $f_{stimulus}$ and $f_{firing\ rate}$ as target firing rates increase, indicating stimulus locking. This effect is not seen when the ratio is 2 : 1 or 1 : 2 (Figure 5.7C).

5.4 Locking of the Firing Rate to the Stimulus Frequency is Correlated with High Reliability

In this section, we check whether the results for the stimulus frequency $f_{stimulus}$ corresponding to the highest reliability value, and for $f_{stimulus}$ corresponding to the locking of the neuron's spike response to the stimulus are in agreement.

Let us therefore reconsider Figure 5.2, and investigate how the peaks in reliability in the $f_{stimulus}$ vs. reliability plot (Figures 5.2E, F and G) correspond to the intersections of the data with the lines corresponding to the values of $spikes/cycle = 2$, 1 and 0.5 in the $f_{stimulus}$ vs. $spikes/cycle$ plot (Figure 5.2D). Ideally, we would expect three peaks in a $f_{stimulus}$ vs. reliability plot, when timing resonance leads to increased spike response reliability for the 2 : 1, 1 : 1 and 1 : 2 locking regimes. Likewise, we would expect a certain amount of data points in a $f_{stimulus}$ vs. $spikes/cycle$ plot to be parallel with lines at values of $spikes/cycle = 2$, 1 and 0.5, corresponding to 2 : 1, 1 : 1 and 1 : 2 locking, respectively, as $f_{stimulus}$ increases. Thus, the task is to match the three peaks in the

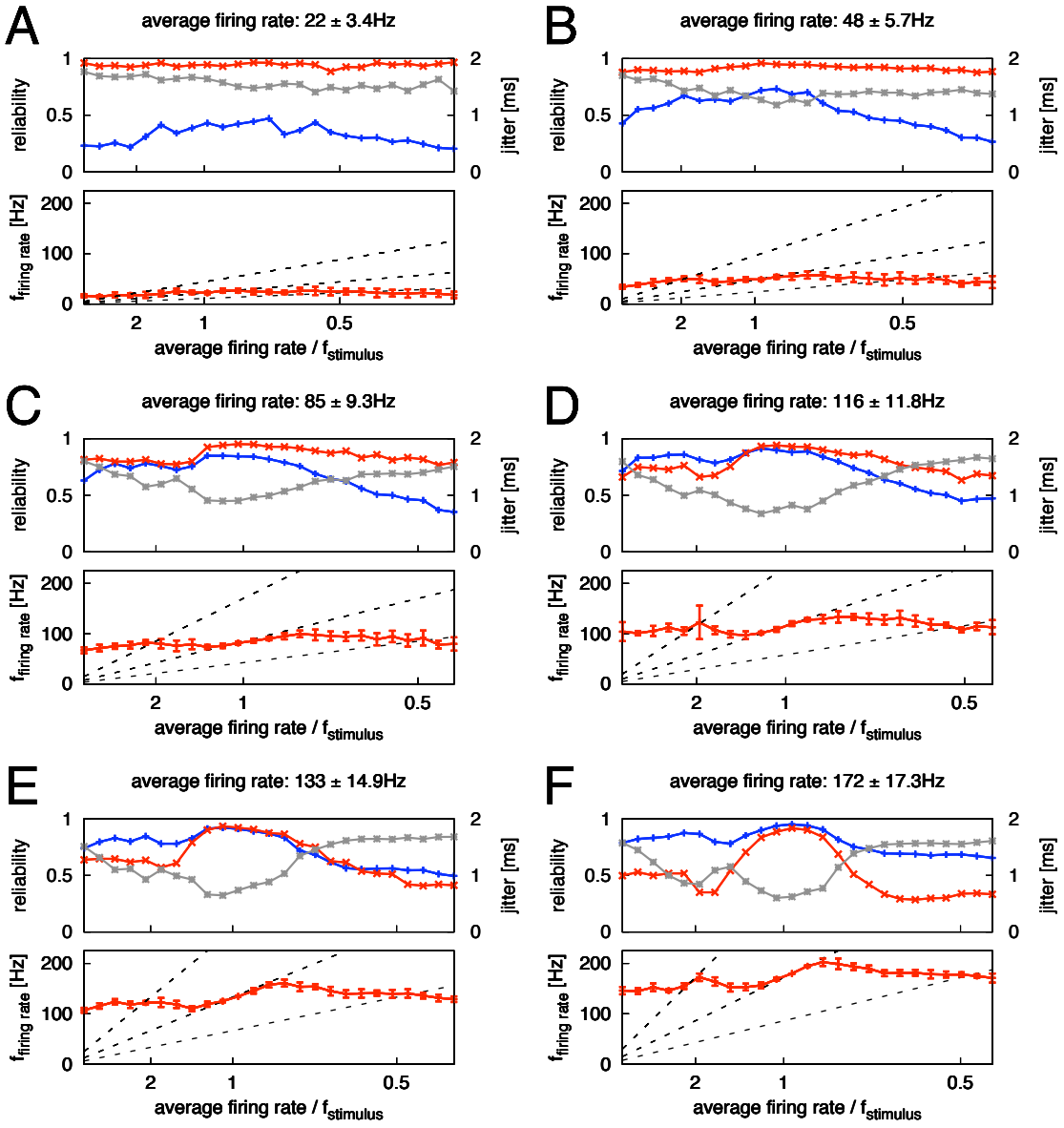

Figure 5.6: Reliability of the spike responses for different average firing rates to sine wave stimuli at different stimulus frequencies $f_{stimulus}$ at a stimulus amplitude $\epsilon_{stimulus} = 6\,\mathrm{dB}$. Overall stimulus intensities were adjusted in order to elicit six different target firing rates, ranging from 25 Hz to 150 Hz in 25 Hz increments. The range of $f_{stimulus}$ and the $f_{stimulus}$ increments were chosen with respect to the target firing rate in order to obtain 25 $f_{stimulus}$ for every target firing rate. The x-axis shows the ratio between the average firing rate (calculated over all $f_{stimulus}$) and $f_{stimulus}$. The resulting average firing rates, averaged over all values of $f_{stimulus}$, were 22 ± 3.4, 48 ± 5.7, 85 ± 9.3, 116 ± 11.8, 133 ± 14.9 and 172 ± 17.3 Hz. In each subfigure, the top plot shows the three reliability measures (blue: correlation-based reliability ($\sigma = 1.1$ ms), red: vector strength, grey: spike time jitter) vs. the stimulus frequency $f_{stimulus}$. The lower plot shows the firing rate $f_{firing\ rate}$ vs. $f_{stimulus}$. For the six different average firing rates, spike timing precision increased and spike time jitter decreased for values of $f_{stimulus}$ around the average firing rate and around its subharmonic. For lower average firing rates, the peaks become less pronounced. As the average firing rate is increased, phase locking decreases for all values of $f_{stimulus}$ except for values around the average firing rate. In the $f_{firing\ rate}$ vs. $f_{stimulus}$ plots, the neuron's spike response starts to lock onto the stimulus as the average firing rate is increased. **(A)** Average firing rate $= 22 \pm 3.4$ Hz. **(B)** Average firing rate $= 48 \pm 5.7$ Hz. **(C)** Average firing rate $= 85 \pm 9.3$ Hz. **(D)** Average firing rate $= 116 \pm 11.8$ Hz. **(E)** Average firing rate $= 133 \pm 14.9$ Hz. **(F)** Average firing rate $= 172 \pm 17.3$ Hz. (Data from neuron 05-08-29-ad)

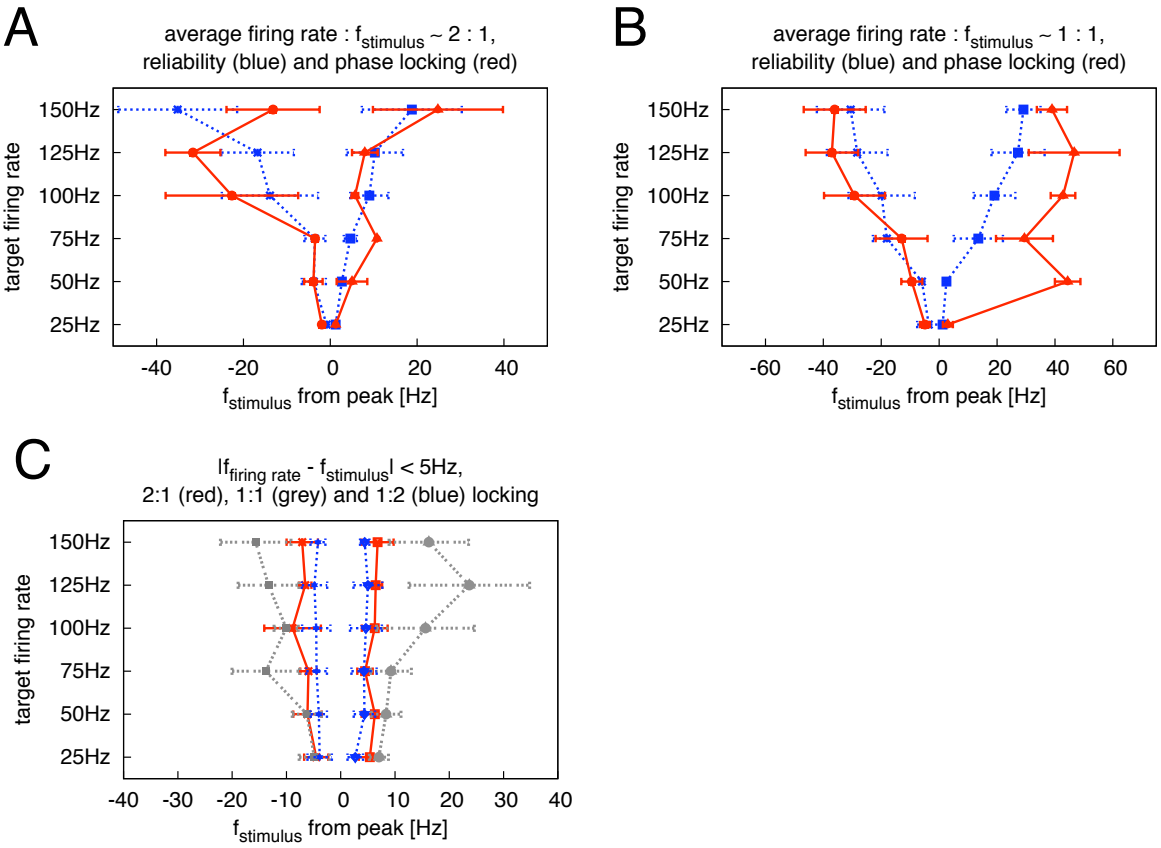

Figure 5.7: Areas of increased reliability and stimulus locking for different target firing rates, averaged over five receptor neurons stimulated with a sine wave stimulus. The stimulus amplitude $\epsilon_{stimulus}$ was 6 dB. **(A)** For a ratio between average firing rate and stimulus frequency of approximately $2:1$, the spike time reliability (blue), determined using the correlation-based reliability with $\sigma = 1.1$ ms, and the phase locking (red), determined by the vector strength, show an increase in the range of $f_{stimulus}$, for which these two parameters are increased, as target firing rates are increased from 25 Hz to 150 Hz. The sample size ranges from $n = 1$ to $n = 5$, with a median of 3. **(B)** For a ratio between average firing rate and stimulus frequency of approximately $1:1$, the range of $f_{stimulus}$ with increased correlation-based reliability (blue, $\sigma = 1.1$ ms) and increased phase locking (red) widens, as target firing rates increase. The sample size ranges from $n = 1$ to $n = 5$, with a median of 3.5. **(C)** The range of $f_{stimulus}$, for which $|f_{firing\ rate} - f_{stimulus}| < 5$ Hz increases for a $1:1$ ratio between $f_{stimulus}$ and $f_{firing\ rate}$ (grey) for higher target firing rates, indicating locking. This effect is not seen when the ratio is $2:1$ (red) and $1:2$ (blue). The sample size is $n = 5$.

$f_{stimulus}$ vs. reliability plot to the corresponding parallel sections of data points in the $f_{stimulus}$ vs. *spikes/cycle* plot. To achieve this, a couple of measures were used, which are discussed in the following.

In the $f_{stimulus}$ vs. *spikes/cycle* plot, we determine the $f_{stimulus}$ values for which the data points intersect with the horizontal lines at values of *spikes/cycle* $= 2$, 1, 0.5 ($2:1$, $1:1$ and $1:2$ locking, respectively). Additionally, for each of the three *spikes/cycle* values ± 0.05, two parallel lines are set, in order to define the beginning and the end of the data points that correspond to a locking of the neuron's spikes to $f_{stimulus}$ for a given stimulus regime (Figure 5.8A). In the $f_{stimulus}$ vs. reliability plot, peaks in reliability are identified using an algorithm proposed by Todd and Andrews (1999). Calculating the width of a peak can be challenging, as peaks in reliability are often not well defined. For

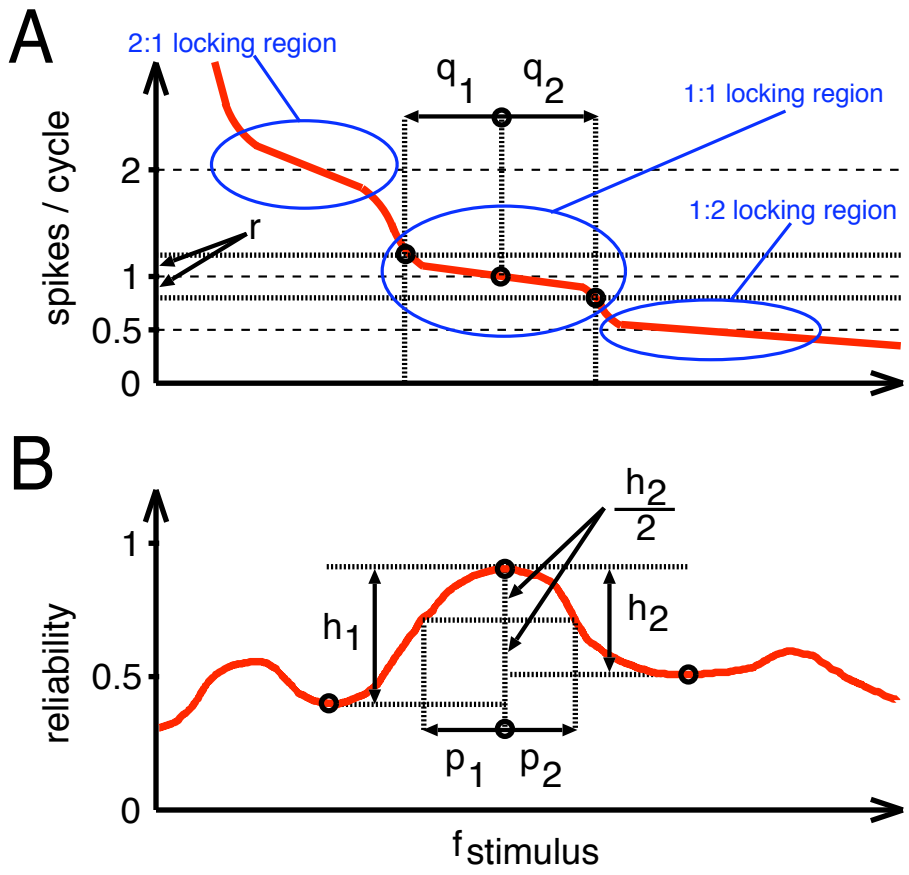

Figure 5.8: Illustration of the computation of the correlation between stimulus frequency ($f_{stimulus}$) corresponding to a phase locking of the spike response, and stimulus frequency corresponding to a peak in reliability. **(A)** In the $f_{stimulus}$ vs. *spikes/cycle* plot, the $f_{stimulus}$ values where the data intersects with the horizontal lines at values of *spikes/cycle* = 2, 1, 0.5 (corresponding to 2 : 1, 1 : 1 and 1 : 2 locking, respectively), are calculated. Then, at values of $r = \pm 0.05$ for each of the three values of *spikes/cycle*, two parallel lines are set in order to define the beginning and the end of the section of data points that correspond to a locking of the neuron's spikes to $f_{stimulus}$ for a given stimulus locking regime. **(B)** The width of a peak is calculated by comparing the difference h_1 between the reliability value of the peak and that of the *left* trough, to the difference h_2 between the peak's reliability value and that of the *right* trough. Of these two, the smaller one, h_2, is used to determine the width of the peak by calculating the $f_{stimulus}$ values at the reliability value corresponding to $h_2/2$. The $f_{stimulus}$ values p_1 and p_2 of the data at $h_2/2$ then yield the peak width.

each identified peak, the difference between the peak reliability value and the reliability value of the *left* trough is compared to the difference between the peak reliability value and the reliability value of the *right* trough, and the smaller difference is chosen. The width of the peak is then determined by calculating the $f_{stimulus}$ values at the reliability value corresponding to *half* of this smaller difference. The smaller difference is chosen in order to make sure that the width of the peak is not overestimated. The $f_{stimulus}$ values of the data at the reliability value corresponding to half of the smaller difference yield the peak width. If two peaks end up in the same range, the higher one is chosen, and the lower peak is considered an artefact (Figure 5.8B).

We analyse the data from 10 shorter recordings and the 11 recordings that have been examined in more detail in Section 5.2. Stimulus frequencies resulting in a peak in

reliability were within the range of the corresponding stimulus locking regimes. Due to the absence of $1:2$ locking in our data, we focus on the $2:1$ and $1:1$ locking regimes. Also, due to the difficulty of determining the width of the troughs in spike time jitter, which was already noted in Section 5.2, we focus on spike time reliability ($\sigma = 1.1\,\text{ms}$) and phase locking, as determined by the vector strength.

When we plot the values of $f_{stimulus}$ determined from the $2:1$ locking regime (Figures 5.9A and B), we find that the peaks in spike time reliability are associated with *lower* $f_{stimulus}$ values, compared to the values of $f_{stimulus}$ for the $2:1$ locking. This effect is also present for the vector strength. Thus, in both cases the scattered data points are below the identity line. The low correlation coefficient for the spike time reliability (correlation coefficient: 0.31, p-value: 0.02) and lack of correlation for the phase locking (correlation coefficient of 0.02, p-value: 0.91) are consistent with the findings in Figure 5.4, where the increase in reliability for the $2:1$ locking was not significant.

For the $1:1$ locking regime (Figures 5.9C and D), we see that the data points are more symmetrically scattered on the identity line, compared to $2:1$ locking in Figures 5.9A and B. The data for the $1:1$ locking has higher correlation coefficients of 0.77 and 0.76 for the correlation-based reliability and the phase locking, respectively, and the correlations are highly significant, with p-values < 0.01. These results show that the $1:1$ locking takes place for approximately the same values of $f_{stimulus}$, which are also associated with the peaks in spike time reliability. Therefore we can conclude that the $1:1$ locking is a solid phenomenon, whereas the $2:1$ locking is very weak.

5.5 No Neuronal Resonance with White Noise Stimuli

To further analyse how the presence of certain frequencies in the stimulus may influence timing resonance, we employ white noise stimuli. White noise is a random signal with a flat power spectrum, meaning that all frequencies have the same power. Much like white light, which is the combination of all the colors of the visible light spectrum in equal proportions, white noise contains sine waves of all frequencies up to a specific cut-off frequency – white noise without a cut-off frequency is purely a theoretical construction, since it would imply infinite total power. Thus, in practice, a signal is considered 'white' if it has a flat frequency spectrum over a defined frequency band.

In the present case, the white noise stimuli were generated from the same instance of white noise. Note that for these stimuli, $\epsilon_{stimulus}$ denotes the standard deviation of the white noise, not the stimulus amplitude. We expected a change in reliability depending on whether frequencies close to the firing rate of the neuron were present in the white noise or not. However, the data gained with the two stimulus protocols presented in the following two subsections was very uniform for all neurons tested (eight recordings gained using the first protocol and 10 for the second protocol). Therefore we will only focus on data from a recording of one neuron for each stimulus protocol, which will act as an example to represent the total data.

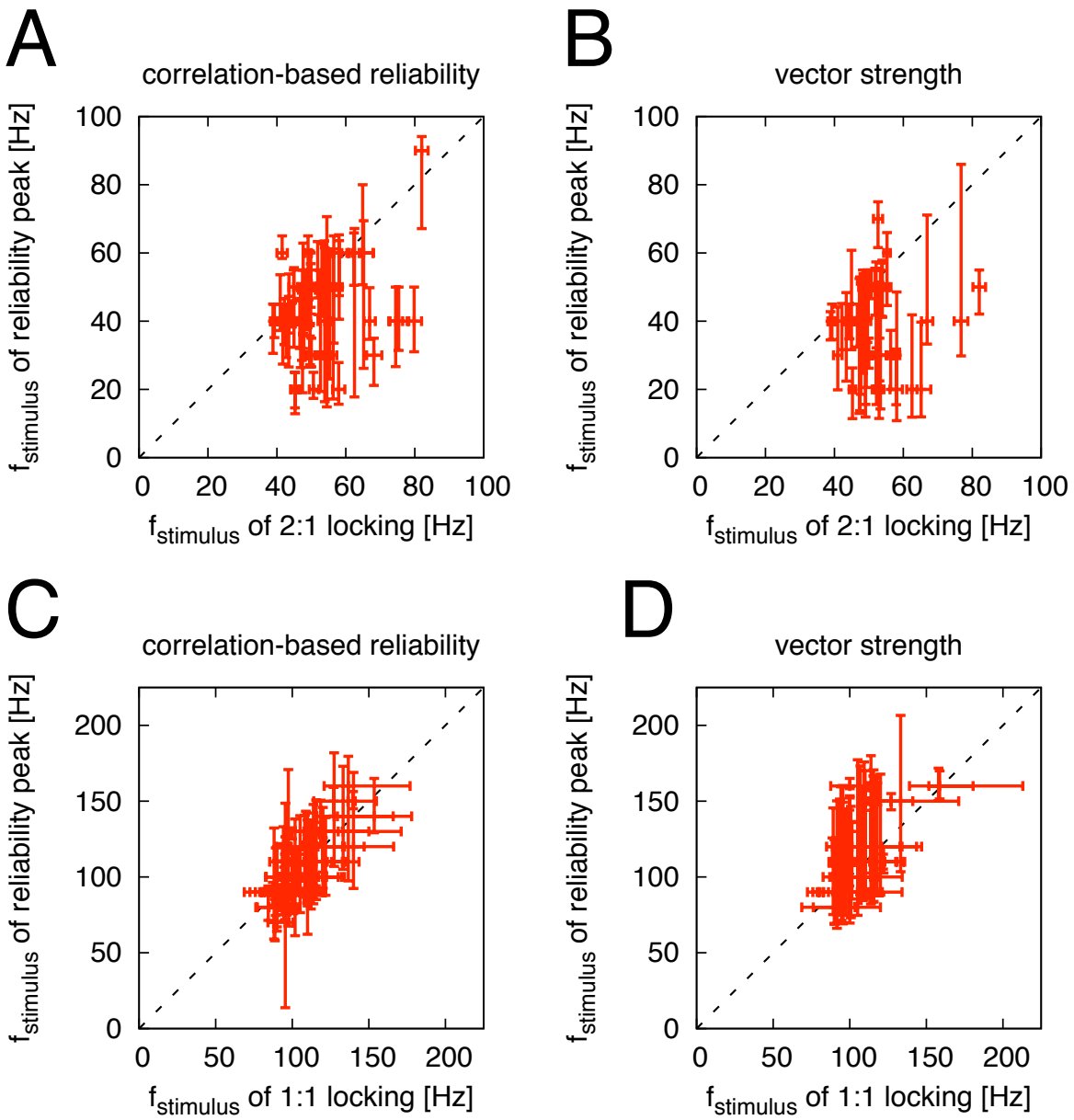

Figure 5.9: Correlation between the stimulus frequency $f_{stimulus}$ corresponding to the highest reliability value, and $f_{stimulus}$ corresponding to the locking of the neuron's spike response to the stimulus. The identity line indicates a perfect match between the stimulus frequency $f_{stimulus}$ corresponding to the highest reliability value, and $f_{stimulus}$ corresponding to the locking of the neuron's spike response to the stimulus. **(A)** $2:1$ locking, using the correlation-based reliability with $\sigma = 1.1\,\text{ms}$. Correlation coefficient: 0.31, p-value: 0.02. The data points are clustered below the identity line, indicating that for the peaks in spike time reliability are associated with *lower* $f_{stimulus}$ values, compared to the $f_{stimulus}$ values of the $2:1$ locking. **(B)** $2:1$ locking, determined by the vector strength. Correlation coefficient: 0.02, p-value: 0.91. The data points are clustered below the identity line. **(C)** $1:1$ locking using the correlation-based reliability with $\sigma = 1.1\,\text{ms}$. Correlation coefficient: 0.77, p-value: < 0.01. The data points are approximately symmetrically scattered around the identity line, indicating that the $1:1$ locking takes place for approximately the same values of $f_{stimulus}$, which are also associated with the peaks in spike time reliability. **(D)** $1:1$ locking, determined by the vector strength. Correlation coefficient: 0.76, p-value: < 0.01. The data points are approximately symmetrically scattered around the identity line.

5.5.1 White Noise Stimuli with Relative Frequency Gaps

In the first set of experiments, we employed white noise stimuli with a frequency gap: A range of frequencies around a 'gap' frequency f_{gap} was missing from the white noise frequency content. The frequency f_{gap} was increased in 10 Hz increments from 10 Hz to 250 Hz. Additionally, the range around f_{gap} was varied: Depending on the stimulus protocol, it was $\pm 10\,\%$, $\pm 20\,\%$ and $\pm 30\,\%$ of f_{gap} for white noise with a cut-off frequency of 800 Hz, or $\pm 15\,\%$ and $\pm 30\,\%$ of f_{gap} for white noise with cut-off frequencies of 200 Hz and 400 Hz. The target firing rate was 100 Hz, and the standard deviation of the stimulus was 6 dB.

In Figures 5.10A – E we analyse the responses of an example neuron to white noise stimuli with a cut-off frequency of 800 Hz and a band-stop filter at frequency f_{gap} with a relative frequency gap of 40 % ($\pm 20\,\%$). There is no significant change in the firing rate, spike time reliability or the phase locking regardless of the frequency f_{gap} of the band-stop filter. Furthermore, when we analyse the spike time reliability using the correlation-based reliability measure ($\sigma = 1.1$ ms) for different relative frequency gaps (20 %, 40 % and 60 % of f_{gap}, Figure 5.10F), we also do not see any significant change in reliability for increased or decreased gap width. Thus, the expectation to see a decrease in reliability, as the frequency f_{gap} of the band-stop filter or its associated gap is close to the average firing rate of the neuron, is not fulfilled.

5.5.2 White Noise Stimuli with Varying Cut-Off Frequencies

In these experiments, the frequency content of the white noise stimulus was decreased by decreasing its cut-off frequency $f_{cut-off}$ over the course of an experiment. Additionally, the standard deviation $\epsilon_{stimulus}$ was varied from 4 dB to 12 dB in 2 dB increments. The stimulus intensity was adjusted in order to elicit an average firing rate in the neuron that closely matched a target firing rate of 100 Hz.

When we analyse the change in reliability and firing rate for the response of another example neuron to white noise stimuli with different cut-off frequencies $f_{cut-off}$ at a standard deviation of $\epsilon_{stimulus} = 8$ dB, the results are uniform (Figures 5.11A – E). For all $f_{cut-off}$ there is no significant change in firing rate or spike time reliability. In Figure 5.11F, no change in spike time reliability, as measured with the correlation-based reliability measure ($\sigma = 1.1$ ms), can be seen for different values of $\epsilon_{stimulus}$. Therefore, even with this coarser experimental protocol compared the protocol used in the previous section, no change in reliability is seen, regardless of whether the frequency equal to the average firing rate is contained in the spectrum of the white noise or not.

5.6 Chapter Summary

In this chapter, we have analysed whether timing resonance can be observed in the responses of locust auditory receptor neurons under acoustic stimulation. For sine wave stimuli, we expected to see resonance effects for ratios of 2 : 1, 1 : 1 and 1 : 2 between the neuron's firing rate and the stimulus frequency $f_{stimulus}$.

Considering spike trains, a ratio of approximately 2 : 1 was seen when $f_{stimulus}$ was approximately half of the average firing rate, and a ratio of approximately 1 : 1, for

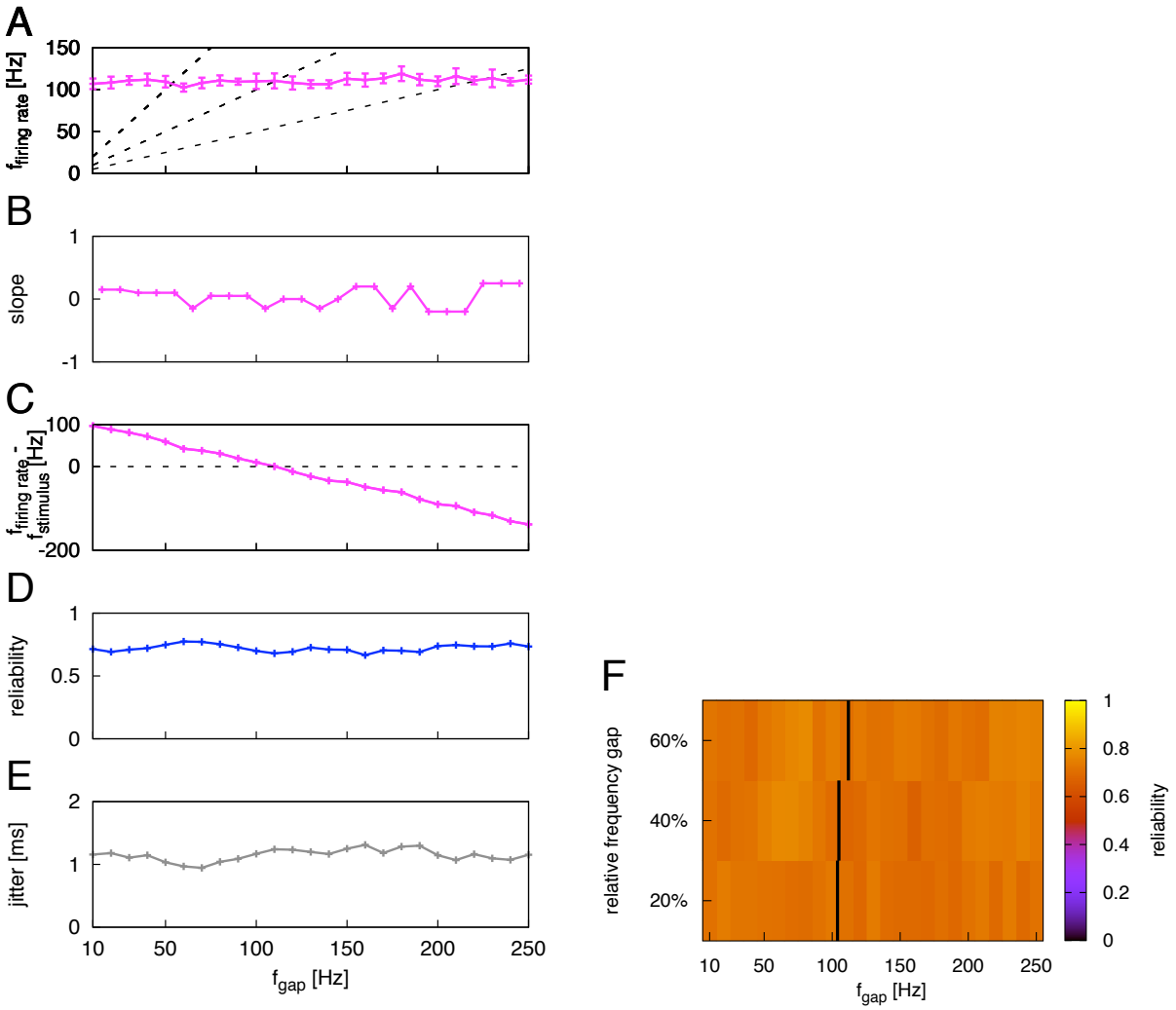

Figure 5.10: Firing rate and reliability of a receptor neuron's spike response to white noise stimuli with a cut-off frequency of 800 Hz, for a band-stop filter at frequency f_{gap} with a relative frequency gap of 40 % (left plots). The standard deviation $\epsilon_{stimulus}$ of the white noise was 6 dB. The average firing rate of the neuron, calculated over all f_{gap}, was 110 ± 3.3 Hz. For all f_{gap} and relative frequency gaps, there is no significant change in the firing rate $f_{firing\ rate}$ or in the reliability of the spike response. **(A)** f_{gap} vs. $f_{firing\ rate}$. The dashed lines indicate 2 : 1 (first line), 1 : 1 (second line) and 1 : 2 (third line) ratios between f_{gap} and $f_{firing\ rate}$ of the neuron. **(B)** Slope of $f_{firing\ rate}$ relative to the 1 : 1 line in the plot above. The data points are filtered using a median filter with a sliding window containing five data points. **(C)** Difference between firing rate and stimulus frequency $f_{firing\ rate} - f_{gap}$. **(D)** Correlation-based reliability ($\sigma = 1.1$ ms). **(E)** Spike time jitter. **(F)** Reliability of the spike response for different stimulus frequencies f_{gap} and relative frequency gaps. The average firing rates were 109 ± 2.3, 110 ± 3.3 and 117 ± 4.4 Hz (black bars), for relative frequency gaps of 20 %, 40 % and 60 %. The reliability measure used is the correlation-based reliability ($\sigma = 1.1$ ms). (Data from neuron 05-09-25-aa)

$f_{stimulus}$ around the average firing rate. A ratio of approximately 1 : 2, albeit with a lot of missing spikes, was present, when $f_{stimulus}$ was approximately twice as high as the average firing rate (Figure 5.1).

The strongest resonance effects were observed for values of $f_{stimulus}$ close to the average firing rate. In this regime, 1 : 1 locking between stimulus and spike response took place, and the neuron's firing rate $f_{firing\ rate}$ followed $f_{stimulus}$ over a considerable range. The

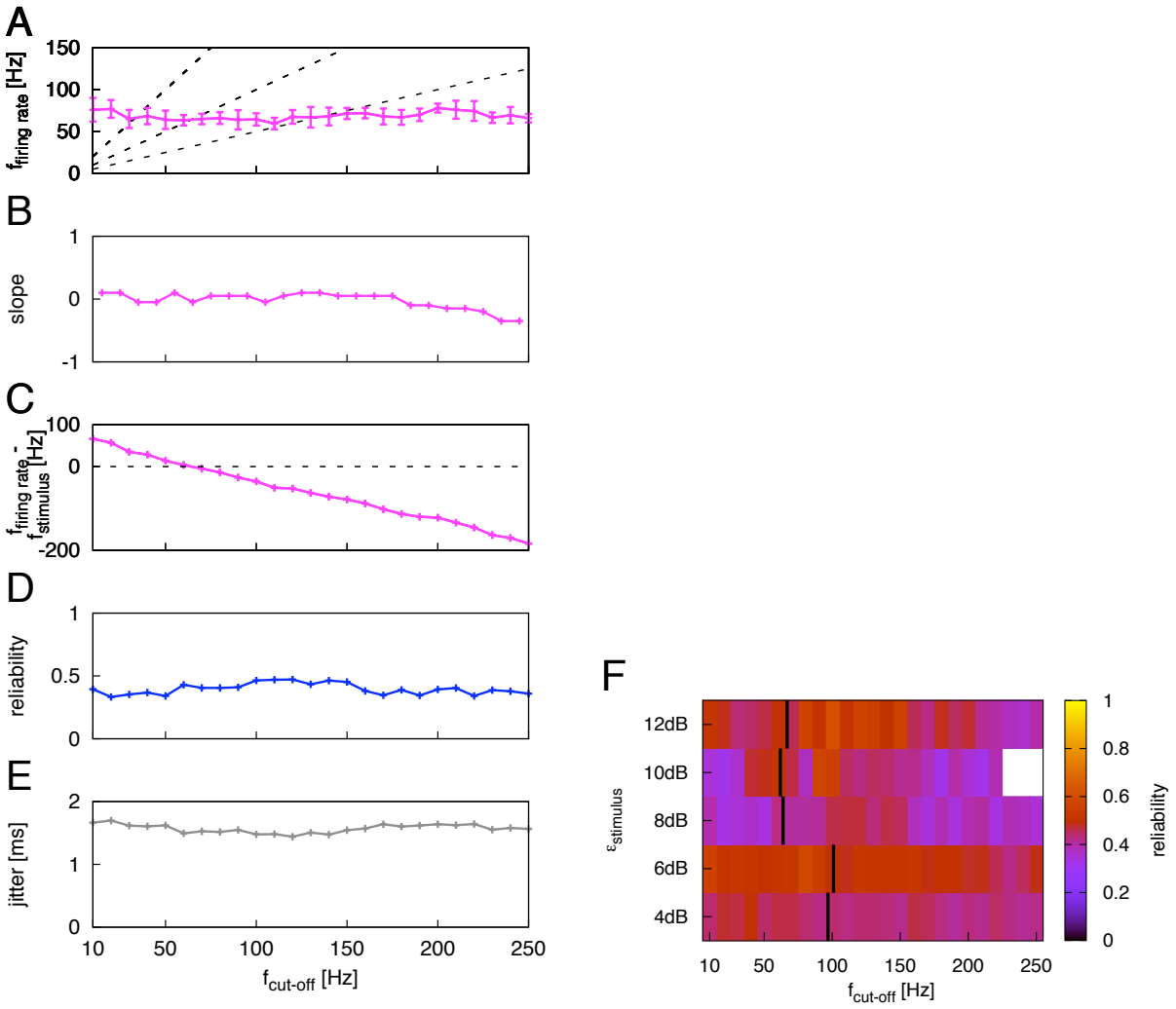

Figure 5.11: Firing rate and reliability of a receptor neuron's spike response to white noise stimuli with different cut-off frequencies $f_{cut-off}$ with a standard deviation of $\epsilon_{stimulus} = 8\,\text{dB}$ (left plots). The average firing rate (calculated over all $f_{cut-off}$) was $69 \pm 4.8\,\text{Hz}$. For all $f_{cut-off}$, at the different $\epsilon_{stimulus}$ there is no significant change in the firing rate $f_{firing\ rate}$ or in the spike time reliability. **(A)** $f_{cut-off}$ vs. $f_{firing\ rate}$. The dashed lines indicate $2:1$ (first line), $1:1$ (second line) and $1:2$ (third line) ratios between $f_{cut-off}$ and $f_{firing\ rate}$ of the neuron. **(B)** Slope of $f_{firing\ rate}$ relative to the $1:1$ line in the plot above. The data points are smoothed using a median filter with a sliding window containing five data points. **(C)** Difference between firing rate and cut-off frequency $f_{firing\ rate} - f_{cut-off}$. **(D)** Correlation-based reliability ($\sigma = 1.1\,\text{ms}$). **(E)** Spike time jitter. **(F)** Reliability of the spike response for different cut-off frequencies $f_{cut-off}$ and standard deviation $\epsilon_{stimulus}$. The average firing rates of the neuron, indicated with a black bar for every $\epsilon_{stimulus}$, were 102 ± 2.3, 106 ± 3.7, 69 ± 4.8, 67 ± 4.8 and $72 \pm 7.5\,\text{Hz}$, for $\epsilon_{stimulus}$ of 4, 6, 8, 10 and 12 dB, respectively. The correlation-based reliability measure is used with $\sigma = 1.1\,\text{ms}$. (Data from neuron 06-03-09-aa)

responses were characterised by high spike time reliability and phase locking, and low spike time jitter. A similar effect, albeit much weaker, was observed at the subharmonic of the firing rate ($2:1$ ratio between $f_{firing\ rate}$ and $f_{stimulus}$). At higher harmonics, no resonance effects were observed (Figure 5.2).

Variation of the stimulus amplitude $\epsilon_{stimulus}$ revealed Arnold tongue structures (Figure 5.3A). Again, the clearest effect was seen around the average firing rate, where the width

of the Arnold tongue increased with increasing $\epsilon_{stimulus}$ (Figure 5.4C). Arnold tongue-like structures could also be seen for the reliability measures, and for many neurons, these structures were also present for a $2:1$ ratio between $f_{firing\ rate}$ and $f_{stimulus}$, when analysed using the correlation-based reliability measure (5.3C) and the spike time jitter (5.3E). Averaged over the population of all recorded neurons, however, the effect at the subharmonic was not significant (Figure 5.4A).

Although the effect of timing resonance with $1:1$ locking was independent of the average firing rate (Figures 5.5 and 5.6), increasing the average firing rate led to a more pronounced manifestation of the effect for a wider range of $f_{stimulus}$ (Figure 5.7).

The results were checked for consistency by analysing the correlation between stimulus frequencies that led to $1:1$ or $2:1$ locking of the response, and stimulus frequencies that elicited responses with increased spike time precision (Figure 5.8). For $1:1$ locking, the values were in good agreement (Figures 5.9C and D), whereas they deviated for $2:1$ locking in many neurons (Figures 5.9A and B). We conclude that in locust auditory receptors, $1:1$ locking leads to more reliable responses than $2:1$ locking.

In contrast to our findings with sine wave stimuli, we found no influence of the frequency content of white noise stimuli on the reliability of the neuronal response (Figures 5.10 and 5.11).

Chapter 6

Neuronal Resonance with Square Wave Stimuli

In this chapter, we examine the spike time reliability of locust auditory receptor neurons using square wave stimuli. There are three important differences between square wave stimuli and sine wave stimuli as used in the previous chapter: First, the slope of a square wave is orthogonal to the base line, and, more importantly, it is independent of the frequency – in a sine wave, these two parameters are connected: For lower frequencies, the sine wave crosses the base line at a shallower angle than for higher frequencies. Second, the square wave gives us the opportunity to vary the fraction of the stimulus cycle which is above threshold by changing the duty cycle. Finally, the sharp transitions between the amplitude extremes in square waves resemble features found in the natural songs produced by grasshoppers.

The focus of this chapter is the correlation of the reliability of the neuron's spike response to the length of the duty cycle of the stimulus: Will the precision change over the length of the duty cycle? When increasing the duty cycle of a square wave stimulus, the stimulus begins to approximate a constant stimulus with no modulation. It is known for layer 5 neurons in rat cortical slices, that in response to repeated current injections of a constant stimulus, over multiple trials the first few spikes after stimulus onset are precisely timed, whereas the later spikes exhibited significant timing jitter across trials (Mainen and Sejnowski, 1995). In addition to the analysis of the effect of duty cycles on spike time reliability, we will compare the spike responses of receptor neurons to square wave stimuli to responses elicited by sine wave stimuli and analyse the effect of 90° slopes.

6.1 Spike Trains Become Irregular for Higher Duty Cycles

The data presented in this section is from a receptor neuron stimulated with square wave stimuli, using 25 stimulus frequencies $f_{stimulus}$ ranging from 10 Hz to 250 Hz in 10 Hz increments, and a stimulus amplitude of $\epsilon_{stimulus} = 6\,\mathrm{dB}$. The overall stimulus intensity was adjusted such that the average firing rate elicited by the neuron was approximately 100 Hz; the stimulus was presented 10 times. Three different duty cycles were used: 25%, 50 % and 75 %.

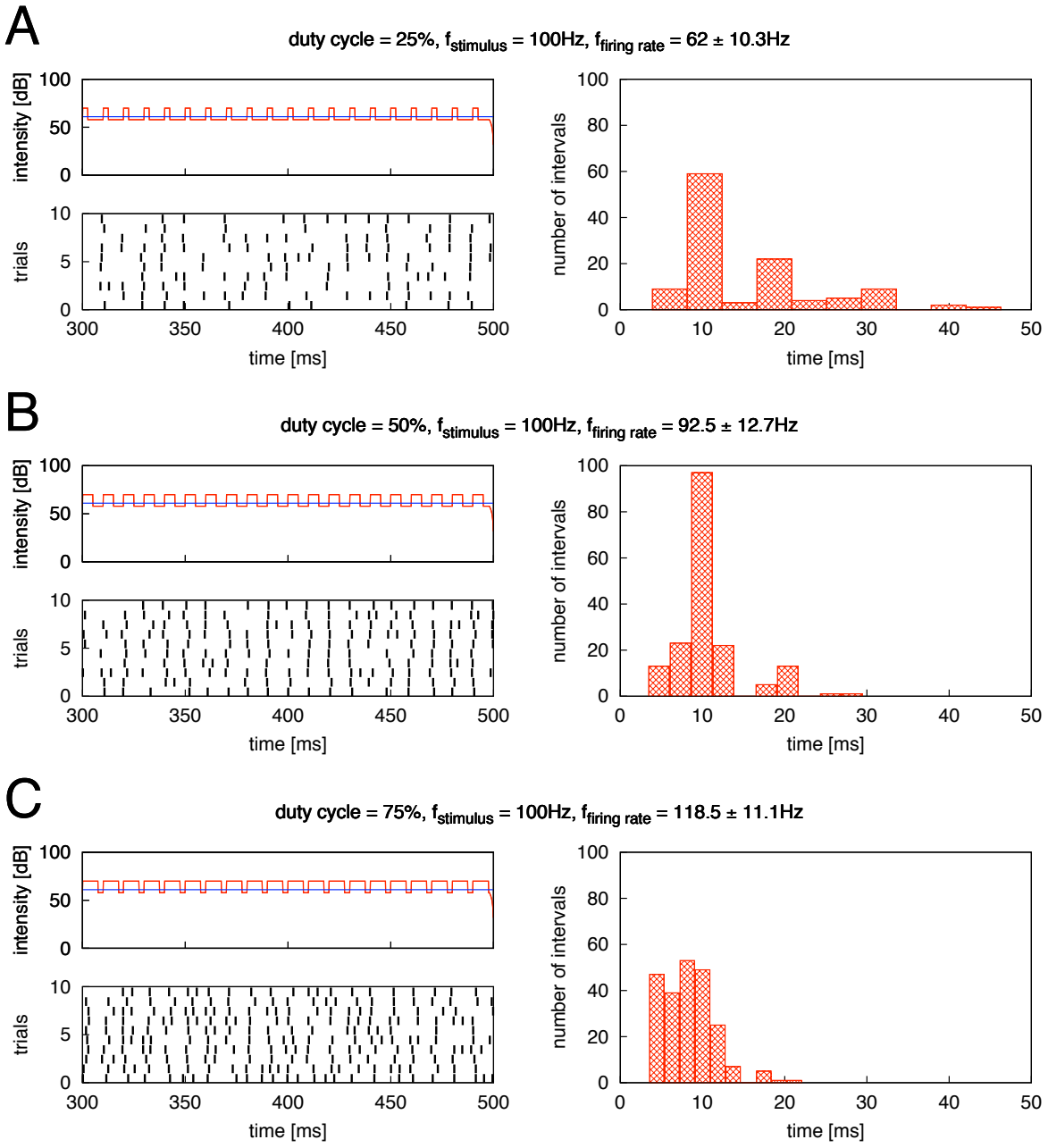

Figure 6.1: Responses of a receptor neuron stimulated with square wave stimuli with duty cycles of 25, 50 and 75 %, at a stimulus frequency $f_{stimulus} = 100\,\text{Hz}$ and amplitude $\epsilon_{stimulus} = 6\,\text{dB}$. The firing threshold of the neuron, indicated with a blue line in the stimulus plots, was 61 dB (left upper plots). The target firing rate was 100 Hz. The neuron's spike responses are depicted as raster plots, the stimulus was presented 10 times (left lower plots). Increasing the duty cycle affects the precision of the spike timing: For the 75 % duty cycle, the distinct peaks in the ISI histograms, which are seen for duty cycles of 25 % and 50 %, are no longer present. **(A)** Duty cycle = 25 %, $f_{firing\ rate} = 62 \pm 10.3\,\text{Hz}$, bin size = 4.25 ms. **(B)** Duty cycle = 50 %, $f_{firing\ rate} = 92.5 \pm 12.7\,\text{Hz}$, bin size = 2.5 ms. **(C)** Duty cycle = 75 %, $f_{firing\ rate} = 118.5 \pm 11.1\,\text{Hz}$, bin size = 1.75 ms. (Data from neuron 05-11-15-ag)

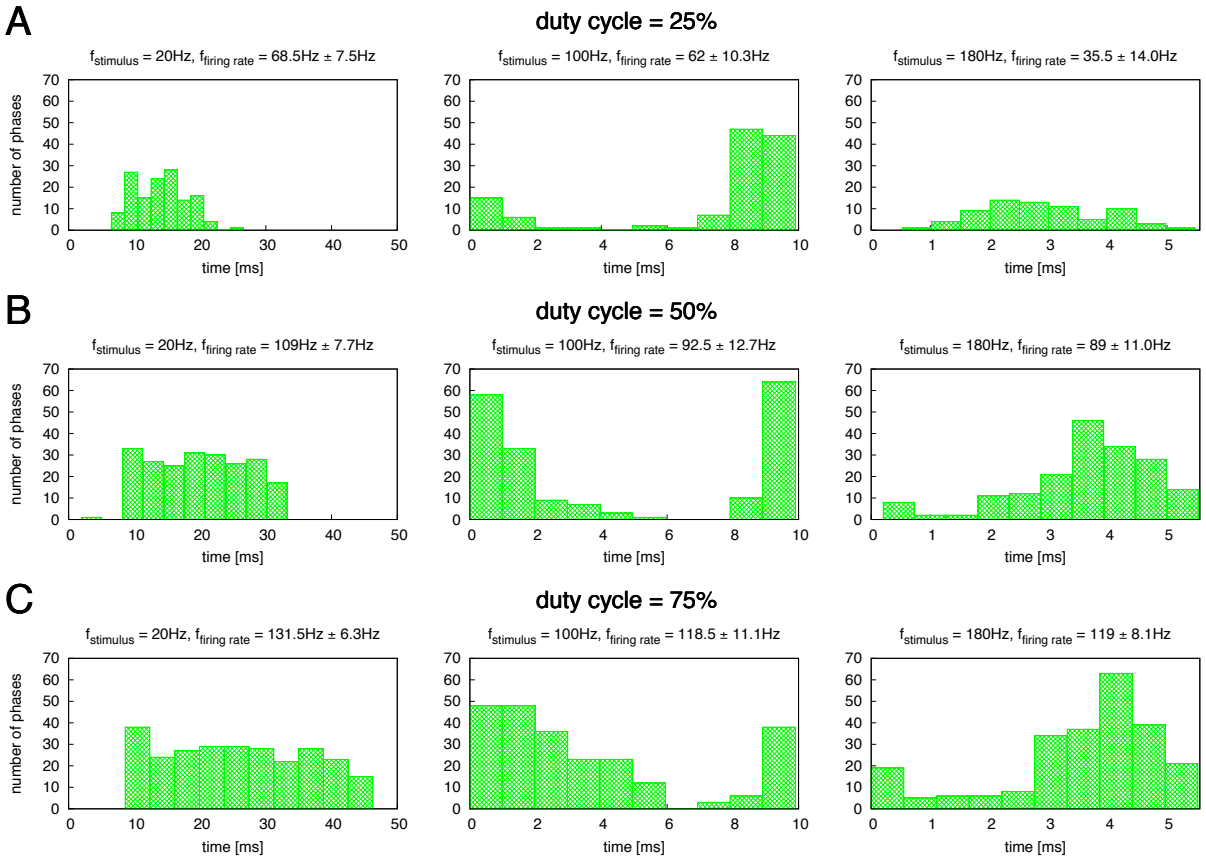

Figure 6.2: Phase histograms of responses to stimuli with three different duty cycles (25, 50 and 75 %) and stimulus frequencies ($f_{stimulus} = 20, 100$ and 180 Hz, from left to right). The stimulus amplitude $\epsilon_{stimulus}$ was 6 dB and the target firing rate was 100 Hz. The phase histograms show that almost all spikes are elicited during the above-threshold phases of the stimuli, after a delay of approximately 8 ms. The peaks of the histograms become broader when the duty cycle is increased. **(A)** Duty cycle = 25 %, $f_{firing\ rate} = 68.5 \pm 7.5, 62 \pm 10.3$ and 35.5 ± 14.0 Hz, bin sizes: 2, 1 and 0.5 ms, from left to right. **(B)** Duty cycle = 50 %, $f_{firing\ rate} = 109 \pm 7.7, 92.5 \pm 12.7$ and 89 ± 11.0 Hz, bin sizes: 3, 1 and 0.5 ms, from left to right. from left to right. **(C)** Duty cycle = 75 %, $f_{firing\ rate} = 131.5 \pm 6.3, 118.5 \pm 11.1$ and 119 ± 8.1 Hz, bin sizes: 3.75, 1 and 0.5 ms, from left to right. (Data from neuron 05-11-15-ag).

Stimulating a receptor neuron with a square wave with $f_{stimulus} = 100$ Hz at these three duty cycles shows an increase in the number of spikes, as the duty cycle gets longer. This is reflected in an increase of the firing rate $f_{firing\ rate}$, from 62 ± 10.3 Hz for the 25% duty cycle stimulus to 92.5 ± 12.7 Hz for the 50% duty cycle stimulus and 118.5 ± 11.1 Hz for the 75% duty cycle stimulus. In order to analyse the spike trains, and specifically, the *intervals* between the spikes of a spike train in the raster plot, in a more systematic way, let us look at interspike interval (ISI) histograms.

For a spike train with spikes elicited with perfect precision at regular intervals, one would expect an ISI histogram with only one sharp peak. However, the ISI histogram for the 25% duty cycle stimulus has two main peaks around 10 ms and 20 ms intervals, with the 10 ms intervals occurring approximately three times as often as the 20 ms intervals (Figure 6.1A). The response thus alternates between one spike every stimulus cycle and one spike every two cycles. Occasional extra spikes cause ISIs < 10 ms, and ISIs > 20 ms sometimes occur when two or three stimulus cycles are missed. For a duty cycle of 50 %,

the ISI histogram has a sharp, well defined peak at an interval length around 10 ms, indicating that one spike is elicited per stimulus cycle most of the time (Figure 6.1B). ISIs around 20 ms, corresponding one spike elicited every other stimulus cycle, occur much less frequently. In contrast to this, for the stimulus with a duty cycle of 75 %, there is only one broad peak around 10 ms in the ISI histogram (Figure 6.1C). On average, the neuron produces more than one spike per cycle, and the spike trains are more irregular compared to the responses to stimuli with 25 % and 50 % duty cycle.

In order to further investigate the change in spike response reliability, let us compare phase histograms of the same neuron for $f_{stimulus} = 20$, 100 and 180 Hz, and the three different duty cycles (Figure 6.2). With phase histograms, we can analyse the occurrence of spikes relative to the stimulus cycle. Therefore, the x-axis is chosen in order reflect the length of a period of $f_{stimulus}$. We see that almost all spikes are elicited during the 'up'-phases of the square wave stimuli, with a delay of approximately 8 ms. This is seen particularly well for $f_{stimulus} = 20$ Hz, where responses were distributed quite evenly over the 'up'-phase and thus peaks of the histograms resemble the square wave shape of the stimuli. For $f_{stimulus} = 100$ Hz, we see bins at times < 8 ms, which belong to the initial reaction of the neuron at 8 ms, but appear due to the periodicity of the plot. For $f_{stimulus} = 180$ Hz, large bins at 4 ms can be seen for a duty cycle of 50 and 75 %, but not for 25 %, where the neuron has difficulty following the stimulus. In general, we see that for increasing duty cycles the peaks in the phase histograms get broader and less well defined.

6.2 Stimulus Locking and Spike Time Reliability Decreases for Higher Duty Cycles

In this section, we analyse the firing rate and the reliability of the spike response of another example neuron to square wave stimuli with a duty cycle of 50 %. As before, the stimulus frequency $f_{stimulus}$ is varied from 10 to 250 Hz in 10 Hz increments. The strongest effect is seen around the average firing rate (calculated over all $f_{stimulus}$) of 140 ± 7.8 Hz: From $f_{stimulus} = 130$ Hz to $f_{stimulus} = 150$ Hz the evoked firing rate $f_{firing\ rate}$ closely matches $f_{stimulus}$. This indicates that 1 : 1 locking occurs, and thus $f_{stimulus}$ modulates $f_{firing\ rate}$ of the neuron (Figure 6.3A). When we compute the slope of $f_{firing\ rate}$ relative to the 1 : 1 line where $f_{stimulus} = f_{firing\ rate}$, we see that the slope is positive between 130 and 150 Hz (Figure 6.3B, data points are smoothed by applying a median filter, see Section 5.1). When we compute the *difference* between $f_{firing\ rate}$ and $f_{stimulus}$, we arrive at the same range of $f_{stimulus} = 130$ Hz to $f_{stimulus} = 150$ Hz, for which the firing rate is approximately equal to the stimulus frequency, resulting in a difference close to 0 Hz (Figure 6.3C). The three reliability measures introduced in Section 2.2 reveal a good agreement: Spike time reliability, phase locking and spike time jitter show their respective peaks and troughs for the same $f_{stimulus}$ (Figures 6.3D, E and F). Therefore, an increased reliability around the range of $f_{stimulus}$ for which the neuron locks on in a 1 : 1 mode is present for square wave stimuli with a duty cycle of 50 %. The three reliability measures also show a weaker increase in reliability at the subharmonic of the average firing rate.

We now use the same example neuron to compare the results of the 50 % duty cycle stimulus with stimuli using duty cycles of 25 % and 75 %. When we evaluate the difference

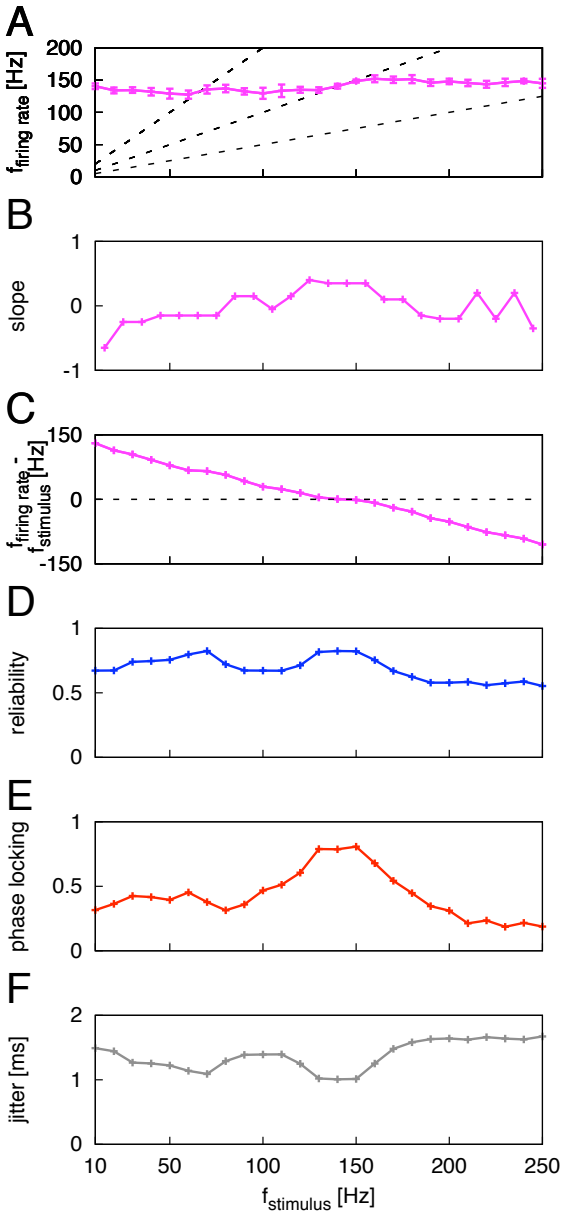

Figure 6.3: Reliability of a receptor neuron's spike response to square wave stimuli and its firing rate $f_{firing\ rate}$ for different stimulus frequencies $f_{stimulus}$ using a duty cycle of 50 %. The average firing rate, calculated over all $f_{stimulus}$, is 140 ± 7.8 Hz. **(A)** $f_{stimulus}$ vs. $f_{firing\ rate}$. The dashed lines indicate 2 : 1 (first line), 1 : 1 (second line) and 1 : 2 (third line) ratios between $f_{stimulus}$ and $f_{firing\ rate}$ of the neuron. The neuron exhibited 1 : 1 locking by increasing $f_{firing\ rate}$ in order to match $f_{stimulus}$ from $f_{stimulus} = 130$ Hz to $f_{stimulus} = 150$ Hz, around the average firing rate. **(B)** Slope of $f_{firing\ rate}$ relative to the 1 : 1 line in the plot above. The data points are smoothed using a median filter with a sliding window containing five data points. The slope is > 0 between 130 and 150 Hz, indicating that 1 : 1 locking occurs. **(C)** Difference between firing rate and stimulus frequency $f_{firing\ rate} - f_{stimulus}$. This difference is close to 0 for $f_{stimulus} = 130$ Hz to $f_{stimulus} = 150$ Hz. **(D)** Correlation-based reliability ($\sigma = 1.1$ ms). The most reliably timed spikes were elicited by $f_{stimulus}$ close to the average firing rate of the neuron. At the subharmonic of the average firing rate ($f_{stimulus} = 70$ Hz), there is a smaller peak, indicating a comparatively weaker increased reliability for 2 : 1 locking. **(E)** Vector strength. Phase locking of the neuron's response is best for $f_{stimulus}$ between 130 and 150 Hz. **(G)** Spike time jitter. The lowest spike time jitter was elicited for $f_{stimulus} = 130$ Hz to $f_{stimulus} = 150$ Hz, and at $f_{stimulus} = 70$ Hz. (Data from neuron 06-05-09-ab)

between the neuron's firing rate and the stimulus frequency, we see that the range of $f_{stimulus}$ for which this difference is 0, or close to 0, decreases for higher duty cycles (Figure 6.4A). Considering the slope of the curve of $f_{firing\ rate}$ vs. $f_{stimulus}$ we find that the slope is positive for values of $f_{stimulus}$ around the average firing rate for all duty cycles. The result indicates that around the average firing rate, the neuron's firing rate is modulated by $f_{stimulus}$, leading to a 1 : 1 locking. The modulation effect is strongest for a duty cycle of 25 %, and becomes narrower when the duty cycle is increased. (Figure 6.4B, data points are smoothed by applying a median filter, see Section 5.1). For the correlation-based reliability using $\sigma = 1.1$ ms, a weak increase in reliability can be seen around the average firing rates for all three duty cycles (Figure 6.4C). For a duty cycle of 50 %, we also see an increase in reliability around the subharmonic of the average firing rate (see also Figure 6.3D). The vector strength shows maximal phase locking around the average firing rate for a duty cycle of 25 %, and the result is similar for the spike time

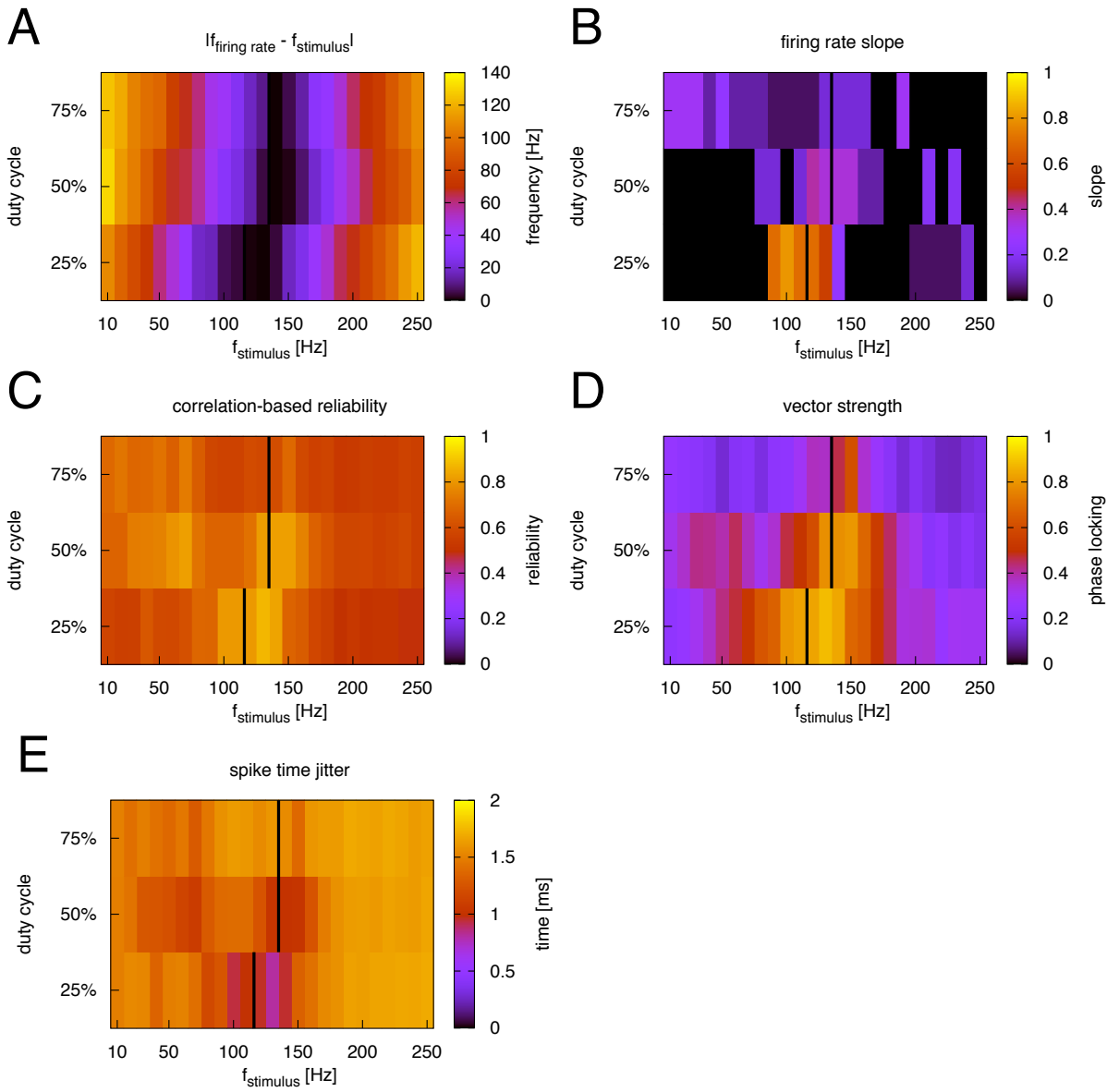

Figure 6.4: Areas of increased reliability and stimulus locking for different duty cycles for a receptor neuron stimulated with a square wave stimulus, with stimulus amplitude $\epsilon_{stimulus} = 6\,\mathrm{dB}$ and target firing rate $= 100\,\mathrm{Hz}$. The average firing rates (indicated with a black bar), calculated over all stimulus frequencies $f_{stimulus}$ for duty cycles of 25, 50 and 75 % were 121 ± 11.1, 140 ± 7.8, and $140 \pm 3.1\,\mathrm{Hz}$, respectively. **(A)** The area where the absolute value of the difference between $f_{firing\ rate}$ and $f_{stimulus}$ is 0, or close to 0, decreases for higher duty cycles. **(B)** Increasing slopes (> 0) of the $f_{firing\ rate}$ vs. $f_{stimulus}$ plot. The data points are smoothed using a median filter with a sliding window containing five data points. The slope increases most prominently around the average firing rate, indicating $1:1$ locking of the firing rate to $f_{stimulus}$. The locking becomes weaker as the duty cycle is increased. **(C)** Correlation-based reliability, using $\sigma = 1.1\,\mathrm{ms}$. Weak increases in reliability can be seen around the average firing rates, and for a duty cycle of 50 % also around the subharmonic of the average firing rate. **(D)** Vector strength, showing maximal phase locking around the average firing rates for low duty cycles. **(E)** Spike time jitter. Low jitter is seen around the average firing rate and decreases for higher duty cycles. For a duty cycle of 50 %, another area of low jitter can be seen around the subharmonic of the average firing rate. (Data from neuron 06-05-09-ab)

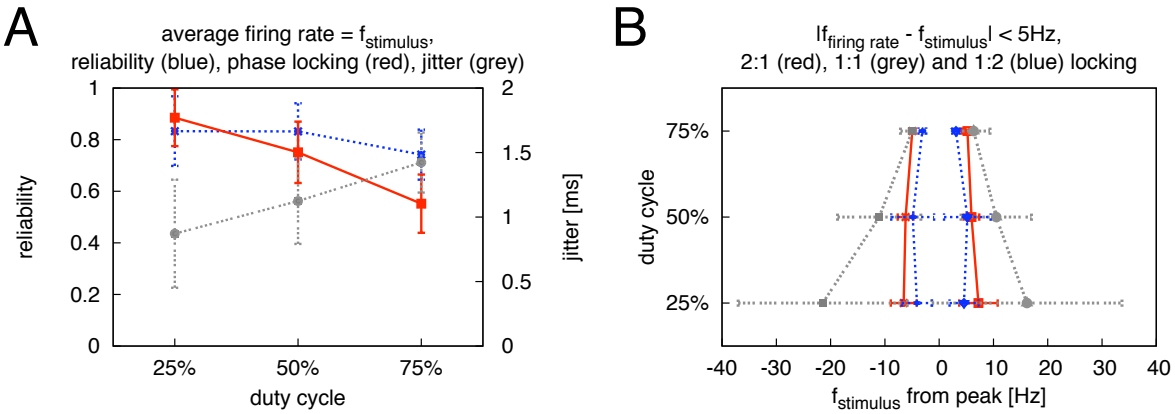

Figure 6.5: **(A)** Reliability values for the three duty cycles at average firing rate = $f_{stimulus}$, averaged over recordings from nine receptor neurons. Blue: correlation-based reliability ($\sigma = 1.1$ ms), red: phase locking, as measured by the vector strength, grey: spike time jitter. The correlation-based reliability remains approximately constant for the three duty cycles. Phase locking, decreases and spike time jitter increases when the duty cycle is increased. **(B)** The range of $f_{stimulus}$, for which $|f_{firing\ rate} - f_{stimulus}| < 5$ Hz, decreases for a $1:1$ ratio between $f_{stimulus}$ and $f_{firing\ rate}$ (grey), as the duty cycle increases, indicating a decrease in stimulus locking. This effect is not seen when the ratio is $2:1$ (red) and $1:2$ (blue). The sample size ranges from $n = 3$ to $n = 9$, with a median of 9.

jitter. For duty cycles of 50 % and 75 %, both measures decrease and increase respectively around the average firing rate (Figures 6.4D and E). All three reliability measures also show a weaker increase in reliability at the subharmonic of the average firing rate at a duty cycle of 50 %, also seen in Figure 6.3F.

The analysis of the reliability of the spike response averaged over the population of neurons presented with square wave stimuli has proven to be challenging. The reason for this is the heterogeneous data, with some data showing prominent peaks while others do not. Therefore, using the same techniques for peak detection presented in Section 5.4 in order to arrive at similar plots as shown in Figures 5.4 and 5.7 did not yield enough samples to determine the range of $f_{stimulus}$ with increased reliability for all three duty cycles.

For this reason, we focus on the case where $f_{stimulus}$ is equal to the average firing rate and analyse the reliability value at this frequency for the three duty cycles (Figure 6.5A). For nine neurons whose recordings were long enough to test all $f_{stimulus}$ for all duty cycles[1], the correlation-based reliability ($\sigma = 1.1$ ms) remains approximately constant for the three duty cycles. However, the vector strength decreases and the spike time jitter increases, when the duty cycle is increased. The decrease in the vector strength, which computes phase locking, can also be seen in the phase histograms (Figure 6.2), where the spikes are distributed over an increasing time window, as the duty cycle is increased. Also note the divergence between the correlation-based reliability and the spike time jitter: For a duty cycle of 75 %, the spike time reliability still remains comparably high, even though the spike time jitter has almost doubled, from 0.8 ms for duty cycles of 25 % to 1.5 ms for duty cycles of 75 %.

The locking of the neuron's firing rate $f_{firing\ rate}$ to $f_{stimulus}$ for the different duty

[1]Of these nine recordings, three where made using 20 Hz increments, instead of the 10 Hz increments used for the other recordings.

cycles was computed as described in Section 5.2. The range of $f_{stimulus}$, for which $|f_{firing\ rate} - f_{stimulus}| < 5\,\text{Hz}$, decreases for increasing duty cycles for the $1:1$ regime, resulting in an inverted 'Arnold tongue-like' structure. The decrease of locking of $f_{firing\ rate}$ to $f_{stimulus}$ shows that the increase in the above-threshold phase has a negative effect on locking, as the stimulus approximates a DC-stimulus which has no modulation. For $2:1$ and $1:2$ ratios between $f_{firing\ rate}$ and $f_{stimulus}$, no locking is seen (Figure 6.5B).

6.3 Comparison to Sine Wave Stimuli

Let us now compare responses elicited by square waves to the responses elicited by sine waves. As outlined in the beginning of this chapter, the slope of a square wave is 90° and independent of the frequency, whereas in a sine wave, the slope increases with frequency. For a duty cycle of 50 %, the fraction of the stimulus cycle which is above-threshold is the same as in a sine wave. Thus, for this duty cycle we now investigate how the spike response to the slope of 90° of the square wave compares to responses for the shallower slopes of a sine wave stimulus. For duty cycles of 25 % and 75 %, we investigate how the responses are influenced by the different length of the above-threshold phases of square waves, compared to sine waves. We evaluate recordings from three different neurons for which both types of stimuli have been tested, and plot reliability values elicited by the square wave stimuli vs. reliability values elicited by the sine wave stimuli for all stimulus frequencies.

Figures 6.6A, C and E show correlation-based reliability values ($\sigma = 1.1\,\text{ms}$) of responses elicited by sine wave stimuli vs. the reliability of responses elicited by square wave stimuli for all $f_{stimulus}$. As the duty cycle increases, the range of reliability values elicited by the square wave stimuli decreases from ≈ 0.75 (25 % duty cycle) to ≈ 0.6 (50 % duty cycle) and ≈ 0.4 (75 % duty cycle), compared to the range of data points of the sine wave stimuli (≈ 0.5). Thus, as duty cycles increase, the correlation-based reliability values become more uniform than for sine wave stimuli.

For the vector strength (Figures 6.6B, D and F), the range of phase locking values elicited by the square wave stimuli also decreases, from ≈ 0.75 (25 % duty cycle) to ≈ 0.6 (50 % duty cycle) and ≈ 0.5 (75 % duty cycle), compared to the range of data points of the sine wave stimuli (≈ 0.55). Moreover, for a duty cycle of 75 %, the phase locking is comparably lower than for sine wave stimuli.

For both reliability measures, the correlation coefficients decrease for higher duty cycles. The p-values for all correlations are < 0.01. From the comparison between the two stimuli, we see that for increasing duty cycles, the correlation-based reliability measure as well as the vector strength are no longer able to resolve peaks, as the range of values for spike time reliability and phase locking decreases. For the vector strength, this decrease is less prominent than for the correlation-based reliability.

6.4 Chapter Summary

We examined the spike time reliability of locust auditory receptor neurons using square wave stimuli, in order to draw comparisons with the results gained from the sine wave stimuli in the previous chapter. We expected to see differences based on the fact that

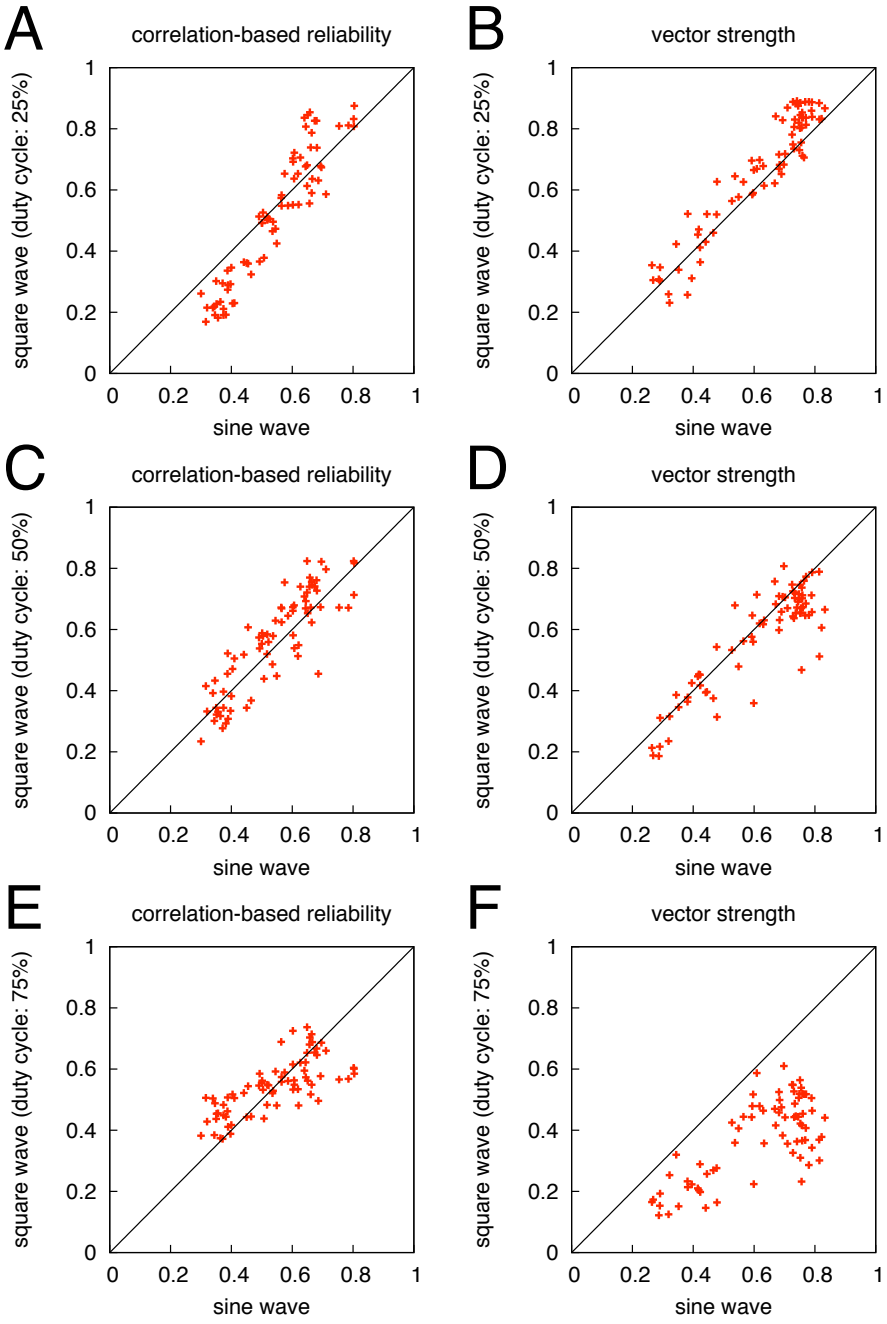

Figure 6.6: Spike response reliability elicited by sine wave stimuli vs. reliability elicited by square wave stimuli, from recordings of three receptor neurons. The target firing rate was 100 Hz and the envelope amplitude was 6 dB. For the correlation-based reliability measure ($\sigma = 1.1$ ms, left plots), the range of reliability values elicited by the square wave stimuli decreases from ≈ 0.75 (25 %) to ≈ 0.6 (50 %) and ≈ 0.4 (75 %), compared to the range of data points of the sine wave stimuli (≈ 0.5). For the vector strength (right plots), the range of reliability values elicited by the square wave stimuli also decreases, from ≈ 0.75 (25 %) to ≈ 0.6 (50 %) and ≈ 0.5 (75 %), compared to the range of data points of the sine wave stimuli (≈ 0.55). For a duty cycle of 75 %, the phase locking is comparably lower than for sine wave stimuli. For both reliability measures, the correlation coefficients decrease for higher duty cycles. The p-values for all correlations are < 0.01. **(A)** Correlation-based reliability, duty cycle = 25 %, correlation coefficient: 0.94. **(B)** Vector strength, duty cycle = 25 %, correlation coefficient: 0.95. **(C)** Correlation-based reliability, duty cycle = 50 %, correlation coefficient: 0.87. **(D)** Vector strength, duty cycle = 50 %, correlation coefficient: 0.89. **(E)** Correlation-based reliability, duty cycle = 75 %, correlation coefficient: 0.74. **(F)** Vector strength, duty cycle = 75 %, correlation coefficient: 0.72.

square waves have slopes of 90°, independent of the frequency; and due to the sharper transitions between the amplitude extremes they resemble the natural communication signals used by grasshoppers and locusts more closely than sine wave stimuli, possibly leading to different responses from these neurons. Additionally, square waves give us the opportunity to control the fraction of the stimulus cycle which is above-threshold by varying the duty cycle.

Stimulating a receptor neuron with a square wave with $f_{stimulus} = 100\,\text{Hz}$ at duty cycles of 25%, 50 % and 75 % shows an increase in the number of spikes as the duty cycle gets longer, reflected in an increase of the firing rate $f_{firing\ rate}$. For a duty cycle of 75 %, the spike trains are more irregular compared to the responses to stimuli with a 25 % and 50 % duty cycle. Interspike interval histograms show the strongest peaks for the 50 % duty cycle (Figure 6.1).

Phase histograms show that almost all spikes are elicited during the 'up'-phases of the square wave stimuli, with a delay of approximately 8 ms. As the duty cycle is increased, the peaks in the phase histograms get broader and less well defined (Figure 6.2).

For a duty cycle of 50 %, $1:1$ locking of $f_{firing\ rate}$ to $f_{stimulus}$ and timing resonance effects were seen around the average firing rate and to a weaker degree also around its subharmonic with the reliability measures. No $1:2$ locking was observed (Figure 6.3).

Expanding the scope by comparing these results with stimuli using duty cycles of 25 % and 75 %, we observed the highest spike response reliability and stimulus locking for duty cycles of 25 %. As the duty cycle was increased to 50 % and 75 %, the values of these measures decreased. Increased reliability around the subharmonic of the average firing rate was weakly present for duty cycles of 50 % (Figure 6.4).

Analysing the reliability values where $f_{stimulus}$ is equal to the average firing rate for the three duty cycles averaged over the population of all recorded neurons, the correlation-based reliability remained approximately constant, while the vector strength decreased and the spike time jitter increased for higher duty cycles (Figure 6.5A). The range of $f_{stimulus}$, for which the neuron locked on decreased for increasing duty cycles for the $1:1$ ratio between $f_{firing\ rate}$ and $f_{stimulus}$. For $2:1$ and $1:2$ ratios, no effect is seen (Figure 6.5B).

When comparing responses elicited by square wave stimuli to responses elicited by sine wave stimuli, the correlation-based reliability measure yielded a smaller range of reliability values as the duty cycles decreased to 75 % and peaks were less prominent (Figures 6.6A, C and E). The phase locking, as measured by the vector strength also decreased for longer duty cycles, and it was comparably lower for the square wave stimulus than for the sine wave stimulus (Figures 6.6B, D and F).

Chapter 7

Discussion and Outlook

In this thesis, we investigated the phenomenon of neural timing resonance in auditory receptor neurons of locusts. Neurons are known to have increased spike time reliability around their resonance frequency – their firing rate – (Knight, 1972; Hunter *et al.*, 1998; Fellous *et al.*, 2000), and at harmonics thereof (Beierholm *et al.*, 2001).

This phenomenon is often analysed using direct current stimulation of a neuron's membrane potential using intracellular current injection. The model system in this thesis, the locust *Locusta migratoria*, allows us to use an in-vivo preparation, using acoustic stimulation and thus a more natural form of stimulation. Also, in the experiments with direct current stimulation, the target firing rate was not varied. In our system however, the firing rate is not an intrinsic property of the neuron, but changes with the intensity of the stimulus. Since the firing rate is the neuron's resonance frequency, our model system thus enabled us to use different resonance frequencies.

Neural timing resonance allows a neuron to produce more reliably timed spikes and is therefore important for transmitting information effectively and efficiently. This is especially important for neurons at the periphery of a nervous system, such as receptor neurons, since information that is lost at the beginning is not available to subsequent stages. Hunter *et al.* (1998) suggested that timing resonance may be useful to switch a neuron from a mode where only the firing rate is reliable to a mode where the spike times are reliable as well, by moving the firing rate into a range where the frequency content of the stimulus influences reliability. Thus the same neuron may be able to be either a rate or a spike time encoder.

In our study, we have stimulated locust auditory receptor neurons with different types of acoustic stimuli (sine waves, square waves and white noise) while performing intracellular recordings from the axons of these neurons. Particularly long intracellular recordings of up to 50 min were necessary in order to test all different stimulus parameters in one neuron.

We showed that there is $1:1$ locking between the firing rate of receptor neurons and the stimulus frequency, revealing an Arnold tongue structure for higher stimulus amplitudes. Weak increased reliability was found in the majority of cells at the lower harmonic (around a $2:1$ ratio between firing rate and stimulus frequency), too, but when averaged over the population of all recorded neurons, the effect is not significant. It may prove insightful to revisit this data by using different peak detection algorithms or by increasing the resolution – the increments of the values of the stimulus frequencies – at the

frequencies where secondary harmonics are to be expected, to better quantify the timing resonance effect for the lower harmonic. The disadvantage of this is that the duration of the stimulus protocol will increase further, making it more difficult to complete it during an intracellular recording.

2 : 1 locking of the firing rate to the stimulus frequency was not observed, and for stimulus frequencies with a ratio of 1 : 2 between stimulus frequency and firing rate, neither increased reliability nor locking was observed. We could show that locking of the firing rate to the stimulus frequency is correlated with the increased reliability for ratios of 1 : 1.

We then tested different firing rates at a constant stimulus amplitude to investigate if timing resonance is dependent on the firing rate of the neuron. We saw that the range of stimulus frequencies, for which spike time reliability and phase locking is increased, widens, when the target firing rates are increased, the same is observed for the locking of the firing rate to the stimulus, when the ratio between the two parameters is 1 : 1.

Sine wave stimuli were also used in a study by Beierholm *et al.* (2001) on interneurons of the isolated spinal cord of newborn rats to investigate neural timing resonance. The stimuli were varied in frequency and amplitude. As a result, two increases in spike time reliability were seen, when sine wave frequencies and amplitudes were chosen which allowed these interneurons to either lock onto the stimulus with two spikes per stimulus cycle (2 : 1 locking), or with one spike per stimulus cycle (1 : 1 locking), thus revealing a timing resonance frequency and its lower harmonic at half of the timing resonance frequency.

Hunter *et al.* (1998) measured the reliability of spike timing in slowly adapting motoneurons in *Aplysia* by using sine wave stimuli and white noise (discussed below). Also in this study, the spike time reliability was almost twice as high for a 1 : 1 ratio between stimulus frequency and firing rate, compared to a ratio of 0.65, which led to an irregular response pattern.

The receptor neurons in this thesis are located at the periphery, as opposed to the interneurons studied by in Beierholm *et al.* (2001) and the motoneurons studied by Hunter *et al.* (1998). Receptor neurons need to pass on sensory information with high fidelity, while central neurons show spike responses with a much higher variability. This increase in variability, from the periphery to higher stages of processing has been demonstrated for the auditory system of locusts using simultaneous recordings from receptor neurons and segmental and ascending interneurons in the metathoracic ganglion (Vogel *et al.*, 2005). Increasing variability was also found in the visual system of cats, when recording simultaneously from retinal ganglion cells, relay cells from the LGN (lateral geniculate nucleus) and from cells in the primary visual cortex (Kara *et al.*, 2000). It is therefore intriguing that we were able to find these timing resonance effects in our model system, too, despite the differences in stimulation and preparation.

Bush and Schul (2006) showed that resonance properties may also work on a behavioural level: The phonotaxis response in bushcrickets is also elicited for the lower harmonic of the pulse rate that elicits the strongest phonotaxis response. A modeling study demonstrated that this behaviour could in principle be elicited using a single neuron (Webb *et al.*, 2007). Since we have shown resonant properties in single neurons, our study offers evidence that this behaviour could in principle originate from response properties of a single receptor neuron.

What is the reason for finding locking and increased reliability for 1 : 1 ratios, in some cases for 2 : 1 ratios, but not for 1 : 2 ratios? Since the intensity of the stimulus is encoded with higher firing rates, it makes sense for the locust to encode this information with the highest reliability, and one might speculate whether there might be an active mechanism of the neuron at play, which suppresses the resonances at lower and higher harmonics in order to suppress a potential source of error. A modeling study showed that indeed harmonics of the resonance frequency are weaker (Tiesinga, 2002), and this seems to be confirmed in experimental (Beierholm *et al.*, 2001) and behavioural findings (Bush and Schul, 2006). As for the absence of locking and increased reliability for 1 : 2 ratios, Prinz and Ronacher (2002) found that sinusoidal modulations of more than 300 Hz are unresolvable at 20° Celsius, but not at 30° Celsius, implicating a possible influence of temperature at which our experiments took place. However, we used a target firing rate of 100 Hz in most experiments and thus expected increased reliability for 1 : 2 locking at a stimulus frequency of 200 Hz, e.g. at a significantly lower frequency than 300 Hz.

Regarding the exact mechanism of frequency preference, Schreiber *et al.* (2004a) showed that increased reliability for stimulus frequencies around the firing rate of cortical neurons of rats can be regulated by varying the density of certain ion channels, which has also been suggested by Hudspeth (1985) for the hair cells of the bull frog *Lithobates catesbeianus*. Since ion channel characteristics of locust auditory receptor neurons have not yet been characterized, it remains speculative whether the same mechanism is at play in these neurons.

From our findings with sine wave stimuli, we have seen that the spike time reliability for a given firing rate of the neuron is frequency-dependent. Therefore we investigated if this parameter also depends on the frequency content of white noise stimuli. However, we did not find significant changes in reliability when presenting different white noise stimuli to receptor neurons, regardless of whether frequencies at or close to the neuron's firing rate were present or not.

Hunter *et al.* (1998) not only used sinusoidal stimuli (discussed above), but also white noise stimuli to measure the reliability of spike timing in *Aplysia* motoneurons. They demonstrated that spike time reliability in response to an aperiodic stimulus depended on the frequency content and the modulation amplitude of the stimulus (applied via current injection), as well as on the firing rate of the neuron. For small stimulus amplitudes, the reliability decreased when the frequencies around the firing rate were absent from the frequency content of the white noise, thus implying a timing resonance phenomenon for the mechanism of spike time reliability.

The reasons for the differences between our findings with white noise stimuli and the results of Hunter *et al.* (1998) remain unclear, but may lie in the stimulus type or one of its parameter values, rather than the different system or the stimulus application, due to the consistency of the results with sine wave stimuli as well as with the results from Beierholm *et al.* (2001). For example, Szücs *et al.* (2004) reproduced the findings of Hunter *et al.* (1998) using neurons of the feeding network of the pond snail *Lymnaea stagnalis*, and were able to attain the same levels of precision and reliability by using amplitudes which were smaller by a factor of 10. The difference is probably due to the different biophysical properties of the neurons of the two species, with the *Lymnaea* neurons being less than half the size of the *Aplysia* neurons.

On the other hand, the outcome can even be different in the same experimental

paradigm: Haas and White (2002) applied white noise stimuli to stellate cells in the medial entorhinal cortex of rats and found no subthreshold resonance effects for this stimulus type, while Schreiber *et al.* (2004b) also studied the same cell type with white noise stimuli and reported subthreshold resonance. The reason for the conflicting outcomes of these two studies remains unclear (Oppermann, 2006, suggested that different threshold regimes were examined), but illustrates the variability of experimental results, suggesting that effects not yet fully understood, or subtle differences in experimental techniques may be responsible for the difference.

A possibility to reconcile the findings from the white noise stimuli with the results from the sine wave stimuli is offered by a new stimulus protocol that might lead to interesting insights: Starting out with a sine wave stimulus and increasing the frequency content of the spectrum until the stimulus resembles white noise. Looking at the Fourier spectrum, the stimulus will start with a single peak, since it only includes one frequency, chosen to be identical to the firing rate of the neuron. As more frequencies are added, the spectrum expands, turning into a narrow-band stimulus and ultimately into a white noise stimulus. Investigating at what width of the frequency spectrum the timing resonance effect decreases, and if it is a gradual decrease or not, may help to understand the different outcome of the two stimulus protocols regarding spike time reliability and stimulus locking.

For square wave stimuli, we found that increasing the duty cycle increased the number of spikes and thus the firing rate, and the spike trains became more irregular. At stimulus frequencies equal to the average firing rate for the three duty cycles, the correlation-based reliability remained approximately constant, while the phase locking of the neuron to the stimulus and the spike time jitter increased for higher duty cycles. For a $1:1$ ratio between firing rate and stimulus frequency, the range of stimulus frequencies, for which the neuron locked on to the stimulus, decreased for increasing duty cycles. For $2:1$ and $1:2$ ratios, no effect was seen.

The reliability of responses to square wave stimuli with a duty cycle of 50 % is approximately comparable to that of responses to sine wave stimuli with the same stimulus frequencies (correlation-based reliability). For duty cycles of 25 %, a broader range of spike time reliabilities was elicited, and for a duty cycle of 75 %, the range was narrower than for sine wave stimuli. Phase locking decreased for increasing duty cycles of the square wave, compared to the sine wave stimulus.

The decrease of spike timing precision, as the above-threshold fraction of a stimulus is increased, has also been observed in layer 5 neurons in rat cortical slices: In response to repeated current injections of a constant stimulus, spike timing precision was measured and the first few spikes after stimulus onset were precisely timed, whereas the later spikes exhibited significant timing jitter across trials (Mainen and Sejnowski, 1995). The stimuli in this study had only an onset, while the square wave stimuli in this thesis have on- and offset. A decrease in spike time precision has also been confirmed in a modeling study, simulating cortical neurons (Gutkin *et al.*, 2003). On a behavioural level, the steepness of ramps has been found to play an important role in the phonotaxis behaviour in *Chorthippus biguttulus*: Sound pulses with rectangular shape elicit weaker responses in males than sound pulses with ramps rising gradually over 3 ms and more (von Helversen, 1993). For future experiments, decreasing the amplitude of the square wave stimulus as the duty cycle is increased to keep the number of elicited spikes constant will allow to

isolate the effect of the stimulus shape from the firing rate.

In closing, let us remind ourselves of the two other types of resonance presented in the introductory part of this work: Subthreshold resonance and stochastic resonance. It is unlikely that these two phenomena work in complete isolation from each other in a nervous system, and Reinker *et al.* (2003) have found interactions between the two in models and in experiments using cortical neurons of rats. The challenge for future work will be to elucidate how timing resonance interacts with these two other types of resonance, or if perhaps timing resonance is a consequence of a combination of subthreshold and stochastic resonance.

Bibliography

Balakrishnan, R., von Helversen, D., and von Helversen, O. (2001). Song pattern recognition in the grasshopper *Chorthippus biguttulus*: the mechanism of syllable onset and offset detection. *Journal of Comparative Physiology A*, **1**87, 255 – 264.

Beierholm, U., Nielsen, C. D., Ryge, J., Alstrom, P., and Kiehn, O. (2001). Characterization of reliability of spike timing in spinal interneurons during oscillating inputs. *Journal of Neurophysiology*, **8**6, 1858 – 1868.

Benda, J., Longtin, A., and Maler, L. (2006). A synchronization-desynchronization code for natural communication signals. *Neuron*, **5**2(2), 347 – 358.

Bennet-Clark, H. C. (2003). Wing resonances in the Australian field cricket *Teleogryllus oceanicus*. *The Journal of Experimental Biology*, **2**06, 1479 – 1496.

Berger, H. (1929). Über das Elektroenkephalogramm des Menschen. *Archiv für Psychiatrie und Nervenkrankheiten*, **8**7, 527 – 570.

Billah, K. Y. and Scanlan, R. H. (1991). Resonance, Tacoma Narrows bridge failure and undergraduate physics textbooks. *American Journal of Physics*, **5**9(2), 118 – 124.

Billimoria, C. P., DiCaprio, R. A., Birmingham, J. T., Abbott, L. F., and Marder, E. (2006). Neuromodulation of spike-timing precision in sensory neurons. *The Journal of Neuroscience*, **2**6(22), 5910 – 5919.

Breckow, J. and Sippel, M. (1985). Mechanics of the transduction of sound in the tympanal organ of adults and larvae of locusts. *Journal of Comparative Physiology A*, **1**57, 619 – 629.

Buck, J. and Buck, E. (1968). Mechanism of rhythmic synchronous flashing of fireflies. *Science*, **1**59, 1319 – 1327.

Bush, S. L. and Schul, J. (2006). Pulse-rate recognition in an insect: evidence of a role for oscillatory neurons. *Journal of Comparative Physiology A*, **1**92, 113 – 121.

Carr, C. and Konishi, M. (1990). A circuit for the detection of interaural time difference in the brain stem of the barn owl. *Journal of Neuroscience*, **1**0, 3227–3246.

Carr, C. E. (1993). Processing of temporal information in the brain. *Annual Review Neuroscience*, **1**6, 223 – 243.

Cartwright, J. H. E., Eguiluz, V. M., Hernandez-Garcia, E., and Piro, O. (1999). Dynamics of elastic excitable media. *International Journal of Bifurcation and Chaos*, **9**(11), 2197 – 2202.

Fellous, J.-M., Houweling, A. R., Modi, R. H., Rao, R. P. N., Tiesinga, P. H. E., and Sejnowski, T. J. (2000). Frequency dependence of spike-timing reliability in cortical pyramidal cells and interneurons. *Journal of Neurophysiology*, pages 1782 – 1786.

FitzHugh, R. (1955). Mathematical models of threshold phenomena in the nerve membrane. *Bulletin of mathematical biophysics*, **1**7, 257 – 277.

Goldberg, J. and Brown, P. (1969). Response of binaural neurons of dog superior olivary complex to dichotic tonal stimuli: Some physiological mechanisms of sound localization. *Journal of Neurophysiology*, **3**2(4), 613 – 636.

Gollisch, T. (2004). *The Auditory Transduction Chain: Identification of the functional modules involved in sound encoding*. Ph.D. thesis, Humboldt Universität zu Berlin.

Gray, E. G. (1960). The fine structure of the insect ear. *Philosophical Transactions of the Royal Society of London. Series B, Biological Sciences*, **2**43(700), 75 – 94.

Gu, G., Caldwell, G. A., and Chalfie, M. (1996). Genetic interactions affecting touch sensitivity in *Caenorhabditis elegans*. *Proc. Natl. Acad. Sci. USA*, **9**3, 6577 – 6582.

Gutkin, B., Ermentrout, G. B., and Rudolph, M. (2003). Spike generating dynamics and the conditions for spike-time precision in cortical neurons. *Journal of Computational Neuroscience*, **1**5, 91 – 103.

Haas, J. and White, J. (2002). Frequency selectivity of layer II stellate cells in the medial entorhinal cortex. *Journal of Neurophysiology*, **8**8, 2422 – 2429.

Hough, S. E., Friberg, P. A., Busby, R., Field, E. F., Jacob, K., and Borcherdt, R. D. (1990). Sediment-induced amplification and the collapse of the Nimitz freeway. *Nature*, **3**44, 853 – 855.

Hoy, R. R. and Robert, D. (1996). Tympanal hearing in insects. *Annual Reviews Entomology*, **4**1, 433 – 450.

Hudspeth, A. J. (1985). The cellular basis of hearing: The biophysics of hair cells. *Science*, **2**30, 745 – 752.

Hudspeth, A. J. and Logothetis, N. K. (2000). Sensory systems. *Current Opinion in Neurobiology*, **1**0, 631 – 641.

Hunter, J., Milton, J., and Cowan, J. (1998). Resonance effect for neural spike time reliability. *Journal of Physiology*, **8**0, 1427 – 1438.

Hutcheon, B. and Yarom, Y. (2000). Resonance, oscillation, and the intrinsic frequency preferences of neurons. *Trends Neurosci.*, **2**3, 216 – 222.

Izhikevich, E. M. (2001). Resonate-and-fire neurons. *Neural Networks*, **1**4, 883 – 894.

Jacobs, W. (1953). *Verhaltensbiologische Studien an Feldheuschrecken*, chapter XI.2, pages pp. 88 – 89. Paul Parey in Berlin + Hamburg. Beiheft 1 zur Zeitschrift für Tierpsychologie.

Jeffress, L. (1948). A place theory for sound localization. *Journal of Comparative and Physiological Psychology*, **4**1, 35–39.

Kara, P., Reinagel, P., and Reid, R. C. (2000). Low response variability in simultaneously recorded retinal, thalamic, and cortical neurons. *Neuron*, **2**7, 635 – 646.

Klappert, K. and Reinhold, K. (2003). Acoustic preference functions and sexual selection on the male calling song in the grasshopper *Chorthippus biguttulus*. *Animal Behaviour*, **6**5, 225 – 233.

Knight, B. (1972). The relationship between the firing rate of a single neuron and the level of activity in a population of neurons. *Journal of General Physiology*, **5**9, 767 – 778.

Kosko, B. and Mitaim, S. (2004). Robust stochastic resonance for simple threshold neurons. *Physical Review E*, **7**0, 031911–1 – 031911–10.

Lang, F. (2000). Acoustic communication distances of a gomphorine grasshopper. *The International Journal of Animal Sound and its Recording*, **1**0, 233 – 258.

Machens, C., Schütze, H., Franz, A., Kolesnikova, O., Stemmler, M., Ronacher, B., and Herz, A. V. M. (2003). Single auditory neurons rapidly discriminate conspecific communication signals. *Nature Neuroscience*, **6**(4), 341 – 342.

Mainen, Z. F. and Sejnowski, T. J. (1995). Reliability of spike timing in neocortical neurons. *Science*, **2**68, 1503 – 1506.

Meyer, J. and Hedwig, B. (1995). The influence of tracheal pressure changes on the responses of the tympanal membrane and auditory receptors in the locust *Locusta migratoria* l. *The Journal of Experimental Biology*, **1**98, 1327 – 1339.

Michelsen, A. (1971a). The physiology of the locust ear - i. frequency sensitivity of single cells in the isolated ear. *Z. vergl. Pysiologie*, **7**1, 49 – 62.

Michelsen, A. (1971b). The physiology of the locust ear - ii. frequency discrimination based upon resonances. *Z. vergl. Pysiologie*, **7**1, 63 – 101.

Miller, L. (1970). Structure of the green lacewing tympanal organ (*Chrysopa carnea*, Neuroptera). *Journal of Morphology*, **1**31, 359 – 382.

Møller, A. R. (2000). *Hearing: Its Physiology and Pathophysiology*, chapter 3, pages 71 – 93. Academic Press, San Diego.

Moss, F., Lawrence, W. M., and Walter, S. G. (2004). Stochastic resonance and sensory information processing: a tutorial and review. *Clinical Neurophysiology*, **1**15, 267 – 281.

Neda, Z., Ravasz, E., Brechet, Y., Vicsek, T., and Barabasy, A.-L. (2000). Tumultuous applause can transform itself into waves of synchronized clapping. *Nature*, **4**03(6772), 849 – 850.

Oppermann, T. (2006). *Rhythmic activity in stellate cells: The underlying dynamical structure and its analysis*. Ph.D. thesis, Humboldt Universität zu Berlin.

Pikovsky, A., Rosenblum, M., and Kurths, J. (2001a). *Synchronization: A universal concept in nonlinear sciences*, chapter Appendix A, pages 357 – 361. Cambridge Nonlinear Science Series 12. An english translation of a personal letter from Christiaan Huygens to his Father, Constantyn Huygens, written in the february of 1665.

Pikovsky, A., Rosenblum, M., and Kurths, J. (2001b). *Synchronization: A universal concept in nonlinear sciences*, chapter 2 and 3, pages 27 – 101. Cambridge Nonlinear Science Series 12.

Popov, A. V. and Svetlogorskaya, I. D. (1971). Receptor interaction and ultrastructural organization of the auditory nerve in *Locusta migratoria*. *Zhurnal Evolyutsionnoi Biokhimii i Fiziologii*, **7**(5), 516 – 521.

Prinz, P. and Ronacher, B. (2002). Temporal modulation transfer functions in auditory receptor fibres of the locust (*Locusta migratoria* l.). *Journal of Comparative Physiology A*, **1**88, 577 – 587.

Reinker, S., Puil, E., and Miura, R. M. (2003). Membrane resonance and stochastic resonance modulate firing patterns of thalamocortical neurons. *Journal of Computational Neuroscience*, **1**6, 15 – 25.

Rieke, F., Warland, D., de Ruyter van Steveninck, R., and Bialek, W. (1997). *Spikes: Exploring the neural code*, chapter 2, pages 19 – 99. The MIT press.

Rokem, A., Watzl, S., Gollisch, T., Stemmler, M., Herz, A. V. M., and Samengo, I. (2006). Spike-timing precision underlies the coding efficienc of auditory receptor neurons. *Journal of Neurophysiology*, **9**5, 2541 – 2552.

Römer, H. (1985). Anatomical representation of frequency and intensity in the auditory system of Orthoptera. In K. Kalmring and N. Elsner, editors, *Acoustic and Vibrational Communication in Insects, Proceedings XVII International Congress of Entomology*, pages 25 – 32. Paul Parey Berlin.

Ronacher, B. and Stumpner, A. (1988). Filtering of behaviourally relevant temporal parameters of a grasshopper's song by an auditory interneuron. *Journal of Comparative Physiology A*, **1**63, 517 – 523.

Schreiber, S., Fellous, J.-M., Whitmer, D., Tiesinga, P., and Sejnowski, T. (2003). A new correlation based measure of spike timing reliability. *Neurocomputing*, **5**2 - 54, 925 – 931.

Schreiber, S., Fellous, J.-M., Tiesinga, P., and Sejnowski, T. J. (2004a). Influence of ionic conductances on spike timing reliability of cortical neurons for suprathreshold rhythmic inputs. *Journal of Neurophysiology*, **9**1, 194 – 205.

Schreiber, S., Erchova, I., Heinemann, U., and Herz, A. V. M. (2004b). Subthreshold resonance explains the frequency-dependent integration of periodic as well as random stimuli in the entorhinal cortex. *Journal of Neurophysiology*, **9**2, 408 – 415.

Shadlen, M. N. and Newsome, W. T. (1994). Noise, neural codes and cortical organization. *Current Opinion in Neurobiology*, **4**, 569 – 579.

Stacey, W. and Durand, D. (2000). Stochastic resonance improves signal detection in hippocampal CA1 neurons. *Journal of Neurophysiology*, **8**3(3), 1394 – 1402.

Stemmler, M. (1996). A single spike suffices: the simplest form of stochastic resonance. *Computation in Neural Systems*, **7**, 687 – 716.

Stephen, R. O. and Bennet-Clark, H.-C. (1982). The anatomical and mechanical basis of stimulation and frequency analysis in the locust ear. *Journal of Experimental Biology*, **9**9, 279 – 314.

Steriade, M. (2006). Grouping of brain rhythms in corticothalamic systems. *Neuroscience*, **1**37, 1087 – 1106.

Stumpner, A. and von Helversen, D. (2001). Evolution and function of auditory systems in insects. *Naturwissenschaften*, **8**8, 159 – 177.

Szücs, A., Vehovsky, A., Molnar, G., Pinto, R. D., and Abarbanel, H. D. I. (2004). Reliability and precision of neural spike timing : Simulation of spectrally broadband synaptic inputs. *Neuroscience*, **1**26, 1063 – 1073.

Tiesinga, P. E. H. (2002). Precision and reliability of periodically and quasiperiodically driven integrate and fire neurons. *Physical Review E*, **6**5, 041913–1 – 041913–13.

Todd, B. S. and Andrews, D. C. (1999). The identification of peaks in physiological systems. *Computers and Biomedical Research*, **3**2, 322 – 335.

Uhlhaas, P. J. and Singer, W. (2006). Neural synchrony in brain disorders: relevance for cognitive dysfunctions and pathophysiology. *Neuron*, **5**2(1), 155 – 168.

Vogel, A., Hennig, R. M., and Ronacher, B. (2005). Increase of neuronal response variability at higher processing levels as revealed by simultaneous recordings. *Journal of Neurophysiology*, **9**3, 3548 – 3559.

von Helversen, D. (1972). Gesang des Männchens und Lautschema des Weibchens bei der Feldheuschrecke *Chorthippus biguttulus* (Orthoptera, Acrididae). *Journal of Comparative Physiology*, **8**1, 381 – 422.

von Helversen, D. (1993). 'Absolute steepness' of ramps as an essential cue for auditory pattern recognition by a grasshopper (Orthoptera; Acrididae: *Chorthippus biguttulus* l.). *Journal of Comparative Physiology A*, **1**72, 633 – 639.

von Helversen, D. and von Helversen, O. (1975). Verhaltensgenetische Untersuchungen am akustischen Kommunikationssystem der Feldheuschrecken (Orthoptera, Acrididae), i. Der Gesang von Artbastarden zwischen *Chorthippus biguttulus* und *Ch. mollis*. *Journal of Comparative Physiology*, **1**04, 273 – 299.

Webb, B., Wessnitzer, J., Bush, S., Schul, J., Buchli, J., and Ijspeert, A. (2007). Resonant neurons and bushcricket behaviour. *Journal of Comparative Physiology A*, **1**93, 285 – 288.

Yack, J. and Fullard, J. (1993). What is an insect ear? *Annals of the Entomological Society of America*, **8**6(6), 677 – 682.

Appendix

Ringer Solution

The Ringer solution was produced using 500 ml aqua dest. and dissolving the following salts:

NaCl	4.3 g
KaCl	0.37 g
CaCl	0.29 g

1.19 g HEPES (4-(2-hydroxyethyl)-1-piperazineethanesulfonic acid) was added as an organic buffer and the solution was stabilised with 0.05 – 0.07 g NaOH to a pH of 7.2. The solution was stored at 4° Celsius.

Electrodes

Electrode resistance values were usually around 30 – 70 MΩ. The parameter settings for the electrode puller varied over the course of two years of experimentation. Below is an example set of parameters which provided useful electrodes for a period of several weeks:

Heat	330
Pressure	500
Pull	125
Velocity	125
Time	175

Acknowledgements

During my PhD studies I enjoyed the support of the Institute for Theoretical Biology at the Humboldt Universität zu Berlin (ITB).
Foremost, I would like to thank my advisor Andreas Herz for his support and encouragement, and for giving me the opportunity to work in his group. By bringing together scientists with diverse backgrounds and fields of expertise, he created an inspiring environment at the ITB, allowing me to profit from his group's rich expertise on many fields of computational neuroscience.
In addition, my thanks go to the Graduiertenkolleg 120, "Signalketten in lebenden Systemen", and 238, "Schadensmechanismen im Nervensystem", which supported me during most of my work at the ITB.
I am also greatly indebted to Jan Benda. Without Jan's profound knowledge covering experiments, theory, and the intricacies of data analysis, as well as his steadfast optimism, I could not have succeeded in finishing this thesis. I would also like to thank Martin Stemmler for his mathematical support. Several other people have influenced this thesis with their input given in numerous discussions. Bernd Ronacher and his group were a great source of knowledge, and I am especially indebted to Matthias Henning for sharing his vast knowledge of all things electrophysiological. Input and comments from Susanne Schreiber, Roland Schaette and Tim Oppermann were always greatly appreciated.
I would also like to thank the following people who either helped me with setup hardware or MatLab problems, spent a coffee break with me or invited me for dinner, or just cracked the right joke at the right moment: Peter Appleby, Pietro Berkes, Branka and Samuel Bernard, Roberto Fernandez-Galan, Matthias Flor, Mathias Franzius, Florian Geier, Edward Hagen, Aki Naito, Hartmut Schütze, Henning Sprekeler, and Arndt Telschow.
Last but not least, I would like to thank my parents for their love and continual support. This thesis is dedicated to them.

Figure Acknowledgements

The permission to adapt and reproduce the following images and figures is gratefully acknowledged:

Cartoon by Randall Munroe, taken from http://xkcd.com/ and used under the creative commons Attribution-NonCommercial 2.5 license; Figure 3.1 from Balakrishnan *et al.* (2001), with kind permission from Springer Science+Business Media; Figure 3.2 from Gollisch (2004), with kind permission from Tim Gollisch; Figures 3.3 and 3.4 from Gray (1960), with kind permission from Royal Society Publishing.

Deutsche Zusammenfassung

Diese Dissertation befasst sich mit dem Einfluss von Resonanz und Synchronisation auf die Zuverlässigkeit der Antwort von Rezeptorneuronen. Zuverlässigkeit von individuellen Neuronen an der Peripherie eines Nervensystems, beispielsweise sensorische Neurone, ist äusserst wichtig für höhere Stufen der Verarbeitung, um anhand von präzisen Informationen Entscheidungen zu treffen, welche das Überleben des Individuums sichern. In Kapitel 1 und 2 beschäftigen wir uns deshalb mit Synchronisation, Resonanz und insbesondere Resonanz in neuronalen Systemen.
Resonanz ist die Eigenschaft eines Systems, für eine bestimmte Frequenz – der Resonanzfrequenz des Systems – mit maximaler Amplitude zu schwingen. Es möglich, daß mehr als eine Resonanzfrequenz vorhanden ist: üblicherweise bringen auch die Harmonischen der stärksten Resonanzfrequenz das System dazu, zu oszillieren. Komplexe Anregung wie zum Beispiel breitbandiges Rauschen kann auch dazu führen, daß das System alle Frequenzen außer einem Frequenzband um die Resonanzfrequenz herum herausfiltert.
Verschiedene Formen von Resonanz können dazu führen, daß sich die Zuverlässigkeit eines Neurons erhöht. Unterschwellige Resonanz tritt ein, wenn ein unterschwelliges Eingangssignal, welches eine bestimmte Frequenz enthält, auf ein Neuron angewandt wird, und die Amplitude des Membranpotentials des Neurons zu schwingen anfängt. Stochastische Resonanz beschreibt ein Phänomen, bei dem die Detektion eines unterschwelligen Eingangssignals durch die Kombination mit Rauschen erleichtert wird. Es existiert eine optimale Rauschintensität, welche dem Eingangssignal erlaubt, die Schwelle zu überschreiten, aber das Rauschen ist nicht so groß, als daß es das Signal überlagert. Die dritte Form von Resonanz ist neuronale Timing-Resonanz: diese kommt vor, wenn ein Neuron für Signale um seine Resonanzfrequenz – die Feuerrate des Neurons – enthalten, Aktionspotentiale mit höherer zeitlicher Präzision produziert, als für andere Frequenzen.
Auch bei Synchronisation können mehrere Frequenzen vorhanden sein, für die zwei oder mehr Oszillatoren aufgrund einer schwachen Interaktion ihre individuellen Schwingungsfrequenzen an eine gemeinsame Frequenz angleichen. Dieser Synchronisationseffekt wird als Phasen-Kopplung bezeichnet, und ob er stattfindet, hängt von zwei Faktoren ab: der Kopplungsstärke (der Stärke der Interaktion zwischen den Oszillatoren) und der Differenz zwischen den natürlichen Frequenzen der Oszillatoren. Falls diese Differenz nicht zu hoch ist, gleichen sich die beiden Frequenzen an und werden so synchron. Für steigende Amplituden der externen Antriebskraft eines Oszillators, welche auf einen anderen Oszillator wirkt, wird die Frequenzspanne, in der Synchronizität auftritt, breiter, und eine Region entsteht, die als Arnold-Zunge bezeichnet wird.
Wenn die Synchronisation eines Oszillators mit einer externen Antriebskraft durch eine Sequenz von Pulsen geschieht, können komplexere Formen von Synchronisation entstehen. Wenn zum Beispiel jeder zweite Puls ausgelassen wird, die Pulse aber eine Amplitude

haben, welche groß genug ist, um den fehlenden Puls zu kompensieren, dann kann ein Oszillator mit einer externen Antriebskraft, deren Frequenz halb so hoch ist wie die Frequenz des Oszillators, angetrieben werden. Ein solches Verhältnis wird Synchronisation der Ordnung 2 : 1 genannt. Es können Synchronisationsverhältnisse mit arbiträrer Ordung $n{:}m$ (n oszillatorische Zyklen für m Pulse, wobei n und m ganzzahlig sind) beobachtet werden, wodurch Arnold-Zungen an den entsprechenden Stellen entstehen.

Um die Präzision und die Zuverlässigkeit von Aktionspotentialen (Spikes) in Neuronen zu bewerten, werden drei verschiedene Zuverlässigkeitsmaße verwendet: Die Korrelationsbasierte Zuverlässigkeit untersucht die Zuverlässigkeit basierend auf der paarweisen Kreuzkorrelation zwischen den individuellen Spike-Trains, gefiltert mit einem Gauss-Kernel. Das Maß kann die Werte 0 (niedrige Zuverlässigkeit) oder 1 (hohe Zuverlässigkeit) annehmen. Das zweite Maß, die Vektorstärke, misst das Phasen-Kopplung bzw. die Synchronisation an einen periodischen Stimulus. Die Werte können zwischen 0 (keine Synchronisation) und 1 (perfekte Synchronisation) liegen. Das dritte Maß misst den Jitter der Spike-Zeiten in Millisekunden.

In Kapitel 3 und 4 werden das Modellsystem und die experimentellen Techniken vorgestellt. Wir untersuchten Rezeptorneurone im Ohr der Heuschrecke *Locusta migratoria*. In vielen Spezies der Ordnung *Orthoptera*, zu welcher *Locusta migratoria* gehört, spielt die akustische Kommunikation eine wichtige Rolle für das Paarungsverhalten. Arten dieser Ordnung können akustische Signale, sogenannte 'Gesänge', produzieren, indem sie z.B. eine gezahnte Leiste auf der Innenseite ihres Hinterbeines gegen eine hervorstehende Kante des Flügels reiben. Die Produktion und Erkennung dieser konspezifischen Gesänge sind aus zwei Gründen wichtig: erstens sind sie eine wichtige Barriere gegen Hybridisierung, und zweitens beinhaltet die Struktur dieses Gesanges Information über den Zustand des Senders, und damit indirekt über seine Fitness. Das Ohr der Heurschrecke enthält ca. 60 – 80 Rezeptorneurone, von deren Axonen intrazelluläre elektrophysiologische Ableitungen gemacht wurden.

Kapitel 5 zeigt uns die Ergebnisse, welche mit Hilfe von Sinuswellen-Stimuli sowie Weißem Rauschen gewonnen wurden. Die Erwartung war, Resonanz-Effekte für Verhältnisse von 2 : 1, 1 : 1 und 1 : 2 zwischen der Feuerrate des Neurons und der Stimulusfrequenz zu sehen. Tatsächlich werden die stärksten Resonanzeffekte für Stimulusfrequenzen nahe der mittleren Feuerrate beobachtet. Dabei findet eine 1 : 1-Kopplung zwischen der Stimulusfrequenz und der Spike-Antwort statt, indem die Feuerrate des Neurons der Stimulusfrequenz über eine entsprechende Frequenzspanne folgt. In dieser Frequenzspanne sind die Spike-Antworten durch hohe Spike-Zeiten-Zuverlässigkeit, Phasen-Kopplung, und niedrigen Spike-Jitter charakterisiert. Ein ähnlicher Effekt – jedoch viel schwächer – ist für die Subharmonische der mittleren Feuerrate zu sehen, wo ein Verhältnis von 2 : 1 zwischen der Feuerrate und der Stimulusfrequenz herrscht. Für die Zweite Harmonische (1 : 2) werden keine Resonanzeffekte beobachtet.

Durch Variation der Stimulusamplitude werden Arnold-Zungen sichtbar. Auch hier ist der deutlichste Effekt für Stimulusfrequenzen in der Nähe der mittleren Feuerrate (1 : 1-Verhältnis) zu sehen, wo die Breite der Arnold-Zunge ansteigt, wenn die Stimulusamplitude erhöht wird und Arnold-Zungen-ähnliche Strukturen vorhanden sind für die Zuverlässigkeitsmaße. Für viele Neurone sind diese Strukturen auch für 2 : 1-Verhältnisse zwischen Feuerrate und Stimulusfrequenz zu sehen, wenn die Daten unter Verwendung der Korrelations-basierten Zuverlässigkeit und dem Spike-Jitter analysiert werden. Ge-

mittelt über die Population aller mit diesem Stimulus-Protokoll untersuchten Neurone ist dieser Effekt aber nicht signifikant. Obwohl der Effekt der Timing-Resonanz bei einem 1 : 1-Verhältnis unabhängig von der durchschittlichen Feuerrate ist, führt deren Erhöhung zu einer stärkeren Manifestation des Effektes für eine breitere Spanne von Stimulusfrequenzen.
Die Resultate werden auf Konsistenz überprüft, indem die Korrelation zwischen Stimulusfrequenzen, welche zu 1 : 1- oder 2 : 1-Kopplung führen, und Stimulusfrequenzen, welche zu Spike-Antworten mit erhöhter Zuverlässigkeit führen, bestimmt wird. Für 1 : 1-Verhältnisse stimmen die Werte gut überein, während sie für 2 : 1-Verhältnisse abweichen. Wir schließen daraus, daß in auditorischen Rezeptorneuronen von *Locusta migratoria* 1 : 1-Kopplung zu einer zuverlässigeren Spike-Antwort führt als eine 2 : 1-Kopplung.
Im Gegensatz zu den Ergebnissen mit den Sinuswellen-Stimuli wurde keine Veränderung der Spike-Zuverlässigkeit in Abhängigkeit vom Frequenzgehalt des Weißen Rauschens beobachtet.
In Kapitel 6 werden Daten, welche mit Hilfe von Rechteckwellen-Stimuli gewonnen wurden, analysiert. Die Erwartung war, Unterschiede zu den Ergebnissen im vorherigen Kapitel zu sehen, aufgrund der Tatsache, daß Rechtecksignale einen Anstieg von 90° besitzen, unabhängig von der Frequenz. Außerdem gleichen sie durch die schärferen Übergänge zwischen den Amplitudenextremen den natürlichen Stimuli der Heuschrecken stärker als Sinuswellen. Zusätzlich geben uns Rechteckwellen die Möglichkeit, den Anteil des Stimuluszyklus', der überschwellig ist, durch Variation des Arbeitszyklus' zu kontrollieren.
Rasterplots und Phasen-Histogramme zeigen, daß mehr Spikes produziert werden, wenn der Arbeitszyklus von 25% auf 50 % und 75 % erhöht wird. Für einen Arbeitszyklus von 75 % sind die Spike Trains am unregelmäßigsten. Interspike-Interval-Histogramme zeigen die gipfeligste Struktur für den 50 % Arbeitszyklus.
Für einen Arbeitszyklus von 50 % sind 1 : 1-Kopplung der Feuerrate an die Stimulusfrequenz sowie Timing-Resonanz Effekte um die Feuerrate vorhanden, zu einem schwächeren Ausmaß auch um die Subharmonische. Eine 1 : 2-Kopplung ist nicht zu sehen. Wenn diese Resultate mit Resultaten von Stimuli mit Arbeitszyklen von 25 % und 75 % verglichen werden, ist die höchste Zuverlässigkeit der Spike-Antwort und die ausgeprägteste Stimulus-Kopplung für Arbeitszyklen von 25 % zu sehen. Beide Maße fallen ab für Arbeitszyklen von 50 % und 75 %.
Gemittelt über mehrere Zellen bleiben die Zuverlässigkeitwerte für Stimulusfrequenzen, die mit der mittleren Feurerate identisch sind, für das korrelationsbasierte Zuverlässsigkeitmaß ungefähr konstant für die drei Arbeitszyklen. Im Gegensatz dazu nehmen die Werte der Vektorstärke mit Erhöhung des Arbeitszyklus' ab und der Spike-Jitter zu. Die Frequenzspanne, für welche die Neurone ankoppeln, nimmt ab für höhere Arbeitszyklen für ein 1 : 1-Verhältnis zwischen Feuerrate und Stimulusfrequenz. Für 2 : 1- und 1 : 2-Verhältnisse ist kein Effekt zu sehen.
Wenn diese Ergebnisse mit den Daten von den Sinuswellenstimuli verglichen werden, zeigt das Korrelations-basierte Zuverlässigkeitsmaß eine kleinere Spanne an Werten für Arbeitszyklen von 75 %, und Peaks sind weniger stark zu sehen. Phasen-Kopplung, gemessen mit der Vektorstärke, wird ebenfalls schwächer für längere Arbeitszyklen und ist insgesamt niedriger als für die Sinuswellen-Stimuli.
Schliesslich werden in Kapitel 7 die Ergebnisse des experimentellen Teils rekapituliert und diskutiert, und in Kontext zu weiteren Arbeiten in diesem Feld gestellt. Unser Haupt-

ergebnis, Timing-Resonanz für Stimulusfrequenzen nahe der mittleren Feuerrate, stellt möglicherweise einen generellen Mechanismus dar, welcher in neuronalen Systemen aktiv ist, und verhaltensbiologische Studien zeigen, daß bestimmte Verhaltensmuster theoretisch von einem einzigen Rezeptorneuron ausgelöst werden könnten. Die Interaktion dieser Form von Resonanz mit anderen Formen wie unterschwelliger oder stochastischer Resonanz stellt eine spannende Herausfordung für zukünftige Arbeiten dar.

Selbständigkeitserklärung

Ich versichere hiermit, die vorliegende Arbeit selbständig und ausschliesslich unter Verwendung der angegebenen Mittel und ohne unerlaubte Hilfen angefertigt zu haben.

Berlin, 3. 12. 2007

Samuel Glauser